Characterization of the division apparatus in the budding bacterium *Hyphomonas neptunium*

DISSERTATION

zur Erlangung des Doktorgrades
der Naturwissenschaften
(Dr. rer. nat.)

dem Fachbereich Biologie der
Philipps-Universität Marburg
vorgelegt von

Sabrina Eisheuer
aus Mannheim

Marburg, Februar 2016

Vom Fachbereich Biologie der Philipps-Universität Marburg (HKZ: 1180)
als Dissertation angenommen am 16.02.2016

Erstgutachter: Prof. Dr. Martin Thanbichler
Zweitgutachter: Prof. Dr. Lotte Søgaard-Andersen

Tag der mündlichen Prüfung am 28.04.2016

Die Untersuchungen zur vorliegenden Arbeit wurden von Oktober 2011 bis April 2015 am Max-Planck-Institut für terrestrische Mikrobiologie und am Fachbereich Biologie der Philipps-Universität Marburg unter Leitung von Prof. Dr. Martin Thanbichler durchgeführt.

Die während der Promotion erzielten Ergebnisse werden
in folgenden Originalpublikationen veröffentlicht:

Eisheuer, S., Zimmer, J., Heimerl, T., Thanbichler, M. The dynamics of divisome components during asymmetric cell division in *Hyphomonas neptunium* (in Vorbereitung).

Cserti, E., Rosskopf, S., Chang, Y.-W., Regh, C., **Eisheuer, S.**, Jensen, G., Thanbichler, M. Dynamics of the peptidoglycan biogenesis machinery during budding in *Hyphomonas neptunium* (in Vorbereitung).

Ergebnisse aus in dieser Dissertation nicht erwähnten Projekten sind
in folgender Originalpublikation veröffentlicht:

Jung, A., **Eisheuer, S.**, Cserti, E., Leicht, O., Strobel, W., Möll, A., Schlimpert, S., Kühn, J., Thanbichler, M. (2015) Molecular toolbox for genetic manipulation of the stalked budding bacterium *Hyphomonas neptunium*. *Appl Environ Microbiol* 81:736-744.

Dedicated to people who I love

Abstract

Bacteria are phylogenetically diverse and have evolved a variety of different cell shapes, life styles, and reproduction strategies. In the past decades, research has focused mainly on a few model organisms, such as *Escherichia coli*, *Bacillus subtilis* and *Caulobacter crescentus* that all divide by symmetric or asymmetric binary fission and are rod-shaped. Thus, the mechanisms underlying alternative propagation modes such as multiple offspring formation or budding are largely unknown. To further our knowledge in this field, we set out to study the dimorphic α-proteobacterium *Hyphomonas neptunium* as a representative of the stalked budding bacteria. In this work, we investigated the highly asymmetric cell division of *H. neptunium*, which occurs at the junction between the stalk and the bud, giving rise to two morphologically and physiologically different cell types. In the majority of bacteria, cell division is mediated by a multiprotein complex called the divisome. In *H. neptunium*, most of the known divisome components are conserved, and a comprehensive localization study confirmed that these proteins localize dynamically to the division site. Remarkably, for the central component FtsZ and the DNA translocase FtsK, we could observe unusual localization patterns, with both of them forming complexes at positions other than the final division site. FtsZ localized at both ends of the stalk. However, only the complex at the division site developed into a mature divisome by the recruitment of other division proteins. FtsK localized in an irregular pattern within the stalk structure, indicating that its function may go beyond mediating the last stages of chromosome segregation. Analysis of an ATPase-deficient FtsK variant and a strain with reduced FtsK expression indeed pointed towards an involvement of FtsK in DNA transport through the stalk in *H. neptunium*. Furthermore, we demonstrated that unlike in the closely related species, the conserved ATPase MipZ is not a critical regulator of Z-ring positioning in *H. neptunium*, in contrast to its close relative *C. crescentus*. Since homologs of other regulatory systems are absent, a novel, yet unidentified, mechanism might position the division site in *H. neptunium*. Taken together, we could show that although cell division proteins are conserved among species, their spatiotemporal regulation and specific role can differ to fit the needs of distinct life styles.

Zusammenfassung

Bakterien sind phylogenetisch divers und haben eine Vielzahl von Zellformen, Lebensstilen und Vemehrungsstrategien entwickelt. Die Forschung in den letzten Jahrzehnten hat sich hauptsächlich auf die Untersuchung einiger weniger Modellorganismen wie *Escherichia coli*, *Bacillus subtilis* and *Caulobacter crescentus* konzentriert, welche sich alle durch asymmetrische oder symmetrische binäre Teilung vermehren und stäbchenförmig sind. Entsprechend sind die Mechanismen, die alternativen Teilungsarten, wie der Knospung, zu Grunde liegen, zum Großteil unbekannt. Um das Wissen auf diesem Gebiet zu erweitern, haben wir begonnen, das dimorphe α-Proteobakterium *Hyphomonas neptunium* als Vertreter der gestielten, knospenden Bakterien zu untersuchen. Im Rahmen dieser Arbeit wurde die asymmetrische Zellteilung von *H. neptunium*, die am Übergang von Stiel und Knospe stattfindet und zwei morphologisch und physiologisch unterschiedliche Zelltypen hervorbringt, analysiert. In den meisten Bakterien erfolgt die Zellteilung mit Hilfe eines Multiprotein-Komplexes, der auch als Divisom bezeichnet wird. In *H. neptunium* sind eine Vielzahl der bekannten Divisom-Komponenten konserviert, deren dynamische Lokalisation in der Zellteilungsebene in einer umfassende Lokalisationsstudie bestätigt werden konnte. Allerdings wurde für den zentralen Faktor der Zellteilung, FtsZ, und die DNA-Translokase FtsK ein ungewöhnliches Lokalisationsmuster beobachtet, da beide Proteine an Stellen außerhalb der Zellteilungsebene Komplexe bildeten. FtsZ ist an beiden Enden des Stiels zu finden. Allerdings führt nur der FtsZ-Komplex an der Zellteilungsebene durch die Rekrutierung weiterer Zellteilungsproteine zu einer reifen Zellteilungsmaschinerie. FtsK hingegen lokalisiert in einem unregelmäßigen Muster in der Stiel-Struktur, was auf eine zusätzliche Rolle in einem anderen Prozess als den letzten Schritten der Chromosomensegregation hinweist. Die Analyse einer ATPase-defekten FtsK-Variante und eines Stammes mit reduzierter FtsK-Expression lieferte Hinweise auf eine Beteiligung von FtsK am Transport der DNA durch den Stiel. Zudem konnte gezeigt werden, dass die konservierte ATPase MipZ, anders als in der Spezies *C. crescentus*, nicht für die räumliche Regulation des Z-Rings in *H. neptunium* benötigt wird. Da Homologe anderer Regulatorproteine nicht gefunden wurden, dürfte ein neuer, bisher nicht identifizierter Mechanismus die Zellteilungsebene

in *H. neptunium* positionieren.

Zusammenfassend konnte in dieser Arbeit gezeigt werden, dass sich die räumliche und zeitliche Regulation und die spezifischen Aufgaben von Zellteilungsproteinen unterscheiden können, auch wenn sie in verschiedenen Bakterien stark konserviert sind.

Table of Contents

1 Introduction

1.1 Bacterial cell division

The bacterial cell cycle culminates in the physical separation of the two daughter cells by cytokinesis. This complex process has to be strictly regulated in time and space and coordinated with other events such as chromosome segregation, cell differentiation, and cell growth. In most bacteria, the cell division machinery is orchestrated by the tubulin homolog FtsZ, which directly or indirectly recruits all other divisome components. In general, FtsZ-based cell division can be divided into three distinct steps: (1) assembly and stabilization of FtsZ into a ring-like structure (Z-ring), (2) maturation of the division machinery through recruitment of downstream divisome components and (3) cell constriction to separate the daughter cells.

1.1.1 FtsZ - key player of cell division

The tubulin homolog FtsZ is the central component of bacterial cell division and by far the most conserved cell division protein [1]. It is present in the vast majority of bacteria as well as in euryarcheota, chloroplasts, and the mitochondria of some eukaryotes [2]. The homology between FtsZ and tubulin is mainly based on structural similarity, while sequence similarity is quite low [3, 4]. FtsZ typically consists of four structural domains (Fig. 1.1 A): (1) an N-terminal globular tubulin-like core containing the GTP-binding site and the T7 synergy loop, (2) a flexible C-terminal linker (CTL) of variable length, possibly involved in force generation, (3) a highly conserved C-terminal tail (CTT) serving as interaction site for several cell division proteins, and (4) the C-terminal variable region (CTV), which is suggested to affect assembly of FtsZ molecules depending on its net charge [5].

At the onset of cytokinesis, FtsZ polymerizes in a GTP-dependent manner into linear protofilaments that assemble into a ring-like structure called the Z-ring. The Z-ring is

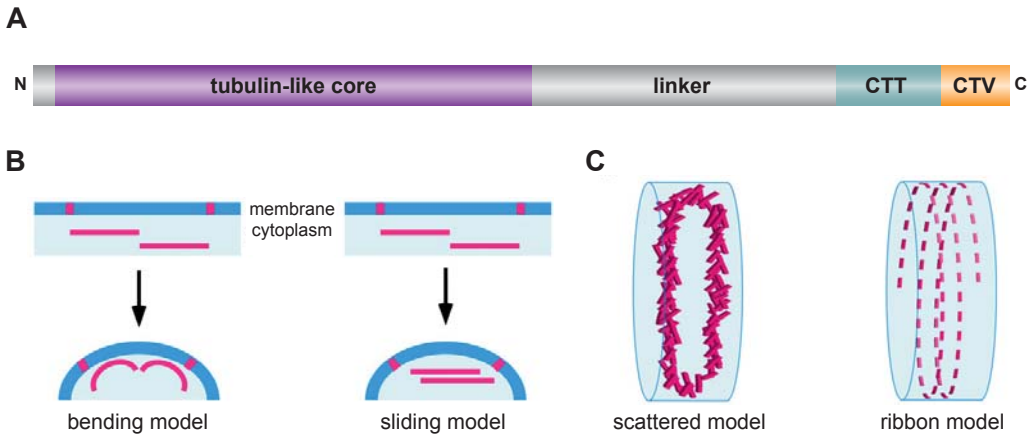

Figure 1.1: Structural and functional models of FtsZ and the Z-ring. **(A)** Schematic representation of the domain organization of FtsZ. The domains are not drawn to scale. Abbreviations: CTT = C-terminal tail; CTV = C-terminal variable region. **(B)** Bending and sliding model for constrictive force generation by the Z-ring. **(C)** Scattered and ribbon model of Z-ring architecture. (B+C) adapted from [8].

the structural basis for cell division and acts as a scaffold for the recruitment of other division proteins, which altogether form the so-called divisome (Fig. 1.2). Although the Z-ring appears like a rigid structure, it is in fact highly dynamic, with FtsZ molecules being rapidly turned over (half-time of 8-10 s) [6, 7].

How the FtsZ polymers are exactly arranged in the Z-ring has still not been completely clarified, although notable progress has been made through the use of advanced visualization techniques such as 3D structured illumination microscopy (3D-SIM), photoactivated localization microscopy (PALM) and cryo-electron tomography (CET). Two models have been advanced for the *in vivo* Z-ring structure (Fig. 1.1 C). The scattered model favors a loose heterogeneous arrangement of filaments generating a multi-layered Z-ring, whereas the ribbon model suggests that the Z-ring is made up of short non-overlapping filaments in a single layer [9]. The scattered model is supported by high-resolution images obtained from various species. In *E. coli*, Fu *et al.* observed a compressed helical Z-ring structure by PALM, which was densely packed and, thus, suggests a loose arrangement of short filaments [10]. Consistent results were obtained in *B. subtilis* using stimulated emission depletion (STED) microscopy and in *C. crescentus* using CET [11, 12]. The rapid turnover times of FtsZ molecules within the Z-ring, as obtained by fluorescence recovery after photobleaching (FRAP), are also compatible

with the presence of rather short protofilaments [6]. The ribbon model is supported by the ability of FtsZ to form long protofilaments assembling on the surface of artificial membranes [13] and under different *in vitro* conditions [14, 15]. Furthermore, in a recent study the Z-ring was observed as a single-layered, continuous structure composed of shorter filaments using CET and *in vitro* reconstitution on liposomes [16].

The Z-ring is also implicated in the generation of the force required for constriction, even though it is unclear to what extent. A variety of *in vitro* experiments have proven that FtsZ either alone, when artificially tethered to the membrane, or in combination with FtsA, is capable of generating a constrictive force driving membrane deformation [17–20]. Two mechanisms have been proposed as the origin of this force (Fig. 1.1 B): in the sliding model, the short FtsZ filaments tend to increase their lateral contacts by gliding along each other, thereby decreasing the diameter of the Z-ring and, thus, pulling the membrane inwards. In the bending model, the constrictive force is based on conformational changes of FtsZ filaments from straight to more curved, driven by GTP hydrolysis [8]. However, the significance of these results *in vivo* remains elusive. Beside the hypothesis that FtsZ alone exerts the required force (FtsZ-centric model), it has been suggested that either peptidoglycan (PG) synthesis pushes the membrane inward (PG-centric model) or that the combined action of the Z-ring and directed PG growth generates the constrictive force [21]. The FtsZ-centric model has recently been challenged by the observation that the Z-ring disassembles before constriction is completed [22].

1.1.2 The bacterial cell division machinery

Assembly of the Z-ring at the future division site requires factors that tether FtsZ to the inner leaflet of the membrane. In *E. coli*, the two membrane-associated proteins ZipA and FtsA are recruited to midcell by FtsZ and mediate membrane attachment via a direct interaction with the FtsZ CTT [23]. ZipA is an essential bitopic protein with a single transmembrane domain and is only conserved in γ-proteobacteria [24]. Additionally to its role in tethering, ZipA recruits downstream division proteins [25] and might be involved in stabilizing the Z-ring [26]. Unlike ZipA, FtsA is associated with the membrane by a short C-terminal amphipathic helix and widely conserved among bacteria

[27, 28]. As a member of the actin/Hsp70 superfamily, it is able to form filaments, but the physiological role of FtsA polymerization in Z-ring assembly *in vivo* has not been clarified yet. However, a gain of function mutant of FtsA can bypass the essential role of ZipA, confirming their overlapping functions [29]. In *C. crescentus*, which lacks ZipA, FtsA is recruited to midcell with a significant delay, indicating that other factors have taken the role of membrane tethering [30, 31]. One promising candidate is the ABC-transporter complex formed by FtsE and FtsX. The ATPase FtsE was shown to interact with FtsZ, albeit not with its C-terminal tail, whereas its partner protein FtsX is embedded in the membrane [32, 33]. Beside a putative role in membrane attachment of the Z-ring in *C. crescentus*, the FtsEX complex in *E. coli* has been implicated in cell wall remodeling [34]. Yang *et al.* demonstrated that FtsX directly recruits EnvC, an activator of the two amidases AmiA and AmiB, to the division site. EnvC activity might, in turn, be regulated by FtsE-mediated ATP hydrolysis and concomitant conformational changes [34]. In *B. subtilis*, by contrast, FtsE and FtsX are not "typical" cell division proteins but rather direct the switch from medial to polar septum formation during sporulation initiation [35].

The stability of the Z-ring in *E. coli* is further promoted by a range of non-essential proteins, named ZapA-D, which have functionally redundant roles in FtsZ protofilament bundling [14, 36–39]. However, out of these four proteins, only ZapA is widely conserved, whereas ZapB, ZapC and ZapD are mainly restricted to γ-proteobacteria. In *E. coli*, ZapB was found to have a putative additional function in chromosome segregation based on the fact that it interacts with the chromosome-structuring factor MatP at the division site. The MatP-ZapB interaction might help to spatiotemporally coordinate the final steps of chromosome segregation with cell constriction [40].

In *C. crescentus*, two additional FtsZ-associated proteins, FzlA and FzlC, have been identified [41]. They are widely conserved in α-proteobacterial species and were shown to bind directly to FtsZ *in vitro*. FzlA, a glutathione S-transferase-like protein, is essential for viability and induces the formation of stable, higher-order structures of FtsZ, thereby influencing protofilament curvature. In contrast, the hypothetical protein FzlC is dispensable under laboratory conditions [41]. In Gram-positive bacteria such as

B. subtilis, which lack many of these non-essential stabilizers, other positive regulators were identified. For instance, SepF from *B. subtilis* modulates the structure of FtsZ bundles [42] and EzrA, although regarded as a negative regulator of Z-ring formation [43], also plays several positive roles during cell division in Gram-positive bacteria [44, 45].

After stabilization of the Z-ring at the incipient division site, there is a delay until downstream cell division proteins are recruited. During this time, factors involved in PG synthesis and remodeling arrive at midcell to carry out medial cell elongation (see section 1.1.3). Finally, in order to promote maturation of the division machinery into a constriction-competent divisome (Fig. 1.2), a number of essential "late" cell division proteins are required. These include FtsK, the FtsQLB complex, FtsI, FtsW and FtsN. The bifunctional DNA-translocase FtsK coordinates cell division with chromosome segregation and is discussed in more detail in section 1.3.2 The bitopic membrane proteins FtsQ, FtsL and FtsB form a subcomplex and are highly conserved among bacterial species [46, 47]. Nevertheless, their precise role is still unknown. Based on the fact that the FtsQLB complex interacts *in vitro* with several other cell division proteins in *E. coli* [48–50] and FtsL is required to localize FtsQ and FtsB as well as FtsI and FtsW in *C. crescentus* [30], it was assumed that the FtsQLB complex has a structural and/or scaffolding role. However, recent work from several groups [51–54] points towards an activating role of the FtsQLB complex in septal PG synthesis mediated by FtsN (as discussed below).

The recruitment of proteins necessary for septal PG synthesis and remodeling mark the transition from cell elongation to cell separation. FtsI is a class B penicillin-binding protein (also called PBP3) and essential for septal PG synthesis [55, 56]. The integral membrane protein FtsW is commonly thought to be the flippase that translocates lipid II PG precursor molecules across the cytoplasmic membrane [57, 58]. In *E. coli*, FtsW recruits FtsI to the division site and both proteins form a subcomplex [59, 60], whereas FtsI arrives prior to FtsW at the division site in *C. crescentus* [30]. Interestingly, a new study by Sham *et al.* claims that in *E. coli*, MurJ is the flippase for lipid II precursors rather than FtsW and RodA [61]. Consequently, further work is necessary to ultimately clarify this issue. Finally, another late cell division protein implicated in PG synthesis and

remodeling is FtsN. It was suggested to regulate PG synthesis and remodeling through interaction with FtsI and PBP1B, and its arrival at the division site coincides with the appearance of a visible constriction [50, 62, 63]. Moreover, several new reports shed light on the question how FtsN might trigger PG synthesis. Collectively, they propose a model in which FtsN activates septal PG synthesis by stimulating its interaction partners FtsA and the FtsQLB complex to convert into an “on” state, which allows PG synthesis to occur [51–54].

In Gram-negative bacteria the final steps of cell division, invagination, and fission of the three cell envelope layers are mediated by the dynamics of the Z-ring (probably including force generation for inner membrane constriction, see section 1.1.1), the Tol-Pal complex (outer membrane constriction), and hydrolytic enzymes such as amidases (PG splitting).The Tol-Pal complex consists of the inner membrane proteins TolA, TolQ, TolR, the periplasmic protein TolB, and the lipoprotein Pal, which is found in the outer membrane. Together, they bridge the different layers of the cell envelope via multiple

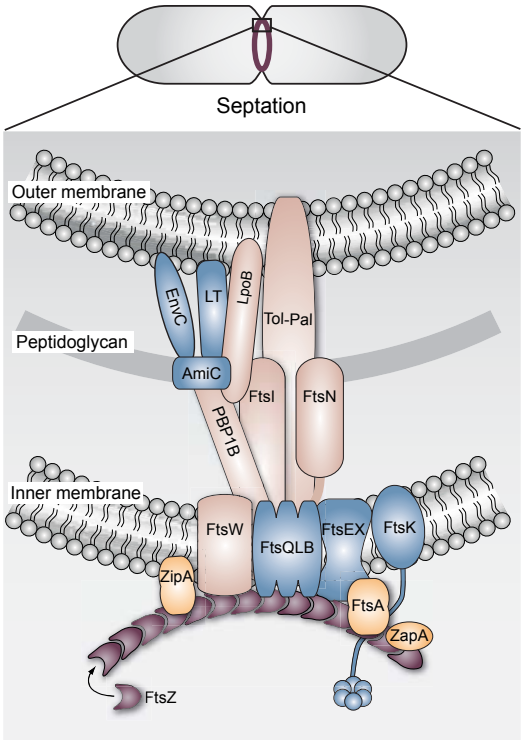

Figure 1.2: The *E. coli* divisome. Schematic representation of the subcellular localization of divisome components at a late stage of cell division. Abbreviation: LT = lytic transglycosylases. Modified from [64].

interactions [65, 66]. In *E. coli*, unlike in *C. crescentus*, the Tol-Pal complex is not essential [66], because a redundant system consisting of PBP1B and LpoB is present [67, 68]. In *C. crescentus*, the Tol-Pal complex is furthermore involved in maintaining cell envelope integrity and in proper localization of the polarity factor TipN [66]. In addition to the Tol-Pal complex, a periplasmic protein called DipM was proposed to facilitate remodeling of the PG layer and outer membrane invagination in *C. crescentus* [69–71].

1.1.3 Peptidoglycan synthesis in the context of cell division

The Gram-negative bacterial cell envelope consists of the inner membrane, a thin layer of peptidoglycan located in the periplasm, and the outer membrane. All together help the cell to maintain its shape and withstand osmotic pressure. PG is made of alternating repeats of N-acetylglucosamine (GlcNAc) and N-acetylmuramic acid (MurNAc) moieties linked by 1,4-glycosidic bonds. These glycan chains are cross-linked by short peptide chains, thereby forming a mesh-like structure [72].

Synthesis of PG is a complex process involving many different steps (reviewed in [64]). Briefly, the lipid II precursor molecules are synthesized in the cytoplasm and at the inner surface of the cytoplasmic membrane, respectively, and then flipped into the periplasm, where they are inserted in the existing PG sacculus. The major PG synthases are penicillin-binding proteins (PBPs), which catalyze the transpeptidation reaction of the peptide side chains (TPases) and some additionally the transglycosylation reaction between MurNAc and GlcNAc (GTases) [73]. Accordingly, they are divided into class A PBPs (bifunctional) and class B PBPS (only TPases). They are usually either specific for cell elongation (PBP1A and PBP2 in *E. coli*) or for cell division (PBP1B and PBP3 (FtsI) in *E. coli*) [74]. In contrast, PG hydrolases are necessary for PG splitting during cell division, while during cell elongation they open the existing sacculus for insertion of new PG material. Depending on which part of PG they act on, they can be roughly divided into lytic transglycosylases (split glycan strands), amidases (split amide bonds) and peptidases (split peptide bonds), with most of these families having again several sub-categories [75].

Generally, one can differentiate between two distinct growth stages: cell elongation and division. During the so-called dispersed cell growth, new PG material is inserted along the lateral cell wall of rod-shaped bacteria. The elongation machinery (elongasome), comprised of PG synthases, e.g. PBP1A and PBP2, hydrolases, the flippase RodA and other associated proteins (MreC, MreD, LpoA etc.), mediates cell growth [76] and is thought to be mainly coordinated and positioned by the cytoskeletal element MreB, an actin homolog essential for rod-shaped growth [77, 78]. During the early stages of divisome assembly and after the Z-ring has been stabilized, the mode of lateral cell growth changes from “dispersed” elongation to “medial” elongation. This switch depends on FtsZ and involves the recruitment of several components of the elongation complex to midcell by direct interaction of FtsZ and MreB [64, 79, 80]. This growth mode contributes significantly to cell elongation in *C. crescentus*, whereas it plays only a minor role during cell elongation in *E. coli* and *B. subtilis* [79, 81]. Finally, at the last stages of cell division, PG has to be remodeled in order to synthesize the new cell poles and separate the daughter cells. This process requires PG biosynthetic enzymes specific for cell division, such as PBP3 (FtsI), FtsW, FtsN, and some hydrolases. Their roles are discussed in more detail in section 1.1.2

1.2 Regulation of Z-ring positioning

Selection of the division site is a crucial step during the bacterial cell cycle that ensures proper cell size and shape as well as faithful transmission of the genetic information to the daughter cells. Even though FtsZ is one of the most conserved proteins in bacteria [1], the systems that regulate the spatiotemporal placement of the Z-ring vary significantly (Fig. 1.3). Beside negative regulators, which were discovered decades ago, recent studies have revealed that positive regulation mechanisms also exist and are more widespread than initially thought.

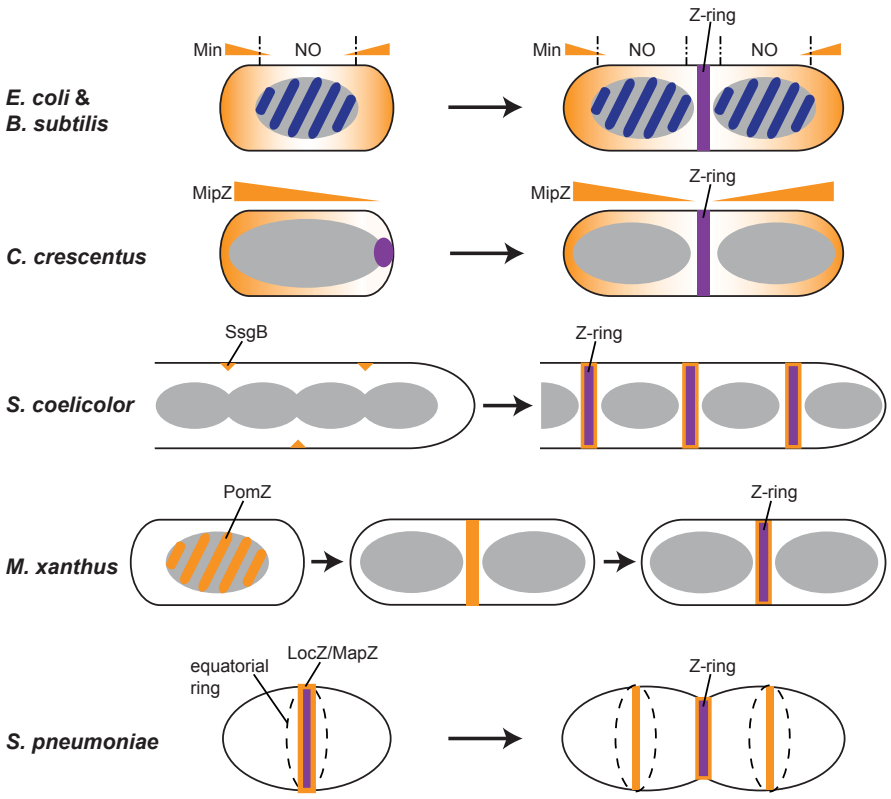

Figure 1.3: Z-ring positioning systems in bacteria. Schematic of negative and positive regulatory mechanisms of the Z-ring from various bacteria. FtsZ/Z-ring is shown in purple, the regulators are shown in orange/dark blue, and the nucleoid is shown in grey. See section 1.2 for more information. Modified from [82, 83].

1.2.1 Negative regulation mechanisms

The best-studied examples of negative regulators are the Min system and nucleoid occlusion, found in *E. coli* and *B. subtilis*. Both systems work in combination to prevent division at inappropriate positions within the cell. In *E. coli*, the Min system comprises the proteins MinC, MinD and MinE, which are encoded in an operon and block the formation of Z-rings at the cell poles [84]. MinC, the actual inhibitor of FtsZ [85, 86], interacts directly with FtsZ and has two distinct domains working in synergy to destabilize the Z-ring by different mechanisms [87, 88]. Additionally, the C-terminus of MinC is involved in its own dimerization, as well as in the interaction with MinD. MinD belongs to the Mrp/MinD family of P-loop ATPases [89] and recruits MinC to the inner membrane [90]. In the ATP-bound, active form, MinD dimerizes and associates with the cytoplasmic membrane via a C-terminal amphipathic helix [91]. The inhibitory activity of the MinCD

complex is restricted to the cell poles by the third protein, the topological factor MinE. MinE stimulates the ATPase activity of MinD via a direct interaction, which results in the release of MinCD from the membrane and its subsequent movement to the opposite cell pole, where the complex binds again to the membrane [92, 93]. This pole-to-pole oscillation generates a temporal gradient in the concentration of MinC that allows Z-ring assembly to occur only at midcell.

B. subtilis uses a different topological factor called DivIVA, which is localized to the cell poles by its intrinsic ability to sense membrane curvature [94–96]. It indirectly recruits MinCD to the poles via an adaptor protein called MinJ, which interacts with DivIVA as well as with MinD [97, 98]. Thus, the Min system in *B. subtilis* is more static than in *E. coli*. Moreover, and unlike in *E. coli*, the Min components in *B. subtilis* are relocated to the constricting divisome at late points of cell division and presumably disassemble the cytokinetic machinery to impair re-initiation of cell division [99–101].

Another negative regulatory mechanism in *E. coli* and *B. subtilis* is nucleoid occlusion (NO). This system prevents Z-ring assembly over the DNA and is mediated by specific factors: the protein SlmA in *E. coli* [102] and the unrelated protein Noc in *B. subtilis* [103]. Both proteins bind specifically to different palindromic binding sites on the DNA that are distributed throughout large parts of the chromosome, but are absent from the terminus region [104–106]. However, the mechanisms by which they antagonize division in the direct vicinity of the nucleoid seem to be quite different. SlmA was shown to interact directly with the conserved C-terminal tail of FtsZ, resulting in disassembly of FtsZ polymers [104, 107, 108]. Nevertheless, the exact mechanism of how FtsZ polymerization is affected by SlmA remains unknown. In contrast, a direct link of Noc from *B. subtilis* to FtsZ or any other protein target could not be demonstrated so far [105, 109]. It was shown though that Noc forms large nucleoprotein complexes at its specific binding sites [105]. Indeed, Adams *et al.* propose a model in their recent work in which these large DNA-Noc complexes physically inhibit division over the nucleoid [110]. They also found that Noc associates with the cell membrane via its N-terminal amphiphatic helix in a DNA-dependent manner. The consequent recruitment of DNA to the membrane was shown to be required for the inhibitory function of Noc, suggesting that the presence of

DNA at the cell periphery might physically occlude divisome assembly [110].

Several recent studies provide evidence for the presence of further positioning mechanisms in these organisms [111, 112]. For example, in outgrown spores of a *B. subtilis* min$^-$ noc$^-$ mutant, the Z-ring can still precisely form at midcell, albeit delayed and less efficiently [111]. In *E. coli*, an unsegregated, only partially replicated chromosome can inhibit Z-ring formation independently of SlmA, MinC, and the SOS system [113]. It was suggested that in slow-growing *E. coli* cells lacking both the Min system and SlmA, the Ter macrodomain serves as a positive signal for divisome assembly [112].

In *C. crescentus*, which lacks homologs of the Min and NO systems, division site positioning is regulated by a bipolar gradient of the ParA-like ATPase MipZ. MipZ is conserved in many other α-proteobacteria and belongs to the Mrp/MinD family of P-loop ATPases. However, unlike MinD, it directly interacts with FtsZ and inhibits its polymerization at least in parts by stimulating the GTPase activity of FtsZ [114, 115]. The bipolar gradient of MipZ is established by interaction with ParB, which is bound to the *parS* sites near the origin of replication (see section 1.3). The duplication and rapid segregation of the origin region to opposite cell poles leads to the highest concentration of MipZ at the cell poles and the lowest concentration at midcell [115]. At a molecular level, this distribution is based on the different oligomerization states of MipZ. Monomeric MipZ is recruited by the origin-bound ParB-*parS* complexes to the cell poles, where it undergoes ATP-dependent dimerization, either directly or indirectly promoted by ParB [114]. Dimerized MipZ is released and binds unspecifically to the nucleoid. Since binding to DNA reduces the diffusion rate of MipZ, it is preferentially bound to DNA regions close to the cell poles, resulting in a gradient-like distribution [114].

1.2.2 Positive regulation mechanisms

A few years ago, the first positive regulator of cell division has been identified in *Streptomyces coelicolor* [116]. During sporulation, SsgB arrives prior to FtsZ at the division site and is assumed to recruit and tether FtsZ via a direct interaction. The localization

of SsgB is in turn controlled by the orthologous protein SsgA [116].

Another positive regulator has been identified in the δ-proteobacterium *Myxococcus xanthus* that lacks all known positioning systems. The protein PomZ, a member of the Mrp/MinD family of P-loop ATPases as well, localizes at midcell prior to and independently of FtsZ, and its loss results in aberrant Z-ring formation [117]. It was proposed that PomZ identifies the correct position and recruits FtsZ there [117].

Quite recently, two groups independently identified a factor involved in the positioning of FtsZ in *Streptococcus pneumoniae*, which was designated MapZ/LocZ [118, 119]. The loss of this protein leads to aberrant division events resulting in anucleate minicells. MapZ/LocZ marks the future division site by being permanently associated with the equatorial ring, a marker for cell division in streptococci and it recruits FtsZ via a direct interaction. Upon cell growth, the equatorial ring is split into two and MapZ/LocZ was observed to move apart with these structures. Phosphorylation of MapZ/LocZ might play a role in regulating the closure of the Z-ring, but is not required for Z-ring positioning [118, 119].

1.3 Chromosome segregation

Before cytokinesis is completed, the genetic material has to be distributed such that each progeny receives a full set of DNA. In contrast to eukaryotes, bacteria segregate their chromosome while replication is still ongoing [120–122]. This requires a high degree of spatial and temporal organization of these processes. Research in the last decades has revealed that there is no universal solution to the problem of chromosome segregation in bacteria, since different species use different mechanisms. Furthermore, in many bacteria the loss of some systems has no major influence on viability, suggesting that redundant systems do exist.

Nevertheless, three different systems have been mainly implicated in chromosome segregation: (1) the *parABS* system involved in *ori* segregation; (2) the SMC (structural

maintenance of chromosome) complex, involved in *ori* and bulk chromosome segregation, and (3) the translocase FtsK, involved in terminus resolution and segregation. The *parABS* system of *C. crescentus* and the DNA translocase FtsK will be discussed in more detail in the following sections.

1.3.1 The *parABS* system of *C. crescentus*

The widely conserved chromosomal *parABS* system can be found in over 65% of all sequenced bacterial genomes [123], including well-known species such as *B. subtilis* [124], *Vibrio cholerae* [125], and *C. crescentus* [126]. However, *C. crescentus* is one of the few species in which this system is essential for viability, likely due to its involvement in the regulation of cell division (see section 1.2.1) [115, 127].

The *parABS* system was first discovered and studied as the segregation mechanism of low-copy plasmids, like F and P1 plasmids [128], but it also works similarly in chromosome segregation. The core components are: (1) the centromere-like DNA sequence *parS*, (2) the DNA-binding protein ParB, and (3) the Walker type ATPase ParA. In general, the ParB protein binds to the *parS* sequences, which are located near the origin of replication. ParA binds non-specifically to the nucleoid upon ATP binding and subsequent dimerization. The intrinsic ATPase activity of ParA is relatively weak, but interaction with the ParB/*parS* nucleoprotein complex can stimulate this activity. The directionality of segregation comes from ParA, but how the movement is accomplished and how the force is generated is still a topic of ongoing debate. Several hypotheses have been proposed in the last years, including the "ParA filament model" [129–131], the "diffusion ratchet model" [132–134], and the "DNA-relay model" [135]. The "ParA filament model" proposes that ParA polymerizes into a long filament, forming a spindle-like structure. Upon binding of the ParB/*parS* complex, the filament depolymerizes due to the stimulation of the ATPase activity of ParA by ParB. Thereby, the *ori* region is "pulled" towards the new cell pole. However, this model is no longer considered to be relevant. In contrast, the "diffusion ratchet model" suggests that ParA forms no filament, but binds unspecifically to DNA in its dimeric form. Binding of ParB then stimulates the ATPase activity of ParA, resulting in a local release of ParA from the nucleoid. By diffusion the ParB/*parS* complex moves to the

next DNA-bound ParA along the ParA dimer gradient and is thereby travelling towards the new cell pole. The “DNA relay model” is a modification of the “diffusion ratchet model” in a way that the DNA-bound ParA dimers are no longer static, but dynamic based on the elasticity of the chromosome. Thus, DNA-bound ParA serves as a transient tether that passes the ParB/*parS* complex along to another DNA-bound ParA dimer across a ParA dimer gradient with the help of the flexible DNA.

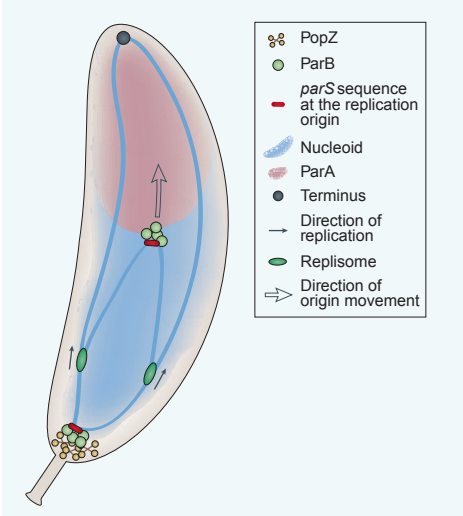

Figure 1.4: The *parABS*-system of *C. crescentus*. See section 1.3.1 for more information. Adapted from [136].

In *C. crescentus*, the origin region is tethered to the cell pole through interaction of the ParB/*parS* complex with the pole-organizing protein PopZ [137, 138]. According to both currently valid models, ParA dimers localize in a cloud-like pattern on the nucleoid that stretches from the new towards the old cell pole (Fig. 1.4). Upon replication and physical separation of the two origin regions, one of the ParB/*parS* complexes comes in contact with the ParA cloud, which stimulates ATP hydrolysis and releases ADP-bound ParA from the nucleoid. Subsequently, the ParB/*parS* complex moves to the neighboring ParA dimers on the nucleoid and the cycle repeats [133, 139–141]. In this way, the origin region is “pulled” towards the new cell pole (Fig. 1.4). At the new cell pole, PopZ acts in concert with the polarity factor TipN to sequester released ParA monomers [139, 142, 143]. In a 3D matrix formed by PopZ, their DNA binding activity is regenerated and they are eventually released to encounter pole-proximal parts of the nucleoid [142]. Thus, PopZ

serves as a polar hub, which induces directionality and prevents reversals in the process of chromosome segregation. The function of TipN in ParA regulation is not completely understood. It might be involved in positioning of PopZ and increasing the effectiveness of ParA recruitment [140, 142, 144].

1.3.2 FtsK - coupling chromosome segregation to cell division

During the last step of chromosome segregation, the cell faces several problems: the terminus regions, which are replicated and segregated last at the division site may become trapped in the closing septum due to a temporal delay in DNA segregation or the presence of chromosome dimers and catenanes, respectively. To resolve these issues, bacteria such as *E. coli* and *C. crescentus* possess a DNA translocase called FtsK, which is part of the division apparatus and couples cytokinesis with chromosome partitioning [145]. It is composed of an N-terminal transmembrane region, required for localization to the division site [145–147], a flexible linker, possibly involved in a function related to cell division [148], and a C-terminal domain, comprising the motor for DNA translocation (Fig. 1.5) [145, 149, 150].

The α and β subunits of the C-terminal domain contain the AAA^+ ATPase domain and form a homohexameric ring around DNA double-strands [151]. The γ-subunit is implicated in several functions. It mediates the sequence-specific recognition of KOPS (FtsK-orienting polar sequences), eight-nucleotide motifs present mainly on the leading strand and oriented towards the terminus region [152–155]. These regions serve as initial loading zones for FtsK and confer directionality to the translocation process [156, 157]. Furthermore, the γ-subunit recruits the XerCD recombinases to the so-called *dif* sites near the *ter* region and stimulates dimer resolution by directly activating XerD [149, 158]. This subunit is also involved in the interaction of FtsK with other proteins and influences whether proteins are removed from the DNA or bypassed during translocation [159]. The C-terminal domain of FtsK is additionally involved in the decatenation of sister chromosomes as it stimulates the activity of the topoisomerase IV component ParC to resolve such structures [160, 161].

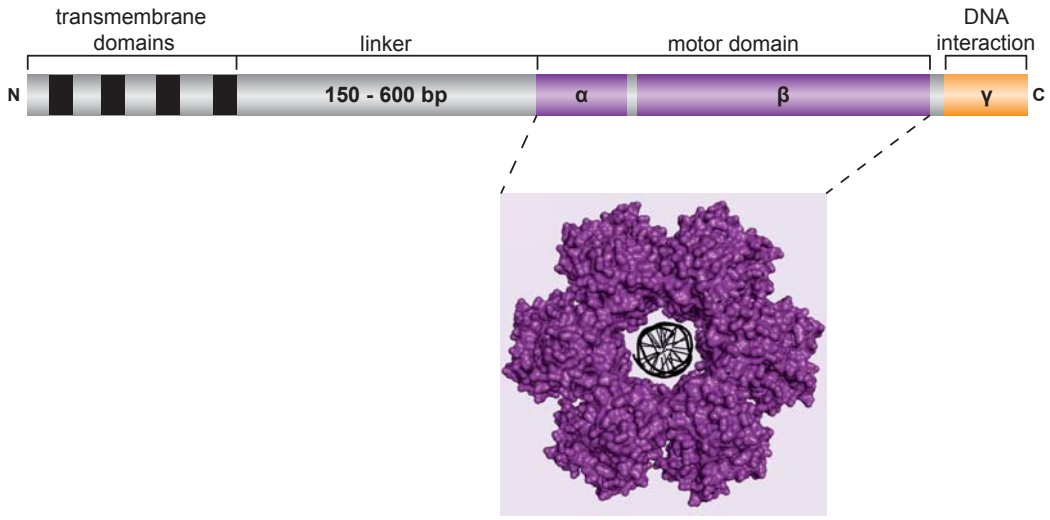

Figure 1.5: Domain organization of FtsK. The motor domain (purple) forms homohexamers around DNA (see inlet). The domains are not drawn to scale. Modified from [162].

Interestingly, the *B. subtilis* homolog of FtsK, SpoIIIE, is additionally involved in sporulation in a way that it pumps 75% of the chromosome into the forespore [163–165], indicating a major role in bulk chromosome segregation.

1.4 *Hyphomonas neptunium* as a new model organism

In the past decades it has become obvious that bacteria are highly organized and dynamic cells. They are capable of localizing DNA and proteins to specific subcellular positions at distinct time points and exhibit a high degree of intracellular organization to coordinate important cellular events. Like their eukaryotic counterparts, they possess cytoskeletal elements and use complex signaling cascades for intra- and intercellular communication.

Despite these huge proceedings, research on prokaryotic cell biology is still focused on a small number of model organisms such as *E. coli*, *B. subtilis*, and *C. crescentus*. As bacteria exist in a variety of different cell shapes and reproduction strategies, the study of the dimorphic budding bacterium *Hyphomonas neptunium* [166] can help to broaden our current knowledge on the organization of bacterial cells.

1.4.1 The cell cycle of *H. neptunium*

The marine α-proteobacterium *H. neptunium* [166] is characterized by a dimorphic lifestyle generating two morphologically and physiologically distinct cell types: a motile swarmer cell and a sessile stalked cell (Fig. 1.6). Additionally, *H. neptunium* features a unique mode of reproduction, whereby the new offspring buds from the tip of a stalk that originates from the mother cell body. Stalks, also known as prosthecae, are thin extensions of the cell envelope and can be mainly found in the class of α-proteobacteria [167].

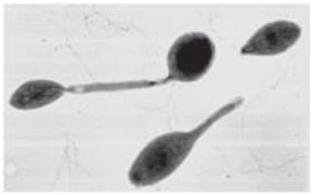

Figure 1.6: Electron micrograph of *H. neptunium*. Shown are a swarmer cell (upper right), a stalked cell (bottom), and a budding cell (upper left). Adapted from [168].

The cell cycle of *H. neptunium* starts at the swarmer stage, in which the cell is motile by means of a single polar flagellum (Fig. 1.7). In order to replicate its chromosome, the swarmer cell has to undergo a transition to a stalked cell. During this differentiation progress, it sheds its flagellum, builds a stalk at the opposite cell pole and produces EPS (extracellular polymeric substance) [169, 170]. After the initiation of DNA replication, a bud emerges at the distal end of the stalk, which necessitates transport of the replicated chromosome and other cellular components through the stalk to the daughter cell. The suggestion that this process occurs via so-called pseudovesicles [171] could not be confirmed by cryo-tomography (A. Briegel, unpublished). At a defined bud size and after a flagellum has been formed at the new pole, the cell undergoes a highly asymmetric division at the junction between the stalk and the bud [169]. This process results in a daughter swarmer cell, which is unable to replicate, and a mother cell that can directly enter a new round of budding.

The process of budding is characterized by local growth and an unequal division. The daughter cells are comprised entirely of newly synthesized cell wall material, whereas the

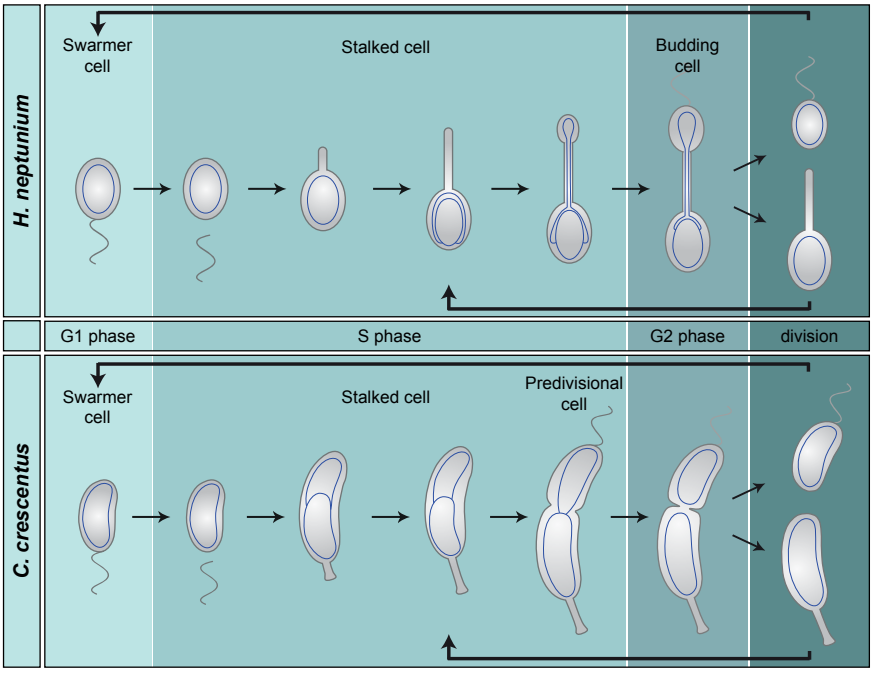

Figure 1.7: The cell cycle of *H. neptunium* and *C. crescentus*. Both species start their cell cycle with a motile swarmer cell, which differentiates into a sessile stalked cell prior to DNA replication. One prominent difference is the mode of poliferation: *H. neptunium* divides by budding whereas *C. crescentus* divides by asymmetric binary fission. See section 1.4 for more information.

mother cell retains its original identity. The propagation by budding is rather unusual in the bacterial phylum since the majority of bacteria rely on binary fission, whereas budding is widely distributed among yeast (e.g. *Saccharomyces cerevisiae*) and other lower eukaryotes (e.g. Porifera spp.). Beside *H. neptunium* and some other species belonging to the α-proteobacteria (*Hirschia*, *Hyphomicrobium*, *Rhodomicrobium* and *Pedomicrobium*), budding can only be found among planctomyces and some cyanobacteria [172–176]. However, the process of budding is closely associated with polar growth, which, in contrast, can be found in many other α-proteobacteria [177].

1.4.2 Characteristic features of *H. neptunium*

H. neptunium was isolated from the harbor of Barcelona (Spain) in 1964 and, based on morphological similarities, originally classified as a member of the genus *Hyphomicrobium* [166]. Later experiments involving DNA-DNA hybridization and metabolic features revealed a closer relationship to the genus *Hyphomonas* [178–180].

According to the current classification based on 16S rRNA gene sequence analysis, *Hyphomonas* belongs to the order *Rhodobacterales* [181]. Interestingly, additional phylogenetic analyses using 23S rRNA sequencing and concatenated protein alignments favor a re-classification to the order *Caulobacterales* [182]. Further support comes from a genome comparison between *H. neptunium* and a well-studied member of the *Caulobacterales*, *C. crescentus*, which indicates a close relationship of the two species [183]. This close relationship becomes equally obvious in terms of their cell cycles, which show many similarities (Fig. 1.7). Both organisms are representatives of the polyphyletic group of dimorphic, prosthecate bacteria (DPBs) [184], which typically have two distinct cell types, one of which has a stalk. Consistent with this close evolutionary relationship, most cell cycle regulators known from *C. crescentus* are conserved in *H. neptunium* [185]. However, there are striking differences between the two organisms with respect to their mode of reproduction and other aspects of their cell biology. *C. crescentus* divides by asymmetric binary fission, whereas *H. neptunium* proliferates by budding and uses the stalk as reproductive structure. The stalk in *H. neptunium* is an integral part of the cell body, whereas the stalk of *C. crescentus* is devoid of DNA and cytoplasmic proteins, compartmentalized by crossbands, and mainly used as an adhesive and, perhaps, nutrient-scavenging structure [186–189]. The position of the stalk is also different, since it is built at the old pole in *C. crescentus* but at the new pole in *H. neptunium*. Unlike *C. crescentus*, *H. neptunium* is a non-saccharolytic organism under laboratory conditions [166, 190], although genes required for glycolysis and pentose phosphate pathway are present in its genome [183]. Instead, *H. neptunium* prefers amino acids as carbon and energy source [178]. Furthermore, it is able to utilize intermediates of the citric acid cycle such as fumarate, malate, and succinate [191].

1.5 Scope

Our knowledge about bacterial cell biology is derived from a small number of model species such as *E. coli*, *B. subtilis*, and *C. crescentus*, which mostly possess a simple symmetric morphology (except *C. crescentus*) and divide by symmetric or asymmetric binary fission. Given the huge diversity in the bacterial phylum with respect to morphologies

and reproduction strategies, it has become obvious that the current research covers only a small area. In particular, the molecular mechanisms underlying alternative reproduction modes such as the formation of multiple offspring or budding are largely unknown. Previously, we have established molecular tools that allow the genetic manipulation of *H. neptunium*, a representative of the stalked budding bacteria [192].

In this work, we aim to broaden the knowledge on bacterial proliferation strategies by analyzing the process of asymmetric growth and division in the budding bacterium *H. neptunium*. In particular, we are interested in the molecular mechanisms involved in divisome assembly and division site positioning and how these fundamental processes are coordinated with other events such as chromosome segregation and cell growth.

2 Results

2.1 Comprehensive localization study of cell division proteins

In order to determine which known cell division proteins are encoded in the *H. neptunium* genome, a bioinformatic analysis using BLAST (*Basic local alignment search tool*) was performed. The protein sequences from the close relative *C. crescentus* were used as a reference. Even though a previous study has already identified part of the cell division proteins [193], the list was extended by the present BLAST analysis, because many new divisome components have been identified in recent years. As shown in table 5.1 (appendix section, p. 95), *H. neptunium* possesses all major cell division proteins, such as FtsZ and FtsA, as well as the proteins typically restricted to α-proteobacteria, such as FzlA and FzlC. Among them, only DipM is absent from the *H. neptunium* genome. Thus, although *H. neptunium* divides by a highly asymmetric budding process and not by binary fission as *C. crescentus*, the involved proteins are conserved. Nevertheless, modifications and differences in the localization patterns of divisome components and in the assembly of the divisome are very likely.

To shed light onto the process of cell division in *H. neptunium*, a broad microscopy-based approach was used to study the subcellular localization of the majority of the cell division proteins. Wherever possible, proteins fused to fluorescent protein tags were endogenously expressed from their native locus as a sole copy. The fusion strategy was guided by previous work in other bacteria such as *C. crescentus* and *E. coli*. However, several problems arose during this approach. For example, the widely used fluorescent protein GFP turned out to be not feasible for fluorescent protein fusions in *H. neptunium*, because of a strong background signal caused by autofluorescence of *H. neptunium* in the corresponding channel. Instead we used YFP and mCherry, but these fluorescent proteins have a weaker fluorescence and are less stable. Furthermore, the localization patterns observed with inducible fusions in *H. neptunium* are not as reliable as in other bacteria, since we realized that some proteins localized differently when the inducible

promoter was replaced by the native one.

In general, the cell cycle-dependent localization of cell division proteins is crucial for successful division, which requires the involved proteins to exhibit a precisely regulated spatiotemporal localization pattern. In *C. crescentus* and other well-studied organisms, this basically means that once the division plane is established by the positioning of FtsZ, the other cell division proteins assemble in a series of functional modules. Nevertheless, there are differences in the hierarchy and content of the factors that arrive at midcell, even in bacteria that divide by binary fission.

The tubulin homolog FtsZ is the key cell division protein providing the structural basis of the division machinery. Since it is an essential protein and C- and N-terminal fluorescent tags generally interfere with its function [194], the fusion protein was expressed from an inducible promoter as an additional copy to the native gene. Time-lapse microscopy revealed that FtsZ-Venus exhibits a dynamic localization pattern (Fig. 2.1 A). In swarmer cells, it localized at the non-flagellated, *i.e.* future stalked pole (Fig. 2.1 A+B) and it remained there during outgrowth of the stalk (Fig. 2.1 A+C). Interestingly, when the bud became visible, a second FtsZ-Venus focus appeared at the junction between the stalk and the bud (the future division site), while the focus at the mother cell pole was still present (Fig. 2.1 A+D). However, this pattern is not as clear to see as the other patterns in the demographs, because stalk length and bud size strongly vary in budding cells. In the majority of cells this dual localization pattern was visible until the cells completed division, suggesting that only the second FtsZ cluster develops into a constriction-competent divisome.

The observed FtsZ localization pattern raised the question whether it is an artifact caused by the use of a non-functional fusion or by the mild overexpression of FtsZ. Therefore, we attempted to verify this localization by various methods (see section 2.4.1). Concurrently, we analyzed the subcellular localization of several proteins that directly associate with FtsZ and thus can serve as reporters to detect the position of FtsZ within the cell.

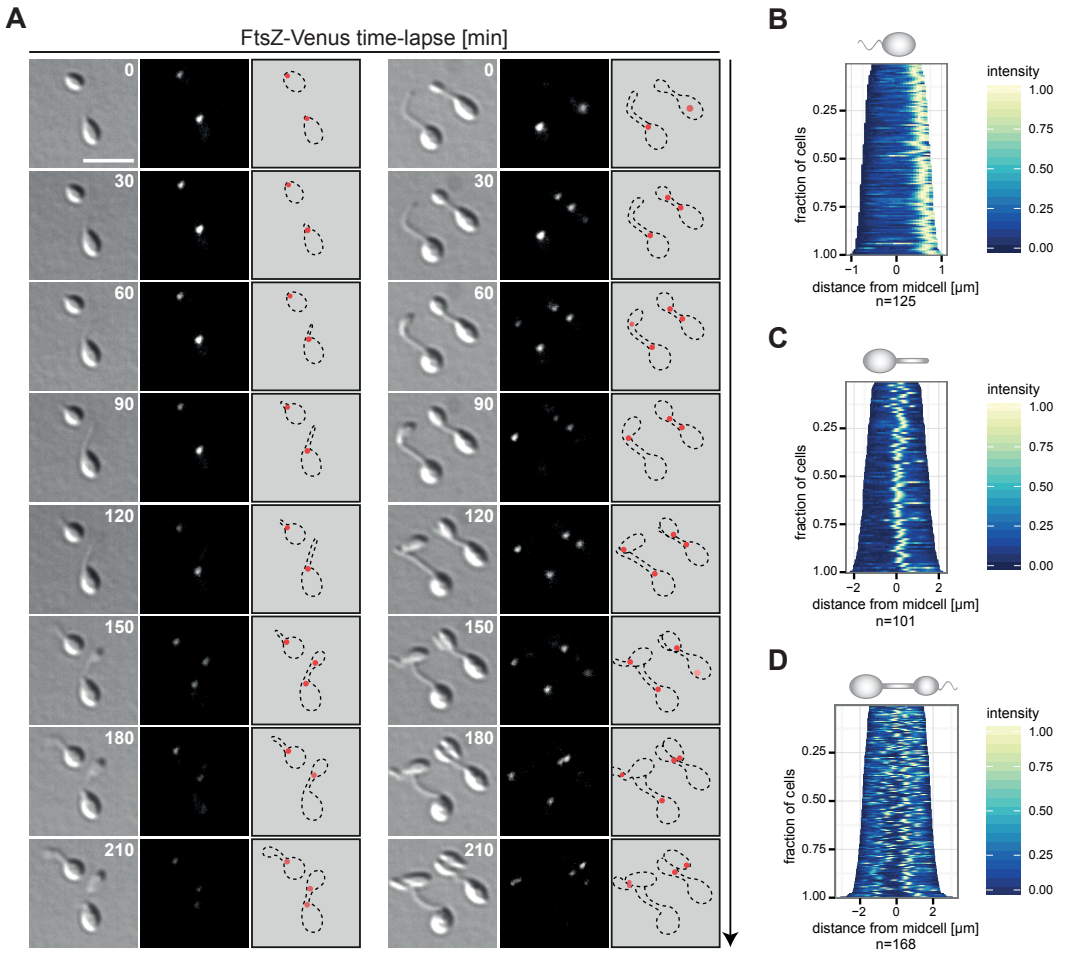

Figure 2.1: Subcellular localization of FtsZ. (A) Cell cycle-dependent localization of FtsZ. Cells of strain SE74 (P_{zn}::P_{zn}-*ftsZ-venus*) were grown in MB to early exponential phase, induced with 0.5 mM $ZnSO_4$ for 2.5 h, and transferred to 1% MB agarose pads. DIC and fluorescence images were taken at the indicated time points while the cells progressed through the cell cycle (scale bar: 3 µm). Since 210 min were not sufficient to observe a complete cell cycle, a second section is shown. **(B-D)** Demographs [195] showing the FtsZ-Venus localization pattern quantitatively in swarmer cells (B), stalked cells (C), and budding cells (D). Cells were analyzed with ImageJ and the corresponding data sets were analyzed with R.

Unfortunately, an inducible version of GFP-ZapA gave no distinct signal, although immunoblot analysis showed that the fusion protein was stably expressed (data not shown). Additionally, the α-proteobacteria-specific proteins FzlA and FzlC, which were shown to interact with FtsZ [41], were examined. In these strains, the native proteins were replaced by N-terminally tagged versions, whose genes were expressed from the corresponding native promoter. The localization pattern observed for Venus-FzlA by time-course microscopy was notably different from the pattern observed for FtsZ-Venus (Fig. 2.2 A). In

swarmer cells, it was either diffuse or formed a distinct focus at one cell pole. In stalked cells a weak focus was observed at the stalked cell pole (similar to FtsZ-Venus). However, in budding cells it localized at the division site and didn't show two foci at any time. In a minor fraction of the cells, Venus-FzlA was diffuse even in budding cells, probably due to weak protein expression levels (data not shown).

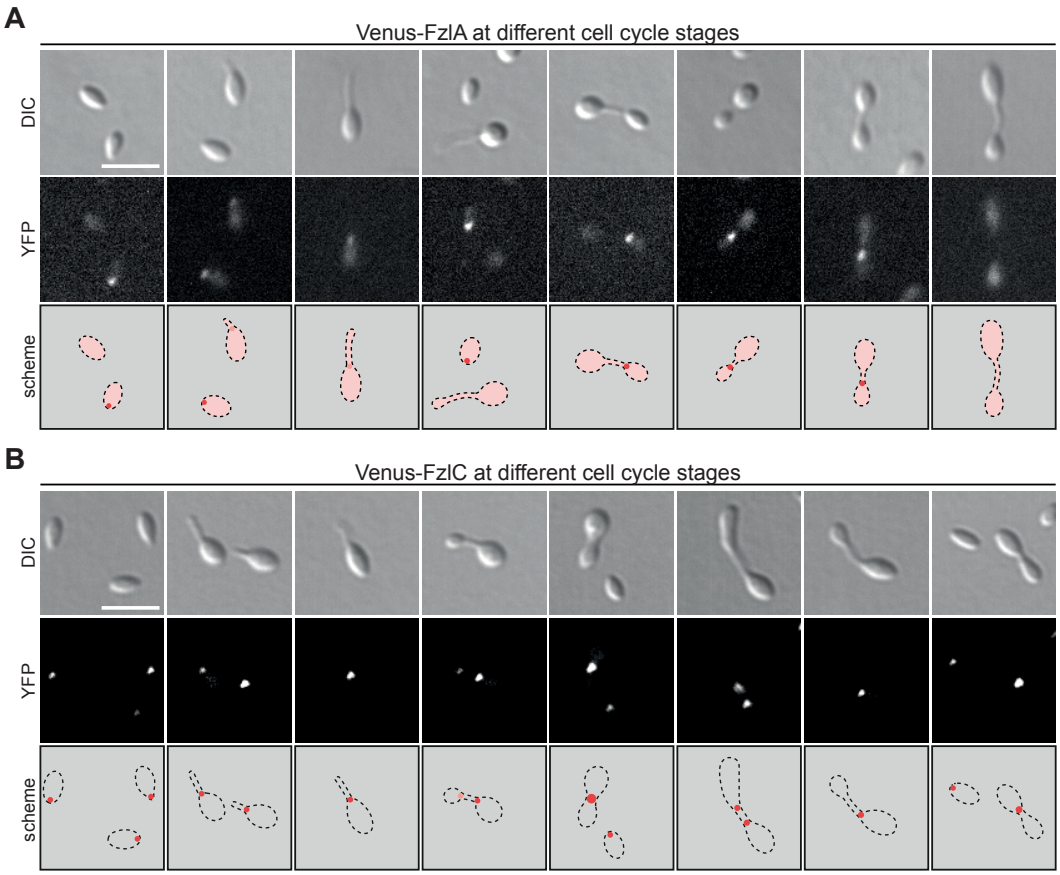

Figure 2.2: Localization of the FtsZ-associated proteins FzlA and FzlC. **(A)** Localization of Venus-FzlA. Cells of strain JZ50 (*fzlA*::*venus-fzlA*) were grown to exponential phase in MB and visualized by DIC and fluorescence microscopy. **(B)** Localization of Venus-FzlC. Cells of strain SE181 (*fzlC*::*venus-fzlC*) were grown to exponential phase in MB and visualized by DIC and fluorescence microscopy (scale bar: 3 µm). Shown are representative cells at different cell cycle stages.

In contrast, the Venus-FzlC localization pattern observed by time-course microscopy resembled the one of FtsZ-Venus (Fig. 2.2 B). At the swarmer cell stage, Venus-FzlC localized at the non-flagellated (= future stalked) pole. In stalked cells, it was observed at the stalked cell pole and in the majority of budding cells additionally at the division site, similar to FtsZ-Venus. Nevertheless, a subset of budding cells had only one focus either

at the mother stalked pole or at the division site. Intriguingly, approximately 40% of budding cells showed an abnormal morphology as reflected by considerably shortened stalks and larger buds, suggesting that the native fusion is only partially functional. This phenotype makes it nearly impossible to distinguish between the mother stalked pole and the division site, resulting in one large Venus-FzlC focus at this restricted area (Fig. 2.2 B).

Next, the actin homolog FtsA, which is involved in membrane attachment of the Z-ring, was analyzed by replacing the native gene with a version encoding an N-terminally tagged protein, expressed from the native promoter. Time-course microscopy could not reveal a clear localization pattern since several bright foci accumulated in an irregular manner in the mother cell body (Fig. 2.3). These might represent inclusion bodies of a non-functional Venus-FtsA protein. Consistent with this assumption, Venus-FtsA accumulated to very high levels in the cell compared to other cell division proteins (data not shown). Furthermore, cells with elongated as well as truncated stalks were observed in the cell culture, suggesting that the function of FtsA was partially impaired by fusion with a fluorescent tag. In *C. crescentus*, the generation of a native FtsA fusion is not possible [30], supporting the notion that a bulky tag has an adverse effect on the function of FtsA.

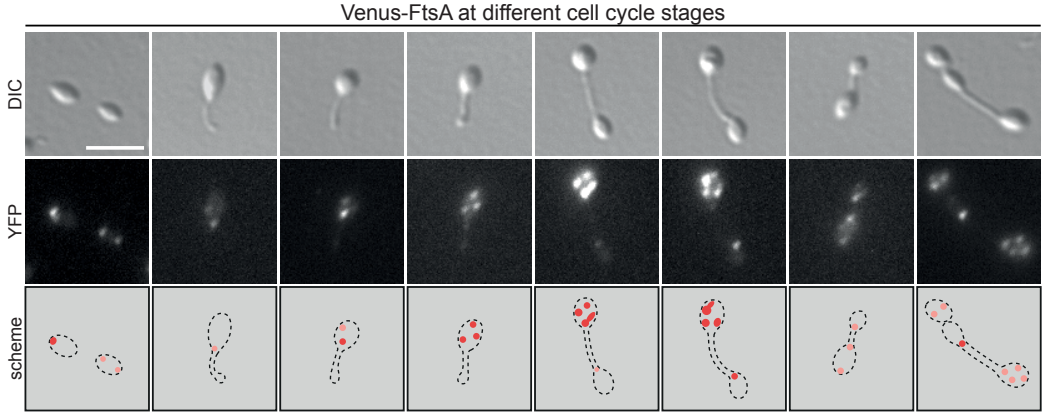

Figure 2.3: Localization of FtsA. Strain JZ49 (*ftsA*::*venus-ftsA*) was grown to exponential phase in MB. Representative cells at different cell cycle stages were visualized by DIC and fluorescence microscopy (scale bar: 3 μm).

In addition to the patchy pattern in the mother cell body, Venus-FtsA localized at the division site in *H. neptunium* budding cells. Accordingly, the cells divided normally, indicating that a portion of Venus-FtsA is functional and can fulfill its putative role during cell division.

In order to visualize the subcellular localization of the FtsEX complex during the *H. neptunium* cell cycle, FtsE was chosen as the representative protein. It is the soluble component of the FtsEX complex, which is implicated in the regulation of cell wall remodeling and, potentially, in Z-ring tethering. The native gene was replaced by a version, encoding an N-terminally tagged protein expressed from the native promoter, but the expression levels (data not shown) and the fluorescence signal were quite low (Fig. 2.4). Before cells started to bud, a weak diffuse signal of Venus-FtsE was observed, which then condensed into a distinct focus at the division site in budding cells.

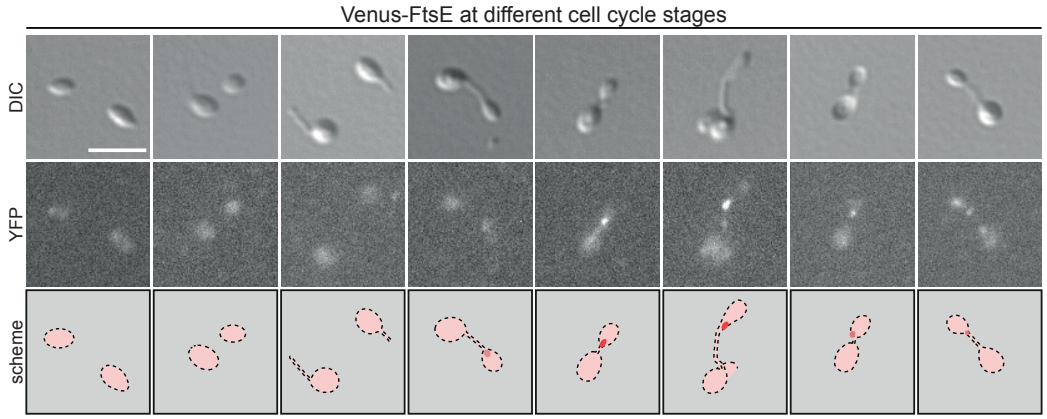

Figure 2.4: Localization of FtsE. Strain JZ29 (*ftsE*::*venus-ftsE*) was grown to exponential phase in MB. Representative cells at different cell cycle stages were visualized by DIC and fluorescence microscopy (scale bar: 3 μm).

For the localization of the bifunctional DNA translocase FtsK, a strain harboring an inducible fusion of FtsK-Venus integrated at the P_{zn} locus was generated, since a previous study revealed that FtsK-Venus expressed from the endogenous promoter could not support normal cell division and cell morphology [193], indicating that this fusion is not fully functional.

Interestingly, the inducible FtsK-Venus fusion localized in a diffuse manner in swarmer

cells but was irregularly distributed in the stalk of stalked and budding cells as observed by time-course microscopy (Fig. 2.5). More precisely, FtsK-Venus appeared to form several distinct clusters occupying the complete stalk structure. This pattern persisted even during cell division, raising the question of whether FtsK is part of the actual divisome (see chapter 2.6 for more experiments on FtsK).

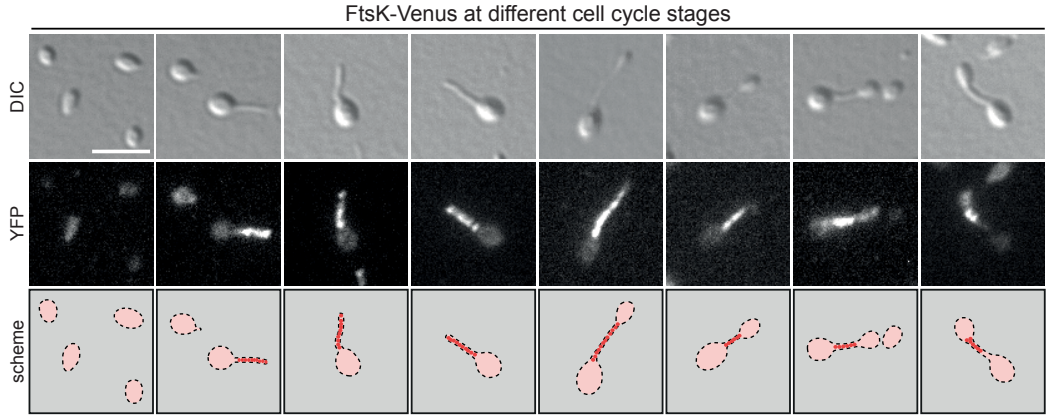

Figure 2.5: Localization of FtsK. Cells of strain SE151 (P_{zn}::P_{zn}-*ftsK-venus*) were grown to early exponential phase in MB, induced with 0.5 mM $ZnSO_4$ for 3.5 h, and visualized by DIC and fluorescence microscopy (scale bar: 3 μm). Shown are representative cells at different cell cycle stages.

Next, the localization of FtsQ as a representative component of the FtsQLB complex, which presumably has a structural or scaffolding function during cell division, was analyzed. In contrast to *C. crescentus*, in which a strain replacing the endogenous *ftsQ* with a fluorescently tagged version could not be generated [30], we were able to generate such a strain in *H. neptunium*. Despite the relatively weak signal, FtsQ-mCherry exhibited a diffuse distribution in the membrane in stalked and budding cells (Fig. 2.6). However, at the swarmer stage, the small size of the cells did not allow us to distinguish between a diffuse periplasmic or cytoplasmic pattern, respectively. Interestingly though, at a late stage of the cell cycle, a weak focus of FtsQ-mCherry was visible either at the division site, at the stalked pole of the mother cell, or at both locations (as FtsZ).

At the late stages of divisome assembly, several proteins involved in PG synthesis and remodeling are recruited to the division site. Out of these, we selected the main division-specific PG synthase FtsI (PBP3), the putative lipid II precursor flippase FtsW, and the PG-binding protein FtsN as representatives of this group.

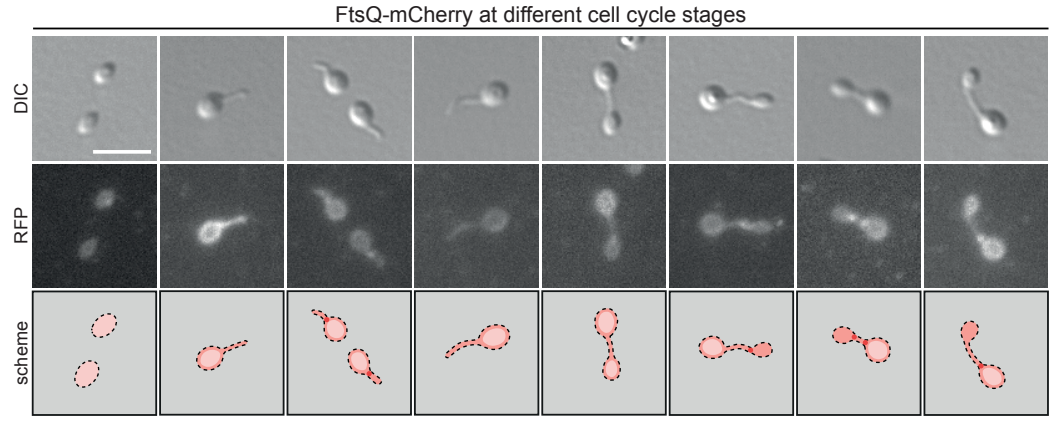

Figure 2.6: Localization of FtsQ. Strain JZ28 (*ftsQ*::*ftsQ-mCherry*) was grown to exponential phase in MB. Representative cells at different cell cycle stages were visualized by DIC and fluorescence microscopy (scale bar: 3 μm).

The Venus-FtsI fusion protein expressed from the native promoter was shown to localize either in a diffuse manner or at one cell pole in swarmer cells (Fig. 2.7). In stalked cells the signal was mostly diffuse, whereas a bright focus appeared at the division site of budding cells, consistent with a role of FtsI in septum synthesis [196].

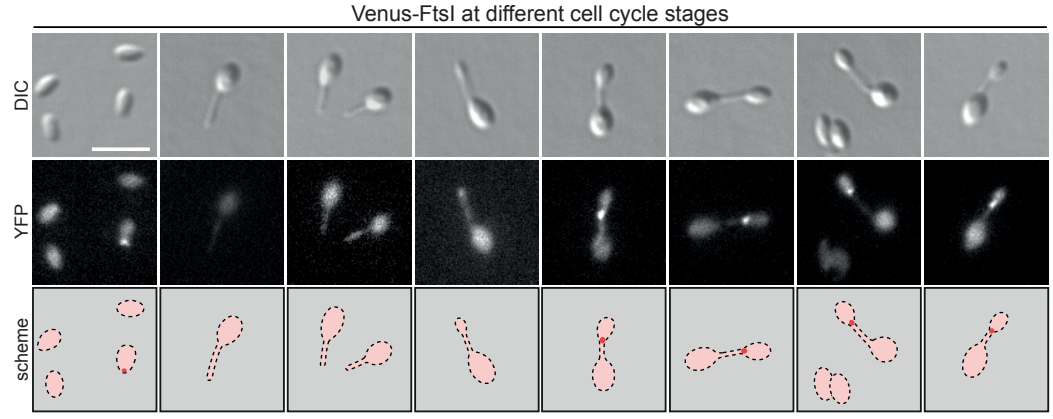

Figure 2.7: Localization of FtsI (PBP3). Strain SE161 (*ftsI*::*venus-ftsI*) was grown to exponential phase in MB and cells representing different cell cycle stages were visualized by DIC and fluorescence microscopy (scale bar: 3 μm).

To localize FtsW, the native gene was replaced by a version, encoding an N-terminally tagged fluorescent fusion, expressed from the endogenous promoter. Time-course microscopy revealed that Venus-FtsW forms a polar focus in swarmer cells, while, in stalked cells, it localized at the stalked cell pole, with a second weak focus often emerging at the

end of the stalk (Fig. 2.8). However, in budding cells, the localization pattern was not that uniform. As expected, there were cells with a distinct focus at the division site, sometimes accompanied by a faint focus at the stalked pole of the mother cell. In a comparable number of cells, Venus-FtsW was absent from the division site and only visible at the stalked pole of the mother cell.

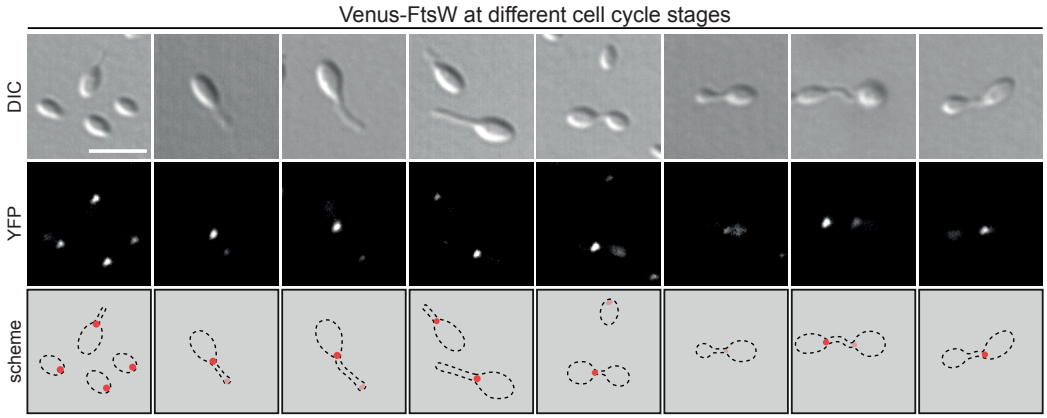

Figure 2.8: Localization of FtsW. Strain JZ51 (*ftsW*::*venus-ftsW*) was grown to exponential phase in MB. Representative cells at different cell cycle stages were visualized by DIC and fluorescence microscopy (scale bar: 3 μm).

At last, the late cell division protein FtsN was examined. Time-course microscopy of a fluorescent fusion, expressed from the native promoter, showed that FtsN localized polarly in swarmer cells, but largely lost its localization during the stalked cell stage (Fig. 2.9). A few stalked cells, however, exhibited a weak focus at the tip of the stalk. Finally, in budding cells featuring a comparable large bud, Venus-FtsN strongly accumulated at the division site, as expected for a late divisome component.

We also attempted to localize TolQ, a member of the Tol-Pal complex, which is involved in membrane invagination [65]. Cells harboring a zinc-inducible Venus-TolQ fusion did not show any distinct localization but only a weak diffuse signal, although the fusion protein was stably expressed (data not shown).

In summary, out of the tested 12 predicted cell division proteins in *H. neptunium*, nine proteins localized as expected at the division site at the junction between the stalk and the bud. The proteins ZapA (SE38) and TolQ (JZ13) did not show any obvious localization pattern (data not shown). Furthermore, the majority of these proteins exhibited a

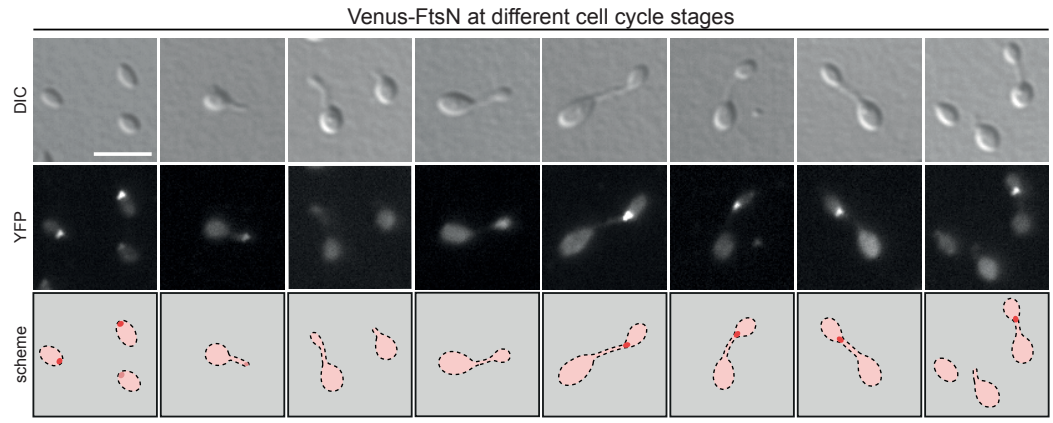

Figure 2.9: Localization of FtsN. Strain SE203 (*ftsN*::*venus-ftsN*) was grown to exponential phase in MB, and cells representing different cell cycle stages were visualized by DIC and fluorescence microscopy (scale bar: 3 μm).

dynamic localization pattern with seven proteins starting the cell cycle at the cell pole (FtsZ, FzlA, FzlC, FtsA, FtsI, FtsW and FtsN). This is mostly the non-flagellated (=new) pole as confirmed by time-lapse microscopy (data not shown). During stalk growth, most division proteins remained at this cell pole. Only FtsI seemed to become diffuse and FtsN had the tendency to localize at the tip of the stalk, albeit with a weak signal. Interestingly, when Venus-FtsN was expressed from an inducible promoter, and thus at elevated levels, the localization at the tip of the stalk was more pronounced (data not shown). During the budding process, however, the proteins switched their position and relocated to the division site, no matter whether they were diffuse or polarly localized before and then remained there until the cells divided. The proteins FtsZ, FzlC and occasionally FtsQ accumulate additionally at the stalked pole. One prominent exception from this scheme is the dynamic localization behavior of FtsK. After being diffuse in swarmer cells, it stably localized within the entire stalk and maintained this localization pattern until cell division was completed.

2.2 The growth pattern of *H. neptunium*

In order to correlate the localization patterns observed for the different divisome components to cell growth and to analyze cell division in more detail, we needed to clarify

how exactly *H. neptunium* grows at different stages of the cell cycle. For that reason, we stained wild type cells with 7-hydroxycoumarin-carbonyl(HCC)-amino-D-alanine (HADA), a fluorescent D-amino acid, which labels the sites of active PG incorporation [197]. In *H. neptunium* wild type cells, we could observe that the growth mode switches between dispersed and zonal as cells progressed through the cell cycle (Fig. 2.10 A). More precisely, swarmer cells showed a dispersed PG incorporation pattern. However, when stalk growth initiated, a distinct focus became visible at the stalked pole, indicating that the stalk grows from its base by a polar mode of growth. At a certain time during the cell cycle, PG incorporation switches from the stalked pole to the tip of the stalk, where the bud is then generated. During bud growth, a diffuse signal is detectable within the complete bud, which again implies a dispersed growth mode. Finally, PG incorporation takes place at the division site, *i.e.* the junction between the bud and the stalk, reflecting formation of the septum. Thus, the dynamic pattern of the active growth sites correlates with the dynamic localization of FtsZ and other cell division proteins. At the stalk base, several cell division proteins accumulated simultaneously to active PG incorporation. And, as expected, cell division proteins colocalized with the site of PG incorporation at the division site. In conclusion, the sites of zonal growth of *H. neptunium* coincide with the local accumulation of cell division proteins, whereas most cell division proteins do not necessarily colocalize with the sites of dispersed growth.

Cryo-electron tomograms of wild type cells illustrate the different cell cycle stages at a higher resolution (Fig. 2.10 B-D). These images revealed that the stalk is indeed a continuous structure without any visible barriers, emanating from the mother cell body (Fig. 2.10 B+D) and it is not devoid of DNA or ribosomes (Fig. 2.10 C) like the stalk of *C. crescentus* [186, 189]. Interestingly, the cryo-electron image of a “mature” bud (with attached flagellum) (Fig. 2.10 D) shows ongoing constriction at the division site, which cannot be visualized by DIC microscopy due to the limited resolution of this technique.

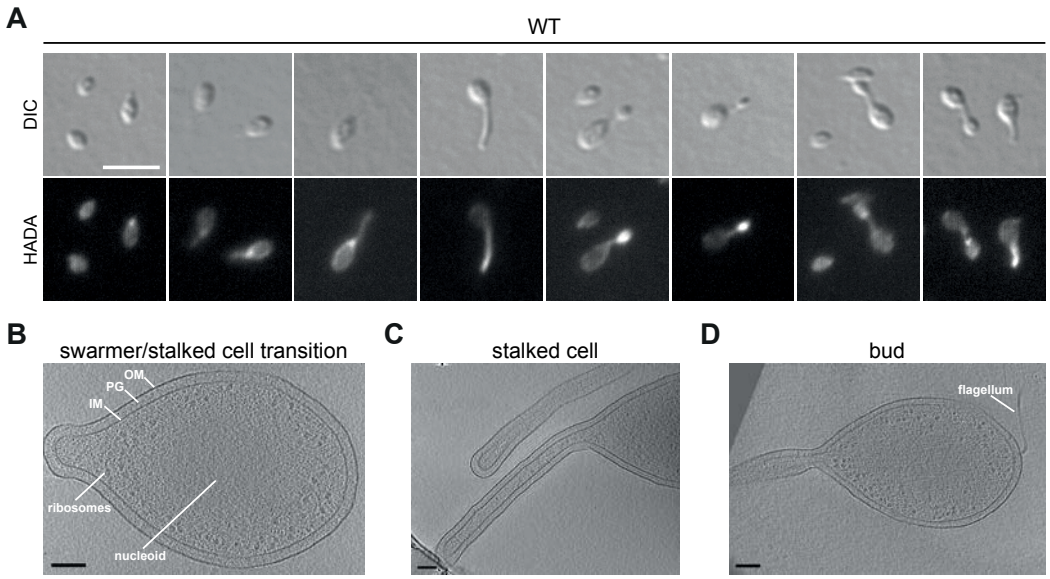

Figure 2.10: Growth of *H. neptunium* wild type. (A) Active PG incorporation. Wild type cells were grown to exponential phase in MB, incubated with 0.5 mM HADA for 9 min, fixed with 70% EtOH, washed, and imaged by DIC and fluorescence microscopy (scale bar: 3 μm). **(B-D)** Cryo-electron tomograms of wild type cells at different cell cycle stages (scale bar: 100 nm). Images were taken by Yi-Wei Chang (California Institute of Technology).

2.3 Regulation of division site placement

Identification of the correct site for cell division is crucial and thus tightly regulated, since an inaccurate positioning of the divisome would have severe consequences such as the formation of anucleated minicells. Most studied bacteria determine precisely their division site, although bacteria exist, which divide with less precision [198, 199].

From the common regulatory systems mentioned in the introduction (see section 1.2) *H. neptunium* possesses only a homolog of MipZ, based on BLAST analysis (table 5.1, p. 95). Homologs of the Min system, nucleoid occlusion, PomZ, SsgB and MapZ/LocZ could not be identified.

2.3.1 MipZ is not required for proper Z-ring positioning

The ParA-like protein MipZ is responsible for Z-ring positioning in *C. crescentus* and essential for viability in this organism. Depletion of MipZ leads to minicell formation and

a significant increase in the average cell length [115]. Since the *H. neptunium* genome encodes a MipZ homolog, we were wondering whether it is required for correct division site placement. Therefore, a strain harboring a deletion of *mipZ* was generated. Surprisingly, we were able to obtain a deletion strain, revealing that MipZ is not essential in *H. neptunium*. Furthermore, phenotypic characterization of Δ*mipZ* cells showed that they exhibited wild type morphology (Fig. 2.11 A) with no hint of irregular division patterns. To rule out a less obvious effect, the lengths of cells in a mixed population (Fig. 2.11 B) were quantified. Usually, viable *H. neptunium* mutants generate normal-looking swarmer cells, irrespective of the severity of their morphological defects at later cell cycle stages. To increase the sensitivity of the analysis, we further quantified specifically the lengths of budding cells to detect minor cell shape defects (Fig. 2.11 C)

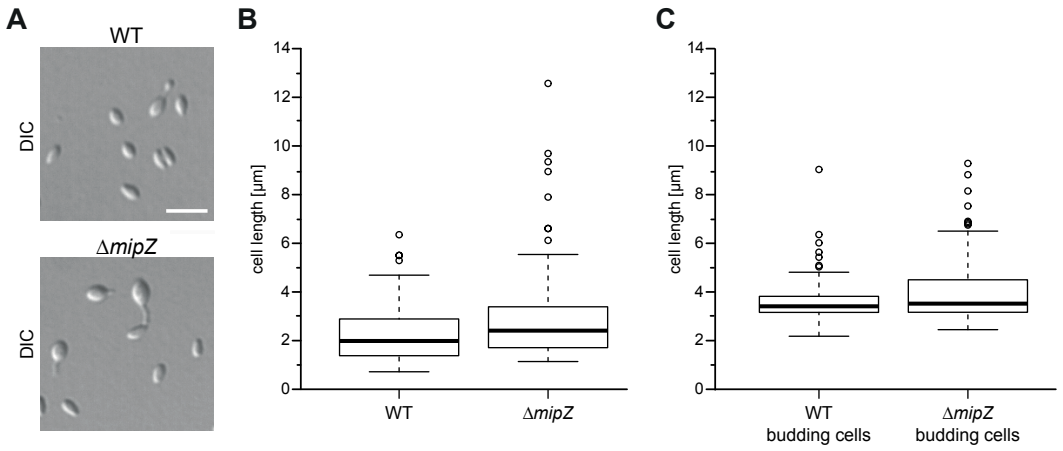

Figure 2.11: Phenotypic analysis of Δ*mipZ* cells. (A) DIC images of exponentially growing wild type (ATCC15444) and Δ*mipZ* (SE124) cells (scale bar: 3 µm). **(B)** Quantification of the cell lengths of cells described in (A). DIC images of exponentially growing mixed cultures of both strains were used to measure the cell length (n= 198 for WT cells and n=185 for Δ*mipZ* cells). Data sets were displayed in box-whisker-plots. Shown are the interquartile range (box), the median (line), the 5th and 95th percentile (whiskers), and outliers (circles). **(C)** Quantification of the budding subpopulation of wild type and Δ*mipZ* cells. Same approach as in (B). The total of 105 and 131 cells, respectively, were measured.

Apart from an increased number of outliers, no significant difference could be observed in the mixed population (Fig. 2.11 B). Similar results were obtained for the budding subpopulation (Fig. 2.11 C). These results are contradictory to a previous study [200], in which a dramatic increase in cell length of budding cells lacking MipZ was reported. However, this previous study included considerably fewer cells for quantification [200].

To further investigate the effect resulting from a loss of MipZ, the localization pattern of FtsZ in the wild type background and in Δ*mipZ* cells were compared (Fig. 2.12 A). From the data obtained by DIC and fluorescence microscopy, no alteration in FtsZ localization was observeable (Fig. 2.12 A and Fig. 2.1), matching the results from the phenotypic analysis and indicating that MipZ is not a critical determinant for division site placement in *H. neptunium*. Based on these results, we were wondering whether MipZ might be part of a redundant system or has no role in Z-ring positioning at all. In *C. crescentus*, the expression of an ATPase-deficient variant of MipZ, $MipZ_{D42A}$, has a dominant negative effect and blocks cell division throughout the entire cell, similar to MipZ overexpression [115]. However, since FtsZ does usually not assemble over the nucleoid in *H. neptunium*, we expected a milder phenotype than in *C. crescentus* when expressing the corresponding mutant.

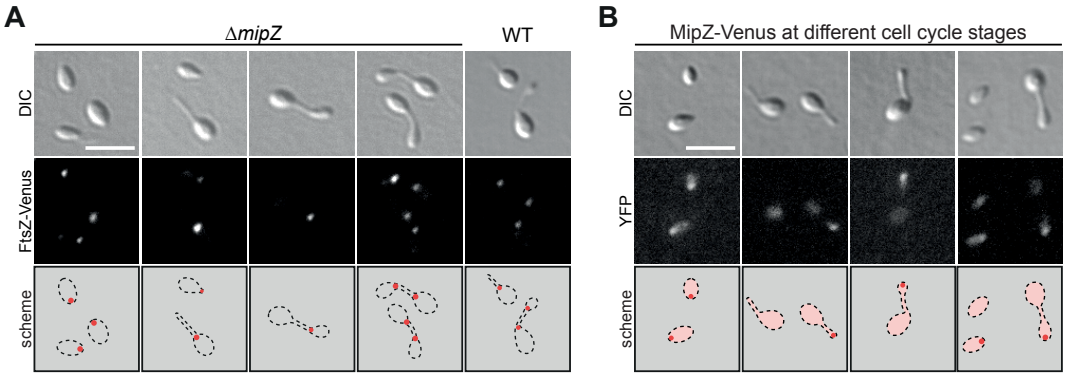

Figure 2.12: Localization of FtsZ in the absence of MipZ and localization of MipZ. (A) Time-course microscopy of FtsZ-Venus in Δ*mipZ* cells. Strain SE113 (Δ*mipZ* P_{zn}::P_{zn}-*ftsZ-venus*) and SE74 (P_{zn}::P_{zn}-*ftsZ-venus*) as control were grown to early exponential phase in MB, induced with 0.5 mM $ZnSO_4$ for 3 h, and visualized by DIC and fluorescence microscopy (scale bar: 3 μm). **(B)** Time-course microscopy of MipZ-Venus. Strain SE106 (P_{zn}::P_{zn}-*mipZ-venus*) was grown to early exponential phase in MB, induced with 0.5 mM $ZnSO_4$ for 5 h, and visualized by DIC and fluorescence microscopy (scale bar: 3 μm). Representative cells are shown.

In general, the MipZ homologs from *C. crescentus* and *H. neptunium* share 50% sequence identity, including the conserved residues of the Walker A and Walker B motifs and a conserved aspartate in the N-terminal ATPase domain (Fig. 2.13 A). A strain expressing the $MipZ_{D62A}$ variant, which is equivalent to the *C. crescentus* $MipZ_{D42A}$ mutant, from an inducible promoter as sole copy of MipZ, did not show any phenotypic aberrations (Fig. 2.13 B). Cells grew at the wild type rate (data not shown), had wild type morphology, and divided normally (Fig. 2.13 B). A quantification of cell lengths revealed no significant variance between the induced and wild type sample (Fig. 2.13 C). The slight increase in cell lengths after 20 h of induction can probably be attributed to the effect of $ZnSO_4$. Taken together, these observations suggest that the MipZ homolog from *H. neptunium* has no or only a redundant role in division site placement under standard laboratory conditions. Thus, another mechanism appears to be responsible for accurate Z-ring positioning.

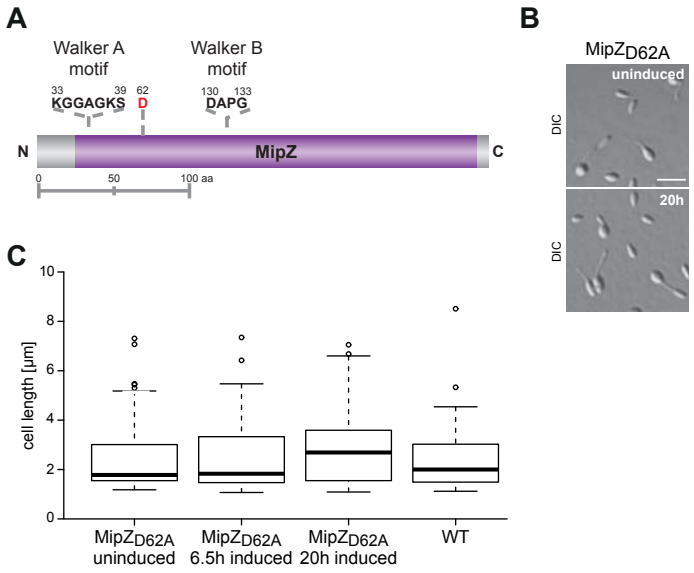

Figure 2.13: Characterization of a putative ATPase-deficient MipZ variant. (A) Schematic representation of the conserved residues in the ATPase domain of $MipZ_{HNE}$. All known conserved residues of $MipZ_{CC}$ are present in $MipZ_{HNE}$. Highlighted in red is the conserved aspartate, which was mutated. **(B)** DIC images of exponentially growing cells of strain SE170 (Δ*mipZ* P_{zn}::P_{zn}-$mipZ_{D62A}$) before and after induction with 0.5 mM $ZnSO_4$ for 20 h (scale bar: 3 µm). **(C)** Quantification of the cell length of wild type and strain SE170 (Δ*mipZ* P_{zn}::P_{zn}-$mipZ_{D62A}$) before and after induction with 0.5 mM $ZnSO_4$ for 6.5 h and 20 h, respectively. DIC images obtained as described in (B) were used to measure the cell lengths. A total of 182, 221, 270 and 168 cells, respectively, were analyzed. Data sets were displayed in box-whisker-plots. Shown are the interquartile range (box), the median (line), the 5^{th} and 95^{th} percentile (whiskers), and outliers (circles).

Consistent with the non-conserved role of MipZ in *H. neptunium*, the localization pattern of an inducible MipZ-Venus fusion differs strongly from the one of *C. crescentus* MipZ. Instead of a bipolar localization, MipZ-Venus in *H. neptunium* localized either at the flagellated pole in swarmer cells or at the bud pole opposite of the stalk in budding cells (Fig. 2.12 B), as reported previously [200]. This again suggests no conserved function of the MipZ homolog of *H. neptunium*.

2.3.2 What else could regulate Z-ring positioning?

After having excluded MipZ as the main division site regulator, we examined the influence of other candidate regulators on FtsZ localization. To that end, an inducible FtsZ-Venus fusion was expressed in different deletion backgrounds.

The first candidates we examined were the bactofilin homologs of *H. neptunium*. Bactofilins are a class of bacteria-specific cytoskeletal elements implicated in various functions. In *M. xanthus*, for instance, they are involved in cell morphology and DNA segregation, whereas in *C. crescentus* they contribute to stalk biogenesis [201–203]. *H. neptunium* possesses two bactofilin homologs, BacA and BacB, whose localization patterns are reminiscent of the one of FtsZ (E. Cserti, unpublished). For that reason, the question arose whether the localization of FtsZ depends on the bactofilins. It was shown before that deletion of *bacAB* has a tremendous effect on cell morphology, leading to amorphous and deformed stalked and budding cells (E. Cserti, unpublished). However, the localization of FtsZ-Venus was not dramatically altered in the absence of BacAB (Fig. 2.14 A). FtsZ-Venus still accumulated in discrete foci and localized polarly in swarmer cells and predominantly to the stalked pole or some junction between the stalk and bud in amorphous cells. However, in cells that were completely amorphous, the localization of FtsZ-Venus could not be correlated to its typical pattern, but the protein still formed foci. Altogether, these results suggest that bactofilins have no role in positioning of the division site.

The next candidate we investigated was the orphan ParA-homolog HNE_0708. A previous study revealed that deletion of *HNE_0708* resulted in cells with elongated stalks, deformed

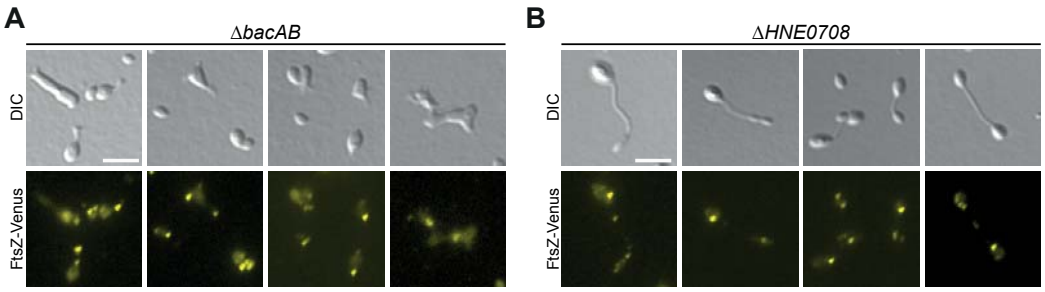

Figure 2.14: Localization of FtsZ in different deletion backgrounds. **(A)** Double deletion of bactofilin homologs BacA and BacB. Strain SE174 (Δ*bacAB* P_{zn}::P_{zn}-*ftsZ-venus*) was grown to exponential phase in MB, induced with 0.5 mM $ZnSO_4$ for 3 h, and visualized by DIC and fluorescence microscopy (scale bar: 3 μm). **(B)** Deletion of the ParA-homolog HNE_0708. Strain SE158 (Δ*HNE_0708* P_{zn}::P_{zn}-*ftsZ-venus*) was treated equally to strain SE174 in (A).

buds, and trapped DNA within the stalk [200]. Furthermore, up to five ParB-YFP foci accumulated in these cells, suggesting a disturbed initiation of replication and/or DNA segregation when HNE_0708 is absent [200]. Regarding cell division, it was shown that a fraction of HNE_0708-deficient cells was not able to divide correctly [200]. Therefore, the localization of FtsZ-Venus was monitored in this genetic background. Interestingly, FtsZ-Venus did not show an altered localization pattern, since cells exhibited discrete foci at the stalked pole and at the junction between the bud and the stalk, as described previously (Fig. 2.1). The fact that no major role could be attributed to HNE_0708 in division site placement is consistent with the absence of a growth defect in HNE_0708-deficient cells [200]. However, a subset of cells with a drastically altered morphology exhibited misplaced FtsZ-Venus foci, even though many cells were able to divide at the correct position. However, the observation of aberrant foci is probably a secondary effect that derives from impaired chromosome replication or segregation and not a direct effect on divisome positioning.

2.4 FtsZ - the key protein of cell division

The studies performed so far indicate that FtsZ in *H. neptunium* shows a behavior quite different from that in the established model organisms and especially in its close relative

C. crescentus. For this reason, we decided to analyze the core divisome component FtsZ in more detail.

The localization pattern observed for FtsZ-Venus (Fig. 2.1) raised the question of whether the polar signal in swarmer cells is a remnant of the last cell division or whether FtsZ is synthesized *de novo* and localized at this position. To clarify this issue, we determined the abundance of FtsZ over the course of the cell cycle using a synchronized wild type population. Immunoblot analysis demonstrated that FtsZ is produced constitutively (Fig. 2.15), unlike FtsZ from *C. crescentus*, which is absent from swarmer cells [204]. Thus, relocalization of FtsZ to the division site is a dynamic process using existing FtsZ molecules, since the expression levels of FtsZ do not change.

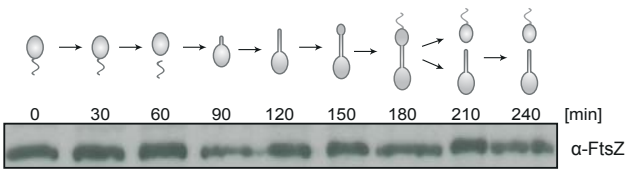

Figure 2.15: Cell cycle-dependent abundance of FtsZ. Isolated swarmer cells of a synchronized wild type culture were grown in MB for 4 h. At the indicated time points, cells were withdrawn and analyzed by immunoblotting using α-FtsZ antibodies. The schematic above illustrates the cell cycle of *H. neptunium*.

2.4.1 Verification of the FtsZ localization pattern

The study of an inducible FtsZ-Venus fusion revealed an unusual localization pattern at both ends of the stalk, in contrast to the expected localization only at the division site. To exclude the possibility that the additional cluster is an artifact caused by the use of a C-terminally tagged fusion protein, we performed immunofluorescence microscopy and immunogold staining on wild type cells. Unfortunately, both approaches were unsuccessful due to *H. neptunium*'s sensitivity to the harsh fixation conditions and non-specific background signals (data not shown). In *E. coli*, it was reported that the insertion of a fluorescent protein within a loop in the tubulin-like domain (between G55 and Q56) results in a fully functional FtsZ protein (H. Erickson, unpublished). Thus, we generated a similar FtsZ-sandwich fusion (FtsZSW) in *H. neptunium* by inserting

Venus at the respective position (after E51) (Fig. 2.16 A+B). Fluorescence microscopy revealed that the FtsZ-sandwich fusion, expressed from the zinc-inducible promoter, localized in the same manner as the C-terminal fusion did (Fig. 2.16 C). Although it was not possible to obtain a strain bearing the sandwich fusion as the sole copy of FtsZ, it is a strong indication that the unusual localization pattern is correct and is not an artifact of the C-terminal fusion.

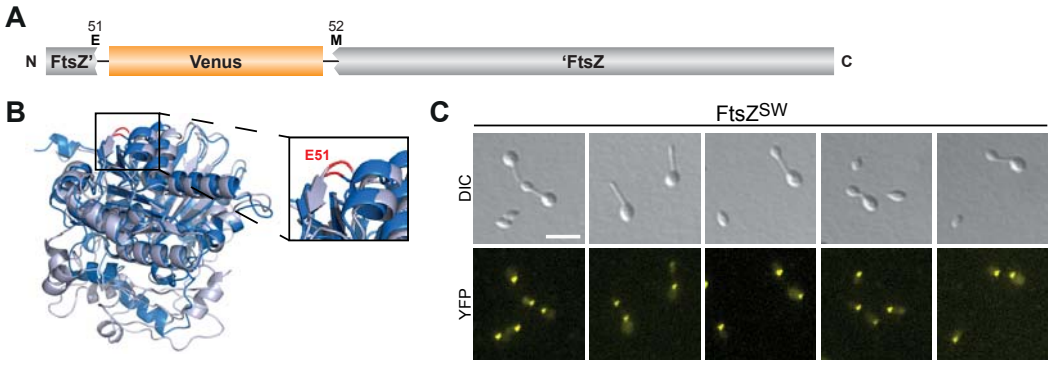

Figure 2.16: FtsZ-sandwich fusion (FtsZSW). (A) Schematic of the FtsZ-sandwich fusion protein. The position of the insertion of Venus and the corresponding residues are indicated. **(B)** Predicted structure of FtsZ proteins with inlet showing residue after which Venus was inserted in red. FtsZ from *H. neptunium* is depicted in grey and FtsZ from *E. coli* in blue. Structural models were generated using I-TASSER [205]. **(C)** Localization of an FtsZ sandwich fusion. Strain SE157 (P_{zn}::P_{zn}-*ftsZ'-venus-'ftsZ*) was grown to exponential phase in MB, induced with 0.5 mM $ZnSO_4$ for 2 h, and visualized by DIC and fluorescence microscopy (scale bar: 3 µm).

2.4.2 Effects of a loss of FtsZ

Due to its central role in cell division, FtsZ is an essential protein in almost all bacteria studied so far, therefore we assumed that this is also the case for *H. neptunium*. In order to examine the effect of FtsZ elimination, we generated a conditional mutant, in which a single ectopic copy of *ftsZ* was placed under control of the zinc-inducible promoter, while the native gene was deleted. When cells were grown in the presence of zinc, they exhibited a wild type phenotype (Fig. 2.17 A, 0h). However, depletion of FtsZ had dramatic effects on the cells. Initially, after around six hours of growth without zinc, the cells elongated their stalks (Fig. 2.17 A). After nine hours, cells started to develop a chaining phenotype and cell bodies became misshapen. Once FtsZ was completely depleted from the cells (Fig. 2.17 C, >9h), the chaining phenotype became more and

more pronounced. Additionally, several, partially branched stalks and a polarity defect, recognizable by stalks emanating from both poles of a cell body, could be observed. This confirms that FtsZ is essential for cell division in *H. neptunium*. Interestingly, cells lacking FtsZ could reach enormous cell lengths of up to 90 µm after 22h and were, on average, eight times longer than wild type cells (Fig. 2.17 B). Along with the chaining phenotype, this suggests that stalk elongation and bud formation are still occurring in the absence of FtsZ.

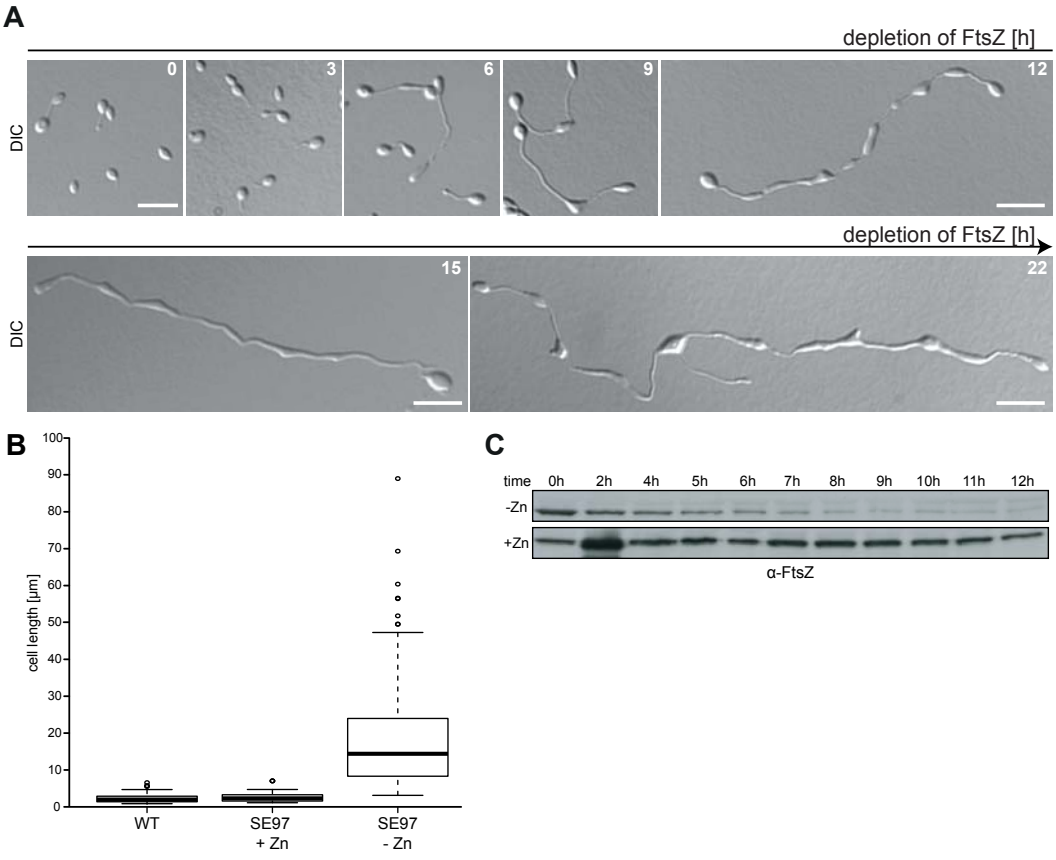

Figure 2.17: Effect of FtsZ depletion. (A) Chaining phenotype and elongated stalks induced by the lack of FtsZ. Cells of strain SE97 (Δ*ftsZ* P_{zn}::P_{zn}-*ftsZ*) were grown to exponential phase in MB supplemented with 0.5 mM $ZnSO_4$, washed twice, and resuspended in medium without $ZnSO_4$. At the indicated time points, cells were withdrawn and imaged by DIC microscopy (scale bar: 5 µm). **(B)** Quantification of cell lengths of SE97, before and after 22 h depletion, and of wild type cells. A total of 198, 201 and 155 cells, respectively were measured using Metamorph. Data sets are displayed in box-whisker plots. Shown are the interquartile range (box), the median (line), the 5^{th} and 95^{th} percentile (whiskers), and outliers (circles). **(C)** Protein level during FtsZ depletion. Immunoblot analysis of the samples described in (A) and of a control culture grown in the presence of $ZnSO_4$.

Given this chaining phenotype, we wondered at which positions growth is achieved in these cells compared to the pattern observed previously for the wild type strain (Fig. 2.10 A).

The conditional mutant of FtsZ exhibited the same morphology and growth zones as wild type cells, as long as FtsZ was present (Fig. 2.18 A, 0h). Interestingly, when FtsZ was depleted for 7.5 h and morphological defects became obvious, the insertion of PG became aberrant (Fig. 2.18 A, 7.5h). On the one hand, PG was inserted in several distinct areas within the cell body, leading to misshaped cells. On the other hand, we could observe that cell bodies between the two terminal compartments were extensively labeled, suggesting that new cells are formed within and not at the end of these cell chains. Furthermore, in several cases PG was incorporated actively into the stalk, consistent with the pronounced stalk elongation that occurs after FtsZ depletion. In cells, which were depleted of FtsZ for a longer time (Fig. 2.18 A, 15h), PG incorporation was mostly dispersed along the complete cell chain, although some local growth was observed, e.g. at a new cell compartment. The interesting observation that the cell chaining originates in between the mother cell and their bud was further confirmed by time-lapse microscopy. Tracking the cells in a

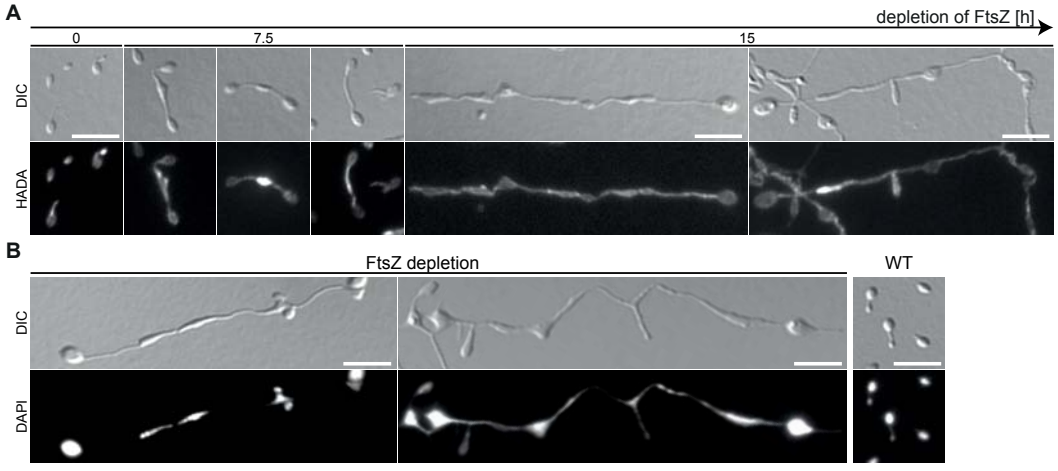

Figure 2.18: Characterization of the FtsZ depletion phenotype. **(A)** PG incorporation in FtsZ-deficient cells. Cells of SE97 (Δ*ftsZ* P_{zn}::P_{zn}-*ftsZ*) were grown to exponential phase in MB supplemented with 0.5 mM $ZnSO_4$, washed twice, and resuspended in medium without $ZnSO_4$. At the indicated time points, cells were withdrawn, incubated with 0.5 mM HADA for 9 min, fixed with 70% EtOH, washed and imaged by DIC and fluorescence microscopy (scale bar: 5 μm). **(B)** FtsZ-deficient cells accumulate chromosomes. Cells of strain SE97 (Δ*ftsZ* P_{zn}::P_{zn}-*ftsZ*), depleted of FtsZ for 22 h, and cells of the wild type grown to exponential phase were stained with DAPI and visualized by DIC and fluorescence microscopy (scale bar: 5 μm).

microfluidic device during depletion of FtsZ clearly showed that new cell compartments are formed by widening of the stalk about halfway between the mother and daughter cell compartment (Fig. 2.19). In some cases, they appear to emerge at random positions in the stalk and in other cases in direct proximity of an existing cell, before they are relocated by the outgrowth of an additional stalk. However, it remains unclear whether the aberrant growth behavior is a direct effect of a loss of FtsZ or an indirect effect caused by a general block in essential pathways of the cell.

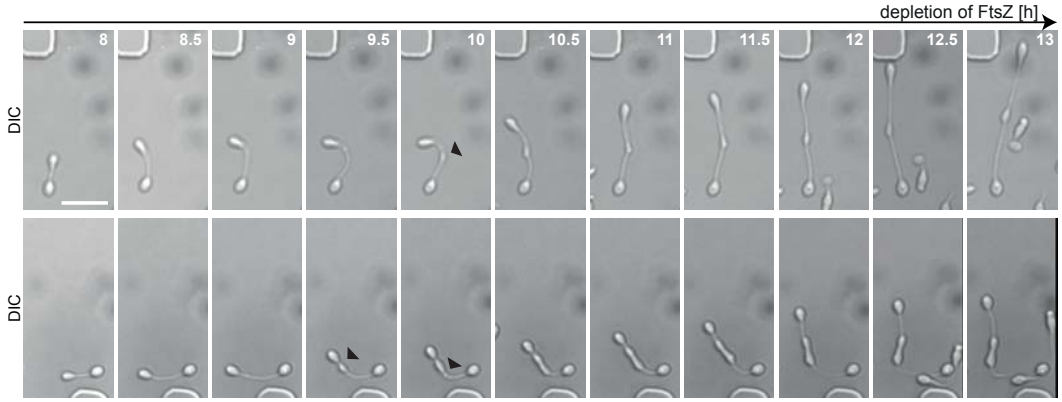

Figure 2.19: New cell bodies are formed in-between existing cell compartments in FtsZ-deficient cells. Time-lapse microscopy showing arising morphological defects during FtsZ depletion. Cells of strain SE97 (Δ*ftsZ* P_{zn}::P_{zn}-*ftsZ*) were grown to exponential phase in MB supplemented with 0.5 mM $ZnSO_4$, washed twice, and resuspended in medium without $ZnSO_4$. After 6 h of depletion, cells were transferred to a microfluidic device and tracked by DIC microscopy in 30 min intervals. Shown are two representative cells between 8 h and 13 h of FtsZ depletion. Triangles highlight nascent cell compartments (scale bar: 5 μm).

Next, we monitored the DNA content in these chaining cells. In *E. coli* and other bacteria, FtsZ depletion results in filamentous cell growth, but DNA segregation is not affected [206]. In *H. neptunium*, staining of DNA with 4',6-diamidino-2-phenylindole (DAPI) revealed that DNA is present in the cell compartments within these cell chains, suggesting that DNA replication and segregation is not abolished, although it might be impaired to some extent (Fig. 2.18 B).

Altogether, these results demonstrate that FtsZ is an essential protein and vital for cell division in *H. neptunium*. Other cellular events such as chromosome segregation, stalk growth, and budding are not directly coupled to cell division in *H. neptunium* and can occur independently of FtsZ, suggesting a different regulatory interplay between these

processes than known from other bacteria.

So far, our attempts to unravel the mechanism responsible for the highly asymmetric placement of the Z-ring were not successful (see section 2.3). Although the key regulator still needs to be determined, observations from re-induction experiments can give insights into the principle of Z-ring positioning in *H. neptunium*. Cells, which were depleted for FtsZ for 11 h, were tracked in a microfluidic device while FtsZ expression was induced again (Fig. 2.20). In the first few hours the cells appeared to be largely inactive, neither dividing nor enhancing the depletion phenotype. However, after 5-6 h, the cells started to divide again. Surprisingly, the site of division was not placed randomly, but in the majority of cases at the junction between a cell body and a stalk, corresponding to the "normal" division site in wild type cells. Even more astonishing was the fact that multiple divisions could occur at the same time within a single cell chain (Fig. 2.20, upper time-lapse). From these results we concluded that whatever mechanism positions the Z-ring, it is still functional in cells that have aberrant morphologies and defects in cell polarity, casting negative regulatory mechanisms into doubt.

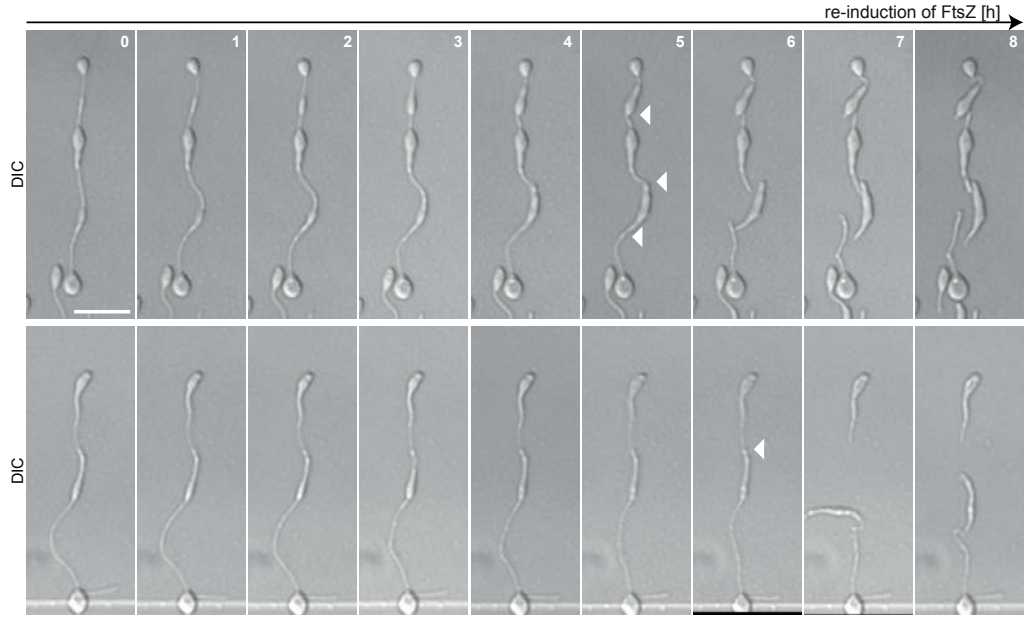

Figure 2.20: Cells divide at junctions between cell bodies and stalks. Cells of strain SE97 (Δ*ftsZ* P_{zn}::P_{zn}-*ftsZ*) were depleted of FtsZ for 11 h, transferred to a microfluidic device, and constitutively induced with 0.5 mM $ZnSO_4$. At the indicated time points, cells were visualized by DIC microscopy (scale bar: 5 µm). White triangles mark the division sites.

This result together with the highly asymmetric mode of division let us speculate about a positively regulated division site placement in *H. neptunium*.

2.4.3 Biochemical characterization of FtsZ

Given the ability of cells devoid of FtsZ to initiate division at the "correct" position after re-induction of FtsZ expression, and, thus, the option of a positive regulatory mechanism responsible for Z-ring positioning, we were wondering whether FtsZ requires a stimulation factor for effective polymerization.

To address this question and to characterize *H. neptunium* FtsZ *in vitro*, native FtsZ was purified in a nucleotide-free state. Therefore, a His_6-SUMO tag was fused to the N-terminus of FtsZ and cleaved off after Ni-NTA purification using the Ulp1 protease. First, we tested the ability of $FtsZ_{HNE}$ to form polymers with different approaches. First, a centrifugation-based polymerization assay was applied. $FtsZ_{HNE}$ was able to polymerize into large structures in the presence of GTP, which were found in the pellet fraction after ultracentrifugation (Fig. 2.21 A). When no GTP was added, hardly any polymers were formed. As control, we used native FtsZ from *C. crescentus*, which is known to form polymers in the presence of GTP and possess GTPase activity [115]. Notably, a higher concentration of $FtsZ_{HNE}$ (12 µm) did not yield higher amounts of polymers (Fig. 2.21 A). These results were confirmed by right angle light scattering (Fig. 2.21 C). $FtsZ_{HNE}$ formed polymers only in the presence of GTP, but to a less extent than $FtsZ_{CC}$. Next, we used electron microscopy to visualize the FtsZ polymers. The EM images showed curved filaments formed by $FtsZ_{HNE}$ in the presence of GTP (Fig. 2.21 B). The filaments looked similar to the filaments formed by $FtsZ_{CC}$ (Fig. 2.21 B).

The ability to undergo polymerization in the presence of GTP implies that $FtsZ_{HNE}$ has GTPase activity. Using a GTPase activity assay, we demonstrated that $FtsZ_{HNE}$ hydrolyzed GTP in a concentration-dependent manner with a turnover number of 2.24 GTP min^{-1} at a concentration of 6 µM (Fig. 2.21 D). However, the experiments on FtsZ cooperativity applying a range of different $FtsZ_{HNE}$ concentrations were not conclusive and have to be repeated in the future (data not shown). Interestingly, when $FtsZ_{HNE}$ was equipped with

a C-terminal His_6-tag, its ability to hydrolyze GTP was strongly reduced (Fig. 2.21 D). In contrast, $FtsZ_{CC}$ equipped with a C-terminal His_6-tag had a GTPase activity comparable to that of the native FtsZ protein (data not shown). In summary, these results demonstrate that FtsZ from *H. neptunium* resembles other FtsZ proteins in terms of polymer formation and GTPase activity.

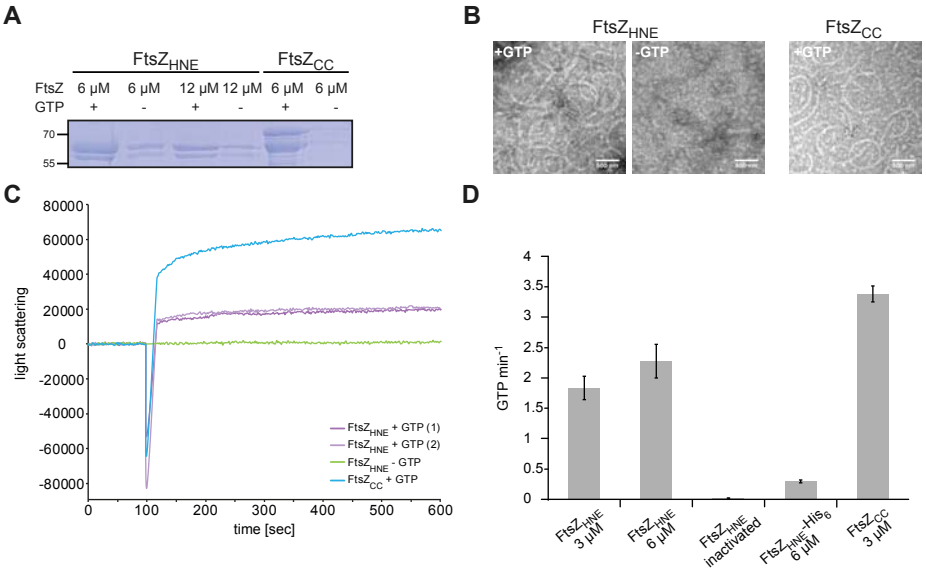

Figure 2.21: FtsZ polymerizes and has GTPase activity *in vitro*. **(A)** Polymerization of FtsZ. $FtsZ_{HNE}$ or $FtsZ_{CC}$ were incubated at the indicated concentrations for 20 min at 25 °C in the presence (+) or absence (-) of 2 mM GTP. After ultracentrifugation at 254,000x g, the pellets were resuspended and visualized by SDS-PAGE. Positions of molecular weigth markers (kDa) are indicated on the left side. **(B)** Structure of FtsZ polymers. $FtsZ_{HNE}$ (6 µM) was incubated for 15 min in the presence or absence of 2 mM GTP. As positive control, $FtsZ_{CC}$ (3 µM) was incubated with 2 mM GTP for 15 min as well. Subsequently, the samples were applied onto carbon-coated grids, stained, and analyzed by transmission electron microscopy in collaboration with T. Heimerl. **(C)** Right angle light scattering. Experiments were performed with 10 µM $FtsZ_{HNE}$ and 10 µM $FtsZ_{CC}$ at 25 °C in the presence or absence of GTP. 2 mM GTP was added after 100 sec (Y. Refes). **(D)** GTPase activity of FtsZ. The specific GTPase activity of different FtsZ proteins was measured. As negative control, $FtsZ_{HNE}$ was heat-inactivated.

We also attempt to identify interaction partners of FtsZ via Co-Immunoprecipitation. FtsZ, equipped with an HA-tag, was expressed in wild type background, proteins were crosslinked and the resulting cell lysate was mixed with α-HA affinity gel (Sigma-Aldrich, Germany). The precipitated proteins were analyzed by mass-spectrometry (in collaboration with J. Kahnt, MPI Marburg) but unfortunately no specific hits could be identified, since the detected proteins were also present in the wild type control sample (data not shown).

2.5 FtsK - an ATPase involved in cell division and DNA segregation

The localization study of the DNA translocase FtsK revealed an interesting and surprising subcellular distribution (Fig. 2.5, p. 27). FtsK localized throughout the stalk in an irregular pattern, suggesting an additional function beside its role in cytokinesis.

2.5.1 Verification of the localization of FtsK

A previous study in *H. neptunium* showed that FtsK, when fused with a fluorescent protein tag at its C-terminal end, is not fully functional, since the only clone obtained had severe morphological defects [193]. Thus, to exclude the possibility that the observed localization pattern obtained with the inducible fusion is an artifact, we conducted further localization studies. First, an N-terminal fusion was generated to check whether a tag at the opposite terminus might lead to a fully functional protein. Unfortunately, this fusion protein was unstable when expressed from an inducible promoter (data not shown). Next, we applied immunofluorescence to visualize the localization pattern of FtsK in its native state. The antibody used was raised against an N-terminally truncated variant of FtsK, which lacks the transmembrane regions. This variant was fused N-terminally to a His_6-tag and purified using the Ni-NTA affinity purification method. Despite intensive efforts to optimize the protocol for *H. neptunium*, fixation of the cells led to significant damage of the cells (Fig. 2.22 A). Nevertheless, the immuno-signals observed suggest that FtsK localized to positions within the stalk as well as to the division site (Fig. 2.22 A).

To finally confirm the localization of FtsK and to circumvent the potential adverse effect of a C-terminal fluorescent tag on the function of the ATPase domain of the full-length protein, we generated a strain expressing only the transmembrane domains of FtsK fused to Venus from an inducible promoter (Fig. 2.22 B). In studies of FtsK homologs from other bacteria, it was shown that this part is sufficient for the correct localization at the division site [146, 147]. Consistently, the localization pattern was the same as obtained

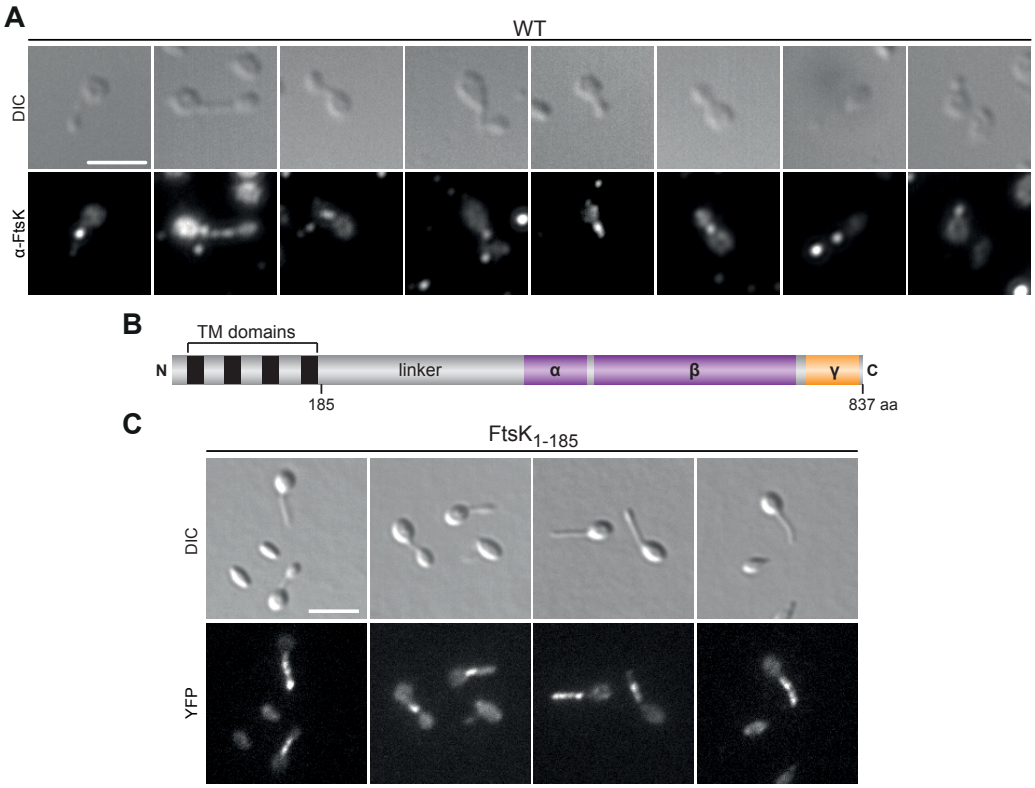

Figure 2.22: FtsK and a C-terminally mutant variant localize to the stalk. **(A)** Localization of FtsK by immunofluorescence. Cells of the wild type were grown to exponential phase in MB, fixed, and probed with α-FtsK antibodies. Immunocomplexes were then detected by application of Alexa-Fluor 594-conjugated secondary antibodies (scale bar: 3 µm). **(B)** Schematic representation of FtsK. Transmembrane domains (TM) are shown in black, the motor domain in purple and the gamma domain in yellow. Numbers indicate the position of amino acid (aa) residues within the protein for the following mutant variant. Adapted from [162] **(C)** Localization of the N-terminal part of FtsK. Cells of strain SE150 (P_{zn}::P_{zn}-*ftsK*$_{aa1-185}$-*venus*) were grown to exponential phase in MB, induced with 0.5 mM $ZnSO_4$ for 3 h, and visualized by DIC and fluorescence microscopy (scale bar: 3 µm).

with the full-length protein. The fusion protein localized in an irregular pattern within the stalk (Fig. 2.22 C), strongly suggesting that the unusual localization, which we observed before, is correct and not an artifact of the fusion.

2.5.2 FtsK localizes independently of FtsZ

Based on the interesting subcellular localization of FtsK in the complete stalk, we wondered whether FtsK is part of the divisome in *H. neptunium*, as it is the case in most other bacteria. To address this issue, we analyzed the dependency of FtsK localization on other

cell division proteins. For instance, in *E. coli* and *C. crescentus*, the localization of FtsK at midcell depends on the key cell division protein FtsZ [30, 147]. When FtsK-Venus was expressed from the copper-inducible promoter in the absence of FtsZ or the late cell division protein FtsN, whose expression were controlled by the zinc-inducible promoter, FtsK maintained its typical patchy distribution within the stalk, even in the strongly elongated stalks (Fig. 2.23 A+B), clearly demonstrating that the localization of FtsK is not dependent on other cell division proteins. Notably, both the FtsZ and FtsN depletion phenotypes were less pronounced when FtsK-Venus was expressed, resulting in shorter stalks and shorter cell chains (Fig. 2.23 A+B), most likely due to a crosstalk of the copper- and zinc-inducible promoters used simultaneously in this experiment.

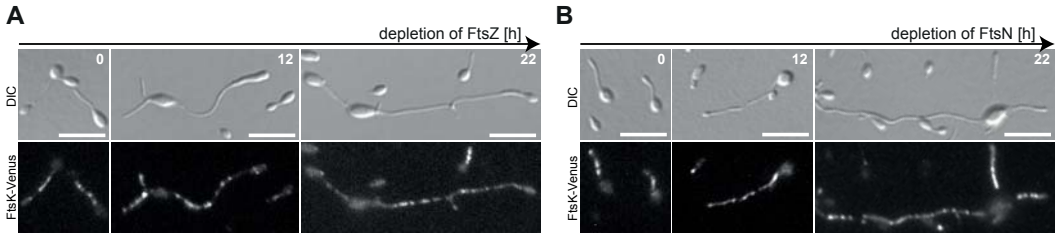

Figure 2.23: The localization of FtsK is not dependent on FtsZ or FtsN. Cells of strain SE147 (Δ*ftsZ* P_{zn}::P_{zn}-*ftsZ* P_{cu}::P_{cu}-*ftsK-venus*) **(A)** and SE148 (Δ*ftsN* P_{zn}::P_{zn}-*ftsN* P_{cu}::P_{cu}-*ftsK-venus*) **(B)** were grown to exponential phase in MB supplemented with 0.5 mM $ZnSO_4$ and induced with 300 μmM $CuSO_4$ for 3 h. After a washing step, cells were resuspended in medium without $ZnSO_4$ but with $CuSO_4$. At the indicated time points, cells were withdrawn and imaged by DIC and fluorescence microscopy (scale bar: 5 μm).

2.5.3 Positioning of FtsK

The unusual localization pattern of FtsK raised the question of how FtsK finds its "destination". One possibility is the recruitment by another protein. In bacteria, such functions are often taken over by cytoskeletal proteins. For instance, bactofilins are involved in positioning of diverse proteins in different bacterial species [203]. Deletion of both bactofilins in *H. neptunium* leads to strong morphological defects (E. Cserti, unpublished). The expression of the inducible FtsK-Venus fusion protein in a Δ*bacAB* background strain, however, did not show an altered localization, since FtsK-Venus was still found in the stalk (Fig. 2.24 A). Therefore bactofilins are not implicated in the positioning of FtsK.

As mentioned before (section 2.4.2), a strain lacking the orphan ParA-homolog HNE_0708 was deficient in chromosome segregation, since it accumulated DNA in the stalk and several ParB foci within the cell [200]. Additionally, HNE_0708 localized in the stalk similar to FtsK, indicating a possible interplay between these two proteins. However, the localization of FtsK-Venus was not affected in the absence of HNE_0708 (Fig. 2.24 B), eliminating HNE_0708 as a positioning factor of FtsK.

The localization pattern of FtsK and its independency from FtsZ raised the question of whether FtsK is part of the division machinery and, consequently, interacts with the divisome. Therefore, we heterologously expressed FtsK from *H. neptunium* ($FtsK_{HNE}$) fused to Venus in the closely related stalked species *C. crescentus*. Intriguingly, $FtsK_{HNE}$-Venus exhibited a completely different localization in *C. crescentus*. It showed a polar localization or a diffuse distribution in swarmer and stalked cells, and accumulated at the division site at midcell in predivisional cells (Fig. 2.24 C). At any time it was absent from the stalk, which is, in contrast to *H. neptunium*, indeed compartmentalized by

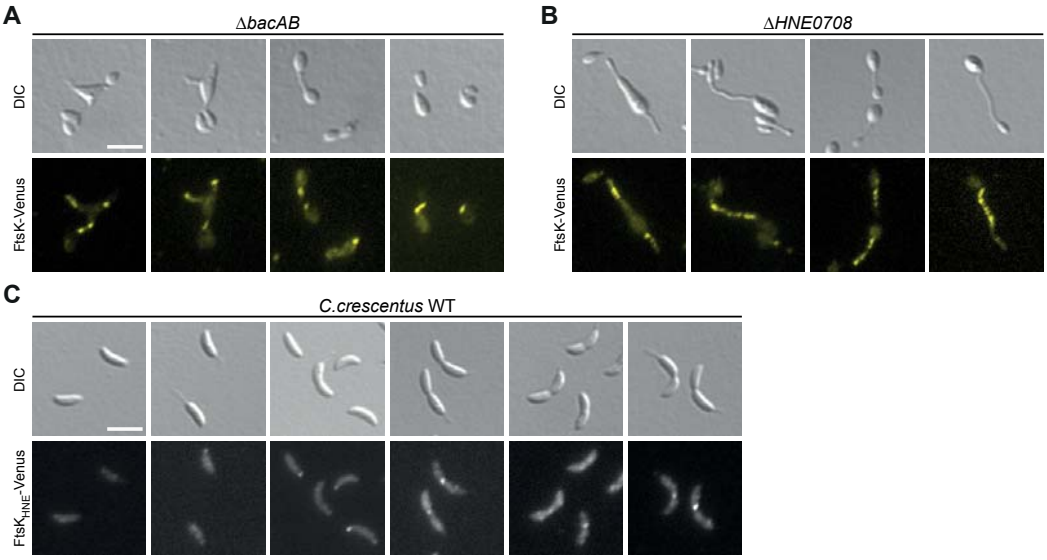

Figure 2.24: Localization of FtsK in different deletion backgrounds and in a heterologous system. (A) Double deletion of bactofilin homologs BacA and BacB. Strain SE175 (Δ*bacAB* P_{zn}::P_{zn}-*ftsK-venus*) was grown to exponential phase in MB, induced with 0.5 mM $ZnSO_4$ for 3 h and visualized by DIC and fluorescence microscopy (scale bar: 3 μm). **(B)** Deletion of the ParA-homolog *HNE_0708*. Strain SE159 (Δ*HNE_0708* P_{zn}::P_{zn}-*ftsK-venus*) was treated equally to strain SE175 in (A). **(C)** Expression of $FtsK_{HNE}$-Venus in *C. crescentus* wild type. Strain SE195 (P_{xyl}::P_{xyl}-*ftsK*$_{HNE}$-*venus*) was grown to exponential phase in PYE, induced with 0.3% xylose for 1.5 h and visualized by DIC and fluorescence microscopy (scale bar: 3 μm).

crossbands, but its first part would still be accessible for FtsK. The fact that $FtsK_{HNE}$ was recruited to midcell in *C. crescentus*, like the endogenous FtsK homolog, implies that it might also be part of the divisome in *H. neptunium*, but may in addition also have a divisiome-independent function in the stalk in.

2.5.4 Generation of a conditional mutant was not successful

The observations of FtsK made so far revealed that FtsK shows a behavior that is strikingly different from that of its homologs from other species. To further elucidate the role of FtsK in *H. neptunium*, we aimed to generate a conditional mutant. Unfortunately, such a strain could not be obtained, despite several attempts. Neither a full-length depletion strain, nor a C-terminal depletion strain, having only the N-terminal part (AA1-330) under the control of an inducible promoter, could be generated. In fact, any manipulation at the *ftsK* locus turned out to be impossible, underscoring the importance of this gene. The analysis of the genomic context of *ftsK* did not reveal any features that could explain these problems. Transcriptome data (A. Jung, unpublished) revealed that *ftsK* is annotated correctly and no alternative start codon was found in close proximity. Additionally, these data verified that *ftsK* is an orphan gene and not part of an operon (Fig. 2.25 A). Of notice, there is a large region (~1 kb) that does not contain any annotated genes, but, according to BLAST analysis, contains a gene homologous to two other hypothetical ORF's of *H. neptunium*. However, this putative gene was excluded as a possible problem, because this region was not significantly transcribed and the reads obtained were in sense direction, whereas the putative gene is oriented in anti-sense direction. Another explanation could be the non-native expression level of *ftsK* in a conditional mutant. To this end, we compared the expression levels of FtsK expressed from either the zinc-inducible promoter or its native promoter. The expression levels obtained with the inducible promoter were only slightly lower than those obtained with the native promoter, which should not cause any problems (Fig. 2.25 C). Additionally, cells which expressed FtsK alone from an inducible promoter in the WT background showed nearly wild type morphology and grew with wild type rate (data not shown).

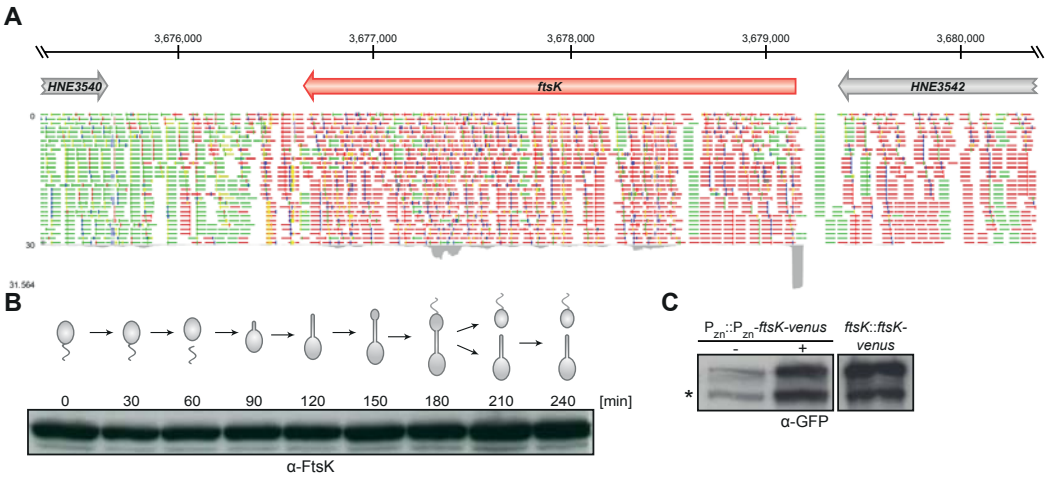

Figure 2.25: Transcription and expression level of FtsK. (A) Region view and transcript levels of the *ftsK* locus. Red lines indicate antisense reads, green lines sense reads. **(B)** Protein level of FtsK over the course of the cell cycle. Swarmer cells of the wild type obtained by synchronization were grown in MB over one cell cycle. At the indicated time points, samples were taken and analyzed by immunoblotting using α-FtsK antibodies. The schematic above illustrates the morphological stages of *H. neptunium* over the course of the cell cycle. **(C)** Comparison of FtsK-Venus levels. Exponentially growing cells of SE151 (P_{zn}::P_{zn}-*ftsK-venus*), induced with 0.5 mM $ZnSO_4$ for 3 h, and WS09 (*ftsK*::*ftsK-venus*) were analyzed by immunoblotting using α-GFP antibodies. The asterisk indicates a degradation product.

Another issue in terms of protein expression is the timing during the cell cycle. Many proteins are cell cycle-regulated and only expressed in certain cell stages. Constant expression of such a protein in a conditional mutant could be lethal. In the case of FtsK, we could exclude this issue, since FtsK is merely very mildly cell cycle-regulated in *H. neptunium*, and present at any time point during the cell cycle (Fig. 2.25 B). This is in contrast to the FtsK level in *C. crescentus*, which varies over the course of the cell cycle and peaks in late pre-divisional cells [30].

2.5.5 Cells with impaired or less FtsK show morphological abnormalities

In order to overcome the problems associated with the genetic manipulation of the *ftsK* locus and study the effects caused by a loss or malfunction of the protein, we generated two different strains in which the native *ftsK* locus was left intact. As a first approach, we generated an ATPase-deficient variant of FtsK, expressed in addition to the native *ftsK* gene. To this end, the conserved lysine (K487) in the Walker A box was substituted with alanine, resulting in a protein that is not capable of binding ATP [151] (Fig. 2.26 A).

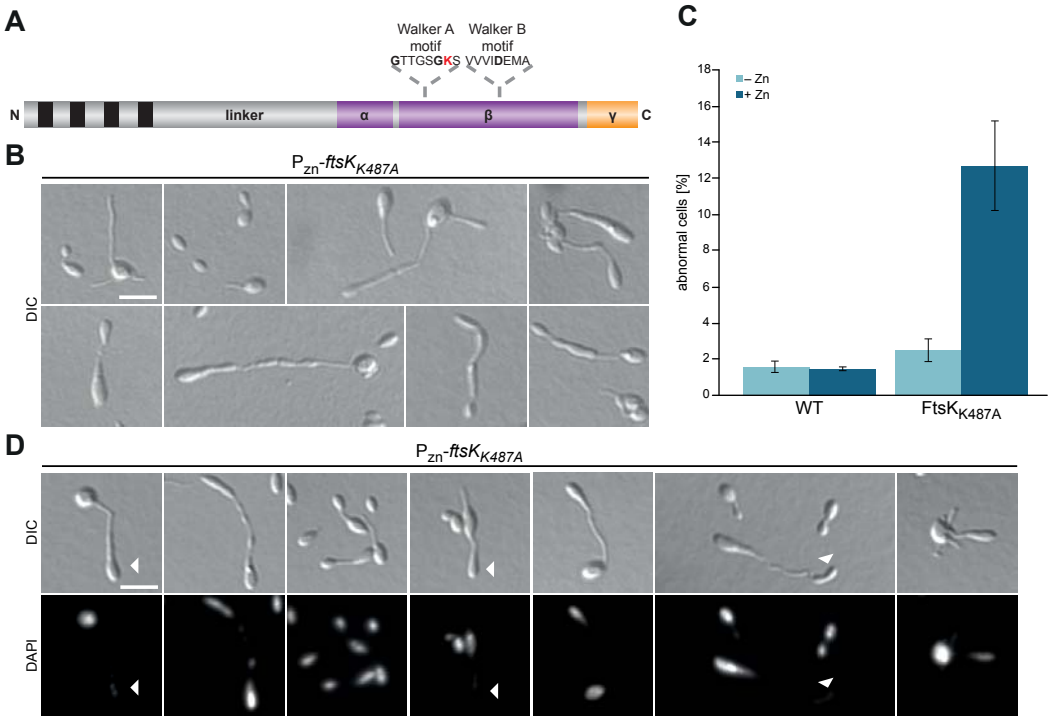

Figure 2.26: Characterization of an ATPase-deficient variant of FtsK. (A) Schematic depicting the Walker A and Walker B motifs located in the β-domain of FtsK. The substituted amino acid is indicated in red. **(B)** Phenotype of the ATPase-deficient FtsK variant. Strain SE156 (P_{zn}::P_{zn}-*ftsK*$_{K487A}$) was grown to exponential phase in MB, induced with 0.5 mM $ZnSO_4$ for 20 h, and visualized by DIC microscopy (scale bar: 3 μm). **(C)** Quantification of abnormal cells from (B) and control strains. Strains SE156 (P_{zn}::P_{zn}-*ftsK*$_{K487A}$) and the wild type were grown in the absence or presence of 0.5 mM $ZnSO_4$ for 20 h (exponential phase). Shown are the average and standard deviation of three independent experiments, with 200-300 cells counted for each strain. **(D)** Expression of FtsK$_{K487A}$ variant results in cell compartments without DNA. Cells from (B) were stained with DAPI and analyzed by DIC and fluorescence microscopy (scale bar: 3 μm). White triangles mark cell compartments without DNA.

In general, such ATPase mutants of FtsK have dominant-negative effects, because they interfere with the proper function of the native protein through the formation of hetero-hexamers [207]. When the FtsK$_{K487A}$ variant was expressed in *H. neptunium*, a fraction of the cell population showed morphological defects. These cells had elongated stalks, misshapen and extended cell bodies, and in some cases a polarity defect (Fig. 2.26 B). However, only 13% of cells showed this phenotype, whereas the majority of cells had a wild type appearance (Fig. 2.26 C). Staining of DNA with DAPI revealed that out of these mutated cells, some lack DNA in one of their cell compartments (Fig. 2.26 D), suggesting an impact on chromosome segregation as hypothesized for FtsK.

In the second approach, we applied a relatively new tool called TALE (transcription activator-like effectors) [208] to manipulate the expression of FtsK. TALEs can be designed such that they specifically recognize and bind user-defined DNA sequences in various organisms (bacteria, yeast, mammalian cells etc.) [209]. Based on the transcription data of *ftsK*, we identified the putative promoter region upstream of the transcriptional start of FtsK and designed a TALE that targets 25 bp within this region. Thus, this TALE should act as a repressor that decreases the FtsK expression level. When we expressed $TALE_{FtsK}$ from an inducible promoter, we could observe changes of the morphology in a fraction of cells (Fig. 2.27 A). They lost their characteristic shape and elongated their stalks. Furthermore, hyper-formation of stalks originating from one cell body could be

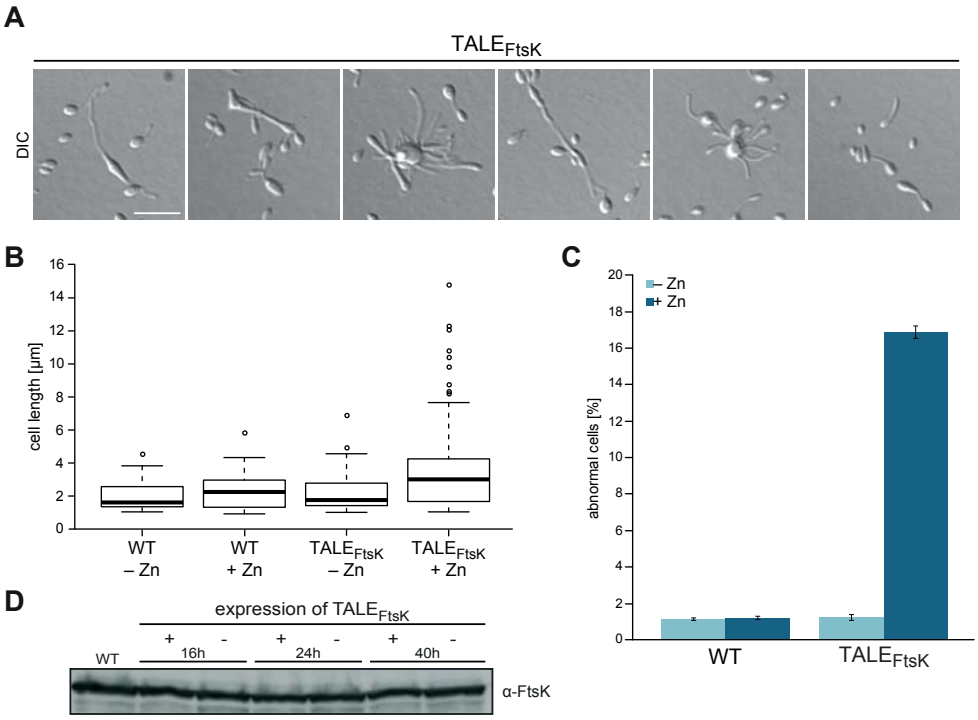

Figure 2.27: $TALE_{FtsK}$ induces morphological defects. (A) Various morphological defects upon $TALE_{FtsK}$ expression. Cells of strain SE197 (P_{zn}::P_{zn}-$TALE_{FtsK}$) were grown in the presence of 0.5 mM $ZnSO_4$ while being kept in exponential phase by constant dilutions, and analyzed by DIC microscopy after 40 h (scale bar: 5 µm). **(B)** Quantification of cell length from wild type and SE197 (P_{zn}::P_{zn}-$TALE_{FtsK}$) cells grown in the absence or presence of $ZnSO_4$ for 40 h. Data sets are displayed in box-whisker plots. Shown are the interquartile range (box), the median (line), the 5^{th} and 95^{th} percentile (whiskers), and outliers (circles). **(C)** Quantification of abnormal cells in wild type and SE197 (P_{zn}::P_{zn}-$TALE_{FtsK}$) cells grown in the absence or presence of $ZnSO_4$ for 40 h. Shown are the average and standard deviation of three independent experiments, with 200-300 cells counted for each strain. **(D)** Protein level of FtsK in the presence (+) or absence (-) of $TALE_{FtsK}$. As control, a wildtype sample is shown.

observed. Even though only a fraction of about 17% of the cell population showed such dramatic defects (Fig. 2.27 C), the expression of $TALE_{FtsK}$ led to a notable increase in the overall cell length of the population (Fig. 2.27 B). However, a decrease in the FtsK expression level could not be verified by immunoblot analysis using an α-FtsK antibody (Fig. 2.27 D), *i.e.* the proof for the efficiency of the TALE in decreasing the expression of FtsK is still missing. Though, it is very unlikely that the observed defects arise from binding of $TALE_{FtsK}$ to a region in the genome that is different from the desired target site, because the binding of TALEs is highly specific [209] and no similar sequence was found in the genome by BLAST analysis. Probably, the FtsK antibody is not as specific as previously thought.

Due to the localization of FtsK in the stalk, we assume that it might play a role during DNA transport through the stalk. To test this hypothesis, we checked the $TALE_{FtsK}$ strain for irregular DNA distribution by DAPI staining. And indeed, a fraction of cells with abnormal morphology showed anucleate cell compartments, but no single DNA-free cells could be observed (Fig. 2.28). These anucleate cell compartments are very likely caused by a reduced level of FtsK and not by the morphological defect itself, since for example FtsZ-depleted cells have no anucleate compartments despite their severe morphological defects (compare Fig. 2.18 B).

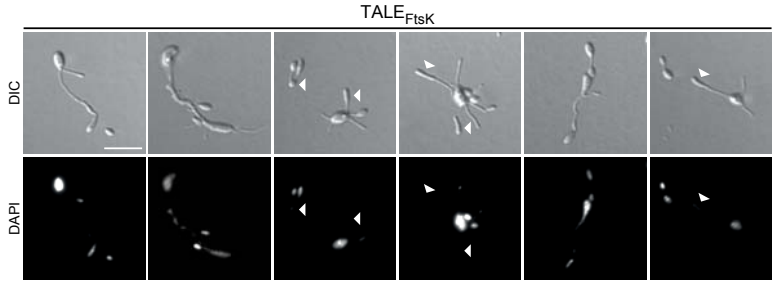

Figure 2.28: $TALE_{FtsK}$ leads to DNA-free cell compartments. Cells of strain SE197 (P_{zn}::P_{zn}-$TALE_{FtsK}$) were grown in the presence of 0.5 mM $ZnSO_4$ for 40 h, while being kept in exponential phase by constant dilutions. Subsequently, cells were stained with DAPI and analyzed by DIC and fluorescence microscopy (scale bar: 5 µm).

2.6 FtsN - a late cell division protein

FtsN is a core component of the cell division machinery. As a representative of late cell division proteins, we decided to analyze FtsN in more detail. The localization of Venus-FtsN in this study revealed that it is present at the pole in swarmer cells, diffuse or at the tip of the stalk in stalked cells and at the division site in budding cells (Fig. 2.9, p. 30).

2.6.1 Loss of FtsN leads to severe defects

In order to draw conclusions about the role of FtsN and cell division in general in *H. neptunium*, we generated a conditional mutant of FtsN. This allowed us to assess the effect of the loss of FtsN and to compare the phenotype to the one caused by loss of an early cell division protein (FtsZ).

To this end, *ftsN* was placed under control of the zinc-inducible promoter while the native gene was deleted. When the cells grew in the presence of zinc, they showed wild type appearance and had no cell length or cell division defect (Fig. 2.29 A+B). After transfer into medium without zinc, the cells started to elongate their stalks after 6 h, similar to the conditional *ftsZ* mutant. Longer depletion of FtsN led to a slight chaining

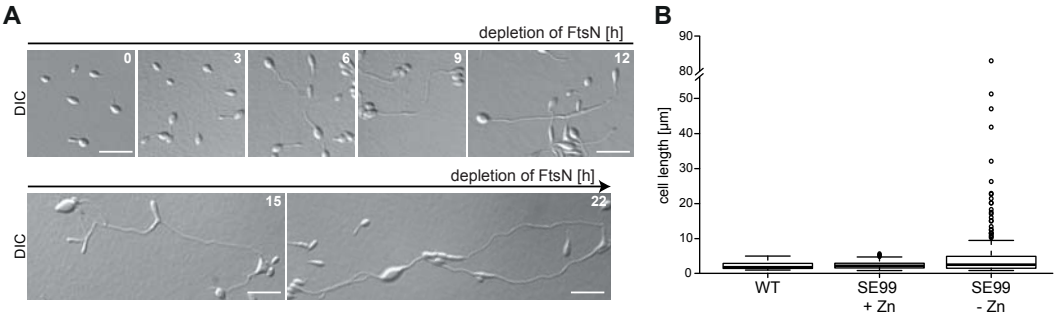

Figure 2.29: Effect of FtsN depletion. (A) Strongly elongated stalks and misshapen cell bodies induced by the lack of FtsN. Cells of strain SE99 (Δ*ftsN* P_{zn}::P_{zn}-*ftsN*) were grown to exponential phase in MB supplemented with 0.5 mM $ZnSO_4$, washed twice, and resuspended in medium without $ZnSO_4$. At the indicated time points, cells were withdrawn and imaged by DIC microscopy (scale bar: 5 µm). **(B)** Quantification of wild type cells and SE99 before and after 22 h depletion. A total of 224, 177 and 200 cells, respectively, were measured using Metamorph. Data sets were displayed in box-whisker plots. Shown are the interquartile range (box), the median (line), the 5th and 95th percentile (whiskers), and outliers (circles).

phenotype, and predominantly, the formation of elongated stalks and polarity defects (Fig. 2.29 A+B), confirming the essential role of FtsN in cell division. A small fraction of the cell population showed wild type morphology, most likely due to an incomplete depletion caused by the relatively high basal activity of the zinc-inducible promoter. Unfortunately, we had no specific antibody against FtsN to determine if it was entirely absent from the cells.

Next, PG synthesis was assessed by staining FtsN-deficient cells with HADA. Similar to the FtsZ conditional mutant, PG incorporation was aberrant, leading to misshapen cells, while new cell bodies arised in the middle of an existing budding cell (Fig. 2.30 A, 7.5h).

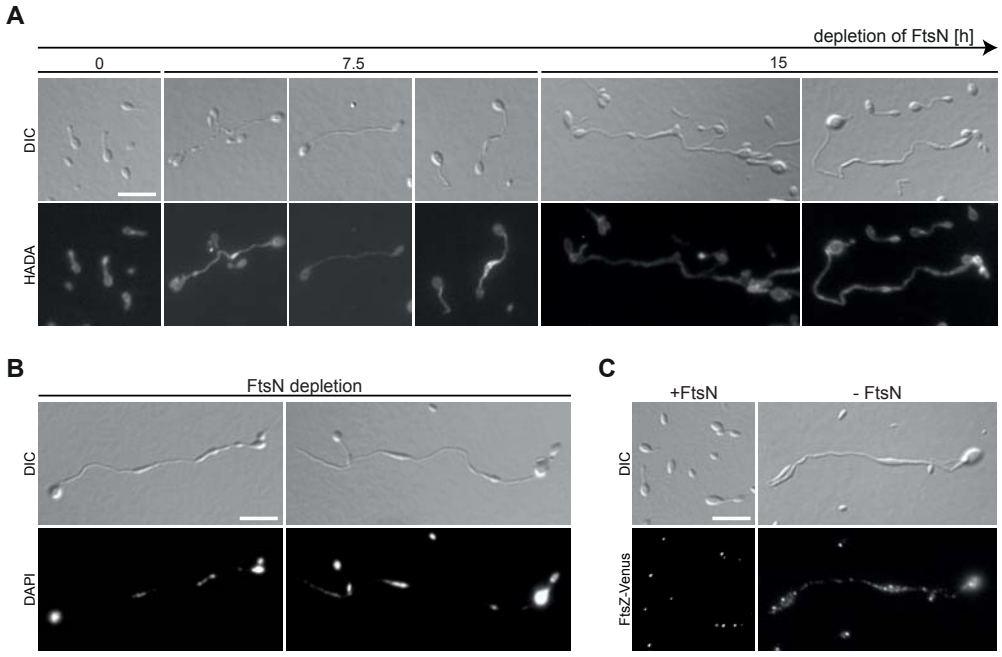

Figure 2.30: Characterization of the FtsN depletion phenotype. (A) PG incorporation in FtsN-deficient cells. Cells of strain SE99 (Δ*ftsN* P_{zn}::P_{zn}-*ftsN*) were grown to exponential phase in MB supplemented with 0.5 mM $ZnSO_4$, washed twice, and resuspended in medium without $ZnSO_4$. At the indicated time points, cells were withdrawn, incubated with 0.5 mM HADA for 9 min, fixed with 70% EtOH, washed, and imaged by DIC and fluorescence microscopy (scale bar: 5 μm). **(B)** FtsN-deficient cells accumulate chromosomes. Cells of strain SE99 (Δ*ftsN* P_{zn}::P_{zn}-*ftsN*) depleted of FtsN for 22 h and cells of the wild type grown to exponential phase were stained with DAPI and visualized by DIC and fluorescence microscopy (scale bar: 5 μm). **(C)** FtsZ is mislocalized in FtsN-deficient cells. Cells of strain SE141 (Δ*ftsN* P_{zn}::P_{zn}-*ftsN* P_{cu}::P_{cu}-*ftsZ-venus*) were grown in the presence of 0.3 mM $CuSO_4$ and 0.5 mM $ZnSO_4$ to exponential phase, washed twice, and resuspended in medium with $CuSO_4$, but without $ZnSO_4$. Directly after resuspension and after 22 h depletion of FtsN, cells were withdrawn and analyzed by DIC and fluorescence microscopy (scale bar: 5 μm).

After longer depletion of FtsN, the HADA signal was less distinct and visible in many spots within the cells, indicating that PG incorporation was entirely misregulated (Fig. 2.30 A, 15 h).

To further characterize the FtsN depletion phenotype, we monitored the DNA content of these elongated cells. Cell elongation caused by loss of a cell division protein such as FtsZ or FtsN has usually no direct effect on DNA segregation. As expected, loss of FtsN in *H. neptunium* does not abolish DNA segregation, since all cell compartments still contained DNA (Fig. 2.30 B). Furthermore, we asked whether FtsZ is able to form distinct Z-rings in the absence of FtsN, as reported for other bacteria [210]. Surprisingly, FtsZ-Venus localized in a patchy, irregular pattern within cell bodies after a short (9 h, data not shown) or a long period of FtsN depletion (22 h, Fig. 2.30 C), indicating that loss of FtsN can influence Z-ring formation, most likely in an indirect manner.

In order to confirm the results obtained with the re-induction experiment of FtsZ, we used the same approach for FtsN. Cells were depleted of FtsN for 11 h, transferred into a microfluidic device and monitored while expression of FtsN was turned on again (Fig. 2.31). Some cells already started to divide after 3 h of induction of FtsN, whereas it took 5-6 h in FtsZ re-induced cells. Consistent with the FtsZ experiment, the position of the division site was always at junctions between cell bodies and stalks, even though the

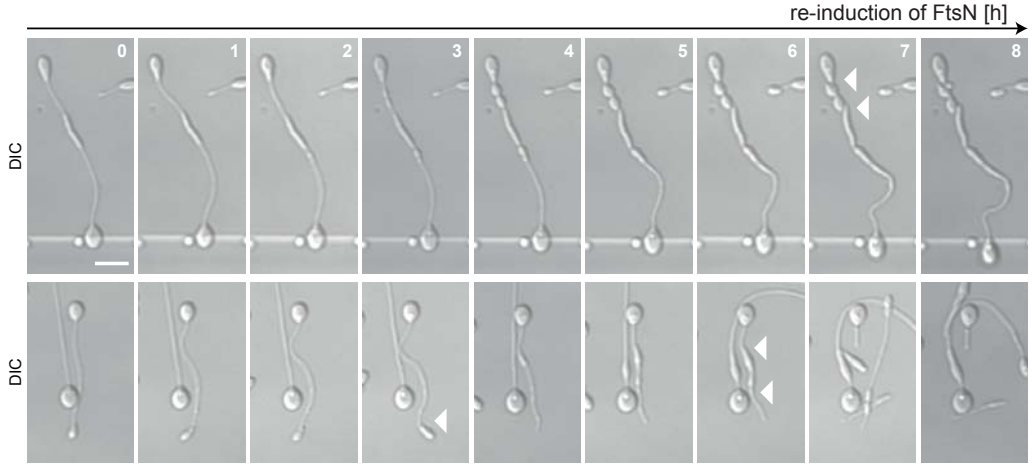

Figure 2.31: Cells divide at junctions between cell bodies and stalks. Cells of strain SE99 (Δ*ftsN* P_{zn}::P_{zn}-*ftsN*) were depleted of FtsN for 11 h, transferred to a microfluidic device and constitutively induced with 0.5 mM $ZnSO_4$. At the indicated time points, cells were visualized by DIC microscopy (scale bar: 5 µm). White triangles mark the division sites.

stalks were not always discernible due to their extremely short length (Fig. 2.31, upper time-lapse). Additionally, multiple divisions occurred at the same time in a single cell, as observed for FtsZ, implying that several divisomes assemble at once. These results confirm that division is not random in cells with aberrant morphologies and disturbed polarity, but still follows a certain pattern.

In summary, we demonstrated that FtsN is an essential protein and vital for cell division in *H. neptunium*. Similar to FtsZ, cellular processes such as budding and chromosome segregation are not directly affected by the absence of FtsN.

3 Discussion

3.1 Cell division proteins show altered localization patterns in *H. neptunium*

A multiprotein complex called the divisome orchestrates bacterial cytokinesis. Its central component is the conserved tubulin homolog FtsZ. In this work, we studied the FtsZ homolog of *H. neptunium* and performed comparative localization studies. Besides its conserved genomic context in an operon with *ftsA* and *ftsQ*, it has 64% sequence similarity and 53% sequence identity to FtsZ from *C. crescentus*. Time-lapse experiments evidenced that FtsZ localization dynamically changes from a unipolar focus at the future stalked pole to a bipolar pattern at both ends of the stalk during the cell cycle (Fig. 2.1, p. 23). From the two clusters observed in budding cells, only the one at the junction to the bud develops into a mature divisome. Although there are other bacteria possessing multiple FtsZ complexes, such as *Agrobacterium tumefaciens* [211], these usually condense into one focus at the onset of division, whereas both clusters are maintained in *H. neptunium* until cytokinesis is finished. Given that a C-terminal FtsZ fusion is not fully functional, we confirmed the unusual localization pattern with an FtsZ sandwich fusion, which is also not fully functional, but was not hindered at its essential C-terminus (Fig. 2.16, p. 39). Thus, *H. neptunium* possesses a unique subcellular FtsZ distribution that clearly differs from known FtsZ pattern, raising several questions about the positioning of the division site, which are discussed below (section 3.4).

From the other cell division proteins studied in *H. neptunium*, only FzlC and occasionally FtsQ have the same localization pattern as FtsZ in budding cells (Fig. 2.2 B and Fig. 2.6, p. 24 and 28). However, cells harboring Venus-FzlC under the control of the native promoter have shortened stalks and larger buds compared to wild type cells, indicating that the fusion is not fully functional and that FzlC malfunction affects the cells. In *C. crescentus*, deletion of *fzlC* did not affect cell morphology or division, rendering FzlC dispensable [41]. Localization of an inducible Venus-FzlC fusion, expressed additionally

to the native gene in *H. neptunium*, was comparable to the endogenously expressed FzlC fusion, but the cells had wild type morphology (data not shown), suggesting that the localization pattern of FzlC, resembling the one of FtsZ, is correct.

Apart from these two proteins, the other proteins (FzlA, FtsE, (FtsA), FtsI, FtsW and FtsN) also had a dynamic localization pattern, but were found exclusively at the division site in budding cells (Fig. 3.1), suggesting that only this FtsZ cluster formed at this site is able to efficiently recruit cell division proteins. The DNA translocase FtsK stands out in this localization study by showing a localization pattern atypical for cell division proteins. Even during divisome assembly and constriction, it remains localized in a patchy pattern in the stalk, instead of accumulating only at the division site (Fig. 3.1). This case is discussed in a following section (3.5).

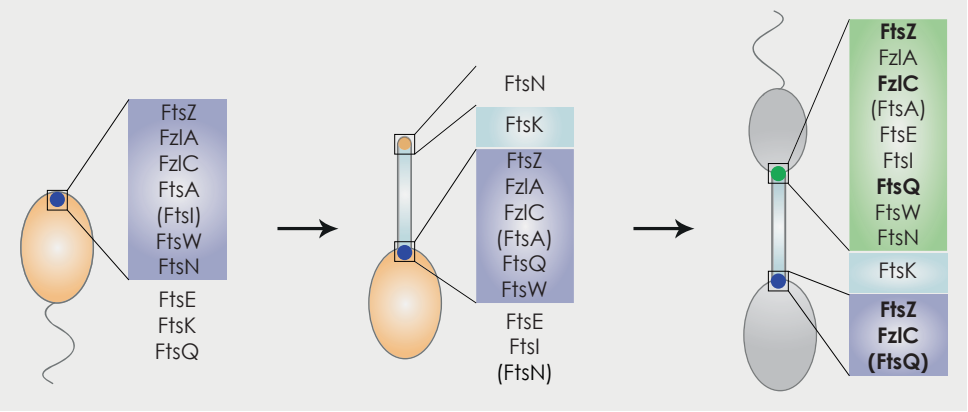

Figure 3.1: Localization scheme of divisome components during the *H. neptunium* cell cycle. Most cell division protein start the cell cycle at the "new" (future stalked) cell pole, whereas FtsE, FtsK, and FtsQ localize diffuse. In stalked cells, many cell division proteins exhibit the same localization pattern as before. Exceptions are FtsK, which localizes to the entire stalk, FtsN, which has left the stalked cell pole and is either diffuse or at the tip of the stalk, FtsI, which became diffuse, and FtsQ (each in bold), which accumulates at the stalked pole now. In budding cells, almost all cell division proteins accumulate at the division site to form the mature divisome. Remarkably, FtsZ, FzlC, and occasionally FtsQ were additionally observed at the stalked mother cell pole. FtsK is still distributed within the entire stalk, but might also be part of the divisome. See text for more information.

The localization pattern of FtsA needs further confirmation, since the native Venus-FtsA fusion accumulated irregular in the mother cell body beside its division site localization. These irregular accumulations could be inclusion bodies composed of misfolded or defective protein caused by the fluorescent tag, but no degredation product, since a

western blot analysis showed a stable expression (data not shown). Remarkably, neither a C-terminal, nor an N-terminal inducible fusion of FtsA gave a distinct localization pattern (data not shown). The weak signals observed there seemed to accumulate randomly within the cell, although the expression level was comparable to native FtsA levels. However, the presence of the native protein in addition to the inducible tagged version could interfere with its correct localization. Furthermore, the fluorescent tag might hinder the protein from interacting with other proteins to find the correct position.

Interestingly, FtsN is capable of localizing at the tip of the stalk during stalk growth, additionally to its localization at the swarmer pole and, later, at the division site. This can be rarely observed in cells harboring Venus-FtsN under the control of the endogenous promoter (Fig. 2.9, p. 30). However, in cells expressing Venus-FtsN from an inducible promoter, the accumulation at the tip of the stalk was observed more frequently (data not shown), likely due to the higher amount of protein in the cells. Remarkably, several other proteins such as BacA, PopZ, MipZ, PBP2, some hydrolytic enzymes, and PleC were found to localize to or near the tip of the stalk in *H. neptunium* (E. Cserti, O. Leicht, S. Rosskopf, A. Jung, unpublished). It is possible that FtsN is interacting with and recruited by one of them in order to form a regulatory complex controlling bud formation. Accordingly, cells lacking FtsN form less buds within the elongated cells than cells lacking FtsZ. That implies that FtsN is most likely not the major factor required for bud formation, but may play a role in this process. The protein fusions of ZapA and TolQ, did not show any specific localization pattern. This could be due to the fact that these fusion proteins were additionally induced to the native protein. For many cell division proteins, only a small amount of molecules is recruited to the division site, due to limited interaction sites. This might be particularly relevant in *H. neptunium*, which has a smaller divisome compared to other bacteria based on its narrow division site. Thus, the fusion protein competes with the native protein for binding sites and probably has a “disadvantage” because of its fluorescent tag. Furthermore, a weak signal at the division site might be covered by a comparably high background signal.

In *C. crescentus*, the expression of some divisome components, such as FtsZ, FtsQ or FtsI, is cell cycle-regulated to ensure correct timing of cell division [30]. We could not

observe variations in the protein levels of FtsZ and FtsK, either due to an insufficient synchrony of the cell population or because they are not regulated on the protein level. This would be in contrast to *C. crescentus*, in which the protein level of FtsZ varies strongly and the one of FtsK varies mildly over the course of the cell cycle. However, RNA-seq data indicate that FtsZ, FtsQ, and FtsK are transcriptionally regulated in *H. neptunium* (O. Leicht, unpublished). Their transcription levels were slightly down-regulated (~2-fold) in the absence of the histidine kinase CckA, which resembles the absence of the master cell cycle regulator CtrA. Moreover, the promotor regions of these genes contain CtrA-binding sites (O. Leicht, unpublished), strongly indicating a cell cycle regulation of FtsZ, FtsQ and FtsK by CtrA, at least on the transcriptional level. Thus, the regulatory network of *C. crescentus* on a transcriptional level regarding cell division proteins seems at least partially conserved in *H. neptunium*. Whether regulation on the protein level is also conserved needs an improved synchronization protocol and further studies.

3.2 FtsZ and FtsN are essential components of the divisome in *H. neptunium*

Deletion of FtsZ and FtsN was not successful in *H. neptunium*, which is consistent with their known essential roles in cell division. Phenotypic analyses of a conditional FtsZ mutant demonstrated that FtsZ is required for cell division (Fig. 2.17, p. 40). The absence of FtsZ leads to a cell division block with highly elongated stalks interrupted by amorphous cell compartments. This indicates that stalk elongation and bud formation do not rely on FtsZ or completed cell division, but are rather independent of cell cycle progression. The phenotype is in contrast to the smooth filaments observed in other bacteria such as *C. crescentus* upon depletion of FtsZ [212] and suggests a decoupling of cell division and cell differentiation in *H. neptunium*.

Compared to the phenotype observed upon depletion of FtsZ, the conditional mutant of the late cell division protein FtsN showed a less severe cell elongation, decreased cell chaining, and less cell compartments. Due to the lack of a functional antibody, we could not determine the level of FtsN in the depleted state to rule out that the less severe

phenotype is caused by an incomplete depletion. Alternatively, FtsN might participate to a minor degree in bud formation.

Surprisingly, FtsZ was mislocalized in the absence of FtsN. However, FtsZ mislocalization is most likely not a direct effect of the absence of FtsN, but might be due to the disturbance of cellular processes and the presence of several chromosomes, respectively, which could also affect the unknown regulatory machinery controlling FtsZ positioning. Possibly, the divisome disassembles if FtsN and, thus, the trigger for constriction are absent, resulting in mislocalized FtsZ. In *C. crescentus* it has been shown that the divisome component FtsK, which requires FtsZ to localize to the division site, is crucial to maintain Z-rings and absence of FtsK lead to random distribution of FtsZ [213], comparable to what happened when FtsN is absent in *H. neptunium*. Alternatively, events such as incomplete chromosome segregation or disturbed PG incorporation upon depletion of FtsN might also, directly or indirectly, lead to mislocalization of divisome components

3.3 MipZ is not the main regulator of Z-ring positioning in *H. neptunium*

Many bacteria rely on negative regulatory mechanisms, like the Min system or MipZ, that identify the middle of the cell as the correct division site through the formation of a gradient, in which an inhibitor regulates FtsZ placement. Such a system is not applicable to *H. neptunium* since the division site is not at the middle of the cell but shifted towards one end. Remarkably, *H. neptunium* possesses a homolog of the negative regulator MipZ.

In this work, we could show that MipZ from *H. neptunium* ($MipZ_{HNE}$) behaves different from MipZ from *C. crescentus* ($MipZ_{CC}$), although the proteins share considerable sequence similarity (50% identity, 68% similarity). Instead of a bipolar distribution reflecting the localization of ParB [115, 200], $MipZ_{HNE}$ showed a unipolar localization, either to the flagellated pole or later on to the bud pole opposite the stalk (Fig. 2.12 B, p. 34), indicating no interaction with ParB. Residues possibly involved in the MipZ-ParB interaction in *C. crescentus* [214] are only partially conserved in $MipZ_{HNE}$, giving no clear indication

about its interaction network. Interestingly, the localization pattern of MipZ resembles the pattern of the pole organizing protein PopZ in *H. neptunium* (A. Jung, unpublished), making PopZ a possible localization factor for $MipZ_{HNE}$. In *C. crescentus*, PopZ is essential, anchors the *ori* region at the cell pole (via direct interaction with *parS*-bound ParB) [137, 138], and is involved in ParA-mediated centromere segregation by recruiting and regenerating inactive ParA [142]. In *H. neptunium*, PopZ is not essential and a deletion has no influence on ParB positioning and chromosome segregation (A. Jung, unpublished), indicating that PopZ fulfills a different role. This is consistent with its altered localization pattern. Interestingly, sequence analysis of MipZ homologs revealed that $MipZ_{HNE}$ has an extended N-terminal tail composed of ~20 amino acids. This extension is conserved in *Hyphomondaceae* (data not shown), but is absent from other MipZ homologs and might be involved in protein-protein interactions that help localize MipZ.

Importantly, we could show that MipZ is not essential in *H. neptunium* and has no obvious effect on Z-ring positioning or cell morphology (Fig. 2.11 / Fig. 2.12 A, p. 33 / 34), which is in stark contrast to its homolog from *C. crescentus*. To date, it remains unclear whether $MipZ_{HNE}$ has the ability to inhibit Z-ring formation at all. Expression of an ATPase-deficient MipZ variant ($MipZ_{D62A}$), which blocked cell division in *C. crescentus* due to unspecific binding to DNA [114], had no effect on *H. neptunium* cells (Fig. 2.13, p. 35). Considering the fact that FtsZ does not assemble over the nucleoid in *H. neptunium* anyway, a missing effect of the $MipZ_{D62A}$ variant can still be consistent with a similar functionality of $MipZ_{HNE}$ and $MipZ_{CC}$. Nevertheless, an altered localization pattern of this variant and, thus, no inhibitory function on FtsZ in *H. neptunium* is also conceivable. One hint for this hypothesis is that $MipZ_{HNE}$ fused to YFP localized in a diffuse manner in *C. crescentus* cells and did not inhibit cell division [215]. Additionally, many putative residues involved in DNA and FtsZ binding of $MipZ_{CC}$ [114, 214] are not conserved in $MipZ_{HNE}$, indicating that $MipZ_{HNE}$ cannot interact with ParB or inhibit Z-ring formation neither in *C. crescentus* nor in *H. neptunium*.

Taken together, these results clearly show that $MipZ_{HNE}$ is not the spatial regulator of division site placement in *H. neptunium*. Probably, MipZ is part of a redundant system or only required under certain conditions. Alternatively, MipZ might act as a nucleoid

occlusion factor, similar to SlmA in *E. coli* and Noc in *B. subtilis* [102, 103]. These proteins are usually not essential, but bind to DNA and thereby prevent assembly of the divisome over DNA. In this scenario, $MipZ_{HNE}$, which accumulates at the old cell pole, would bind (unspecifically) to DNA in a gradient-like pattern with the highest concentration at the old cell pole. This gradient of MipZ dimers, which is not bipolar as the one of $MipZ_{CC}$, would cover part of the chromosome, first in the mother cell, and later on in the bud. In the smaller bud, it might not only cover part of the nucleoid, but the complete nucleoid (over the entire length of the caughter cell) and function as a "failsafe-mechanism" to prevent Z-ring assembly over the nucleoid. Thus, this system could be more important in the bud compartment than in the mother cell compartment. PopZ might then act as a hub recruiting and regenerating MipZ molecules at the old cell pole. This hypothesis is missing experimental evidence so far. However, PopZ was shown to recruit and regenerate the related protein ParA [142]. And the missing effect of an ATPase-deficient MipZ variant we observed, would fit into this model, in which MipZ is only a failsafe-nucleoid occlusion mechanism. This variant would then no longer form a gradient but be distributed over the entire DNA (as the corresponding $MipZ_{CC}$ mutant), which would not give a phenotype as long as Z-ring positioning works accurately. The concentration of the DNA-bound $MipZ_{D62A}$, which would pass the currently assembling Z-ring during DNA segregation, is most likely to low to interfere with FtsZ polymerization.

So far, MipZ from *C. crescentus* is the only characterized MipZ homolog in literature. Thus, it is unclear whether the function of MipZ is conserved across species or whether, as this work indicates, the role of MipZ can differ. There is one example of preliminary data from the MipZ homolog of *Rhodobacter sphaeroides*, which also suggests a different behaviour compared to $MipZ_{CC}$. Although this MipZ homolog colocalizes with the *ori* region, i. e. ParB, of the first chromosome at the cell pole, it additionally colocalizes with FtsZ at the division site, which is not consistent with a role in FtsZ inhibition (N. Dubarry, unpublished). This implies that, although MipZ is highly conserved in α-proteobacterial genomes [115], its function is less conserved and might be adapted to the needs of the individual species.

Besides a putative role in nucleoid occlusion, an unrelated function is within the bounds

of possibility. MipZ forms a putative transcriptional unit with the gene located upstream (*HNE_1127*). HNE_1127 is a hypothetical protein with no conserved domains and is only present in *Hyphomondaceae*. The transcription data proof that $MipZ_{HNE}$ is expressed during standard conditions in a mean level, whereas HNE_1127 is highly expressed. Interestingly, preliminary data revealed that $MipZ_{HNE}$, together with its operon partner HNE_1127, are regulated by the master cell cycle regulator CtrA (O. Leicht, unpublished). Usually, proteins regulated by CtrA in *C. crescentus* fulfil roles in processes such as cell cycle regulation, cell division, polar morphogenesis, and DNA replication, giving a hint about potential MipZ functions. However, a detailed characterization of $MipZ_{HNE}$ is necessary to elucidate its exact role in *H. neptunium*.

3.4 How is the Z-ring positioned in *H. neptunium?*

Given the remarkable distribution of FtsZ at both ends of the stalk, several questions arise: How does FtsZ find these two positions? What determines the second FtsZ focus to become the divisome? And how do the other divisome components know where to localize?

All known spatial regulators target the core divisome component FtsZ directly by either inhibiting FtsZ polymerization at inappropriate positions or by recruiting FtsZ to the correct site. The FtsZ focus at the stalked mother cell pole in *H. neptunium* could simply be kept there by the unknown regulatory system as a remnant of the last cell division, since the FtsZ protein level is constant over the course of the cell cycle. However, the second focus is the result of a dynamic relocalization process, which has to be tightly regulated.

Many negative positioning mechanisms identify the “middle” of the cell as the correct division site by the formation of bipolar regulatory gradients [83]. Such a system cannot work in *H. neptunium*, because the position of the division site is highly asymmetric and does not coincident with the “middle” of the cell, which would be somewhere in the stalk. These circumstances and the fact that the cells divide at the “correct” position after re-induction of FtsZ (Fig. 2.20, p. 43), although the cell shape is strongly

perturbed, argues for a scenario in which a positive regulator recruits FtsZ to the correct position. Positive regulators have been identified in a number of organisms in the last years, but they are not well-conserved. For example, SsgA and SsgB from *S. coelicolor* are only present in *Actinomycetes* [116], PomZ from *M. xanthus* is only conserved in *Myxococcales* and MapZ from *S. pneumonia* is only conserved in lactic acid bacteria [118, 119], suggesting a variety of positive Z-ring placement systems in different bacterial species. So far, there is no obvious candidate protein for such a positive regulator in *H. neptunium*. A more global screening, allowing the identification of unknown, important *Hyphomonas*-specific proteins, might lead to success. One conceivable approach is, for example, a transposon screen, in which the set of essential genes in *H. neptunium* could be identified. Optionally not only in WT cells, but also in a MipZ deletion strain, to identify genes, which become essential in the absence of MipZ.

As reported previously, FtsZ from *M. xanthus*, which is regulated by a positive mechanism, failed to polymerize *in vitro* [117], suggesting a link between positive regulation and polymerization ability *in vitro*. Although it was shown in the meantime that it can form polymers without additional factors (D. Schumacher, personal communication), we characterized $FtsZ_{HNE}$ *in vitro* to elucidate whether a stimulatory factor might be required. The biochemical characterization revealed that it behaves like other characterized FtsZ homologs. It polymerizes in the presence of GTP and Mg^{2+}, as shown by electron microscopy and polymerization assays (Fig. 2.21 A-C, p. 45). Thus, no additional stimulatory factor is needed. The GTPase activity is comparable to that of other FtsZ proteins and increases with increasing FtsZ concentrations (Fig. 2.21 D, p. 45 and data not shown). Since *in vivo* conditions can differ from the *in vitro* conditions used, we cannot rule out that FtsZ requires additional factors to form polymers *in vivo*.

Another determinant of FtsZ placement could be the cell shape. Strikingly, FtsZ localizes to the two sites within a *H. neptunium* cell that exhibit a particular geometric shape: the junctions between the stalk and the cell bodies, which exhibit positively curved membranes. It is conceivable that FtsZ itself, or an interacting protein can sense this geometric cue, similar to DivIVA or SpoVM [216, 217]. In the case of DivIVA, the selective binding is achieved by exposed positively charged or hydrophobic residues and probably

by specific structural features of the two-dimensional lattices formed [217–219]. FtsZ, as a tubulin homolog, can also form three-dimensional polymeric structures. Although FtsZ from *H. neptunium* is highly similar to other FtsZ proteins, its C-terminal linker region is poorly conserved, possibly allowing an adaptation to mediate an unusual localization pattern. Alternatively, FtsZ might sense a special feature of the stalk, such as different PG composition, and would actually localize to the entire stalk structure but is restricted to the ends of the stalk by an inhibitor within the stalk.

In *E. coli*, it was shown that assembly of the Z-ring is a question of the number of FtsZ molecules. Spherical *E. coli* cells, which have a larger diameter, cannot build complete Z-rings at native FtsZ levels. Only after overexpression of the *ftsQAZ* operon, Z-ring formation was successful [220]. Thus, the FtsZ level in *H. neptunium* might be equally low, therefore allowing Z-ring formation only at the narrow stalk-cell junctions. However, even then, FtsZ has to be positioned by some mechanism, to avoid Z-ring assembly in the stalk. Moreover, assuming that the first FtsZ focus is a remnant "immobilized" by the unknown regulatory system, the relocalization to the second position could be regulated by proteins involved in bud formation, e.g. the PG biosynthetic machinery or a hypothetical factor that determines where the bud is generated, or, alternatively, by a relocalization of its (positive) regulator.

As mentioned before, the regulation of division site placement usually occurs at the level of FtsZ. As FtsZ accumulates at two positions in *H. neptunium*, it is conceivable that in this species, the regulation of division site positioning occurs at a later stage. Evidently, only the FtsZ focus at the stalk-bud junction matures into a functional divisome, as confirmed by the localization of almost all analyzed division proteins to only this position. This suggests that the FtsZ accumulation at the mother stalked pole is not able to assemble a stable Z-ring, but might only consist of FtsZ oligomers. Thus, the recruitment of divisome components seems to be restricted specifically to the stalk-bud junction, by a yet unidentified regulatory mechanism. Convenient targets of this unknown regulatory mechanism could be the Z-ring stabilizing/tethering proteins, such as FzlA, FzlC, ZapA, and FtsA, or an unknown factor, allowing the assembly of a functional Z-ring only at this position. Since FzlC colocalized with both FtsZ foci (Fig. 2.2 B, p. 24), it is most likely

not the target of the divisome placement system. The other stabilizers need further investigation to determine whether one of them could be the target. However, as long as the regulatory system has not been identified, this could be a demanding task.

The only known example of another species with two FtsZ cluster is *B. subtilis* during sporulation, resulting in an asymmetric division, too. During sporulation, *B. subtilis* switches from one medial Z-ring to two polar Z-rings (and not only loose accumulations), involving a spiral-like intermediate of FtsZ [221]. Unlike in *H. neptunium*, both Z-rings have the capacity to trigger cytokinesis. However, only one Z-ring forms a septum and the second nascent septum eventually is degraded [222, 223], which is definitely not the case in *H. neptunium*.

3.5 Role of FtsK

DNA translocases play multiple important roles during cell differentiation and chromosome segregation. FtsK, a DNA translocase belonging to the FtsK/SpoIIIE family of AAA^+ ATPases, is involved in cell division as well as in chromosome segregation, dimer resolution, and chromosome decatenation [145, 149, 150]. In this work, we studied the FtsK homolog of *H. neptunium*. The unusual cell shape of this species and the separation of the mother and daughter cell by a thin stalk, implies differences and adaptations in the mechanism of chromosome segregation, its coordination with cell division, and thus very likely in FtsK function.

In most species studied so far, FtsK is part of the division machinery and recruited in an FtsZ-dependent manner to the division site [30, 146, 147]. Surprisingly, we demonstrated that FtsK is distributed in a patchy pattern within the entire stalk in *H. neptunium* and that this localization is not dependent on FtsZ (Fig. 2.5 and Fig. 2.23 A, p. 27 and 48). In fact, FtsK localizes markedly before FtsZ assembles at the division site. Similar to known FtsK proteins, the N-terminal part is sufficient to mediate this localization (Fig. 2.22 C, p. 47). How FtsK finds the stalk remains elusive. Possibly, the localization is mediated by stalk-specific features, e.g. different PG composition or the presence of certain proteins.

During the late stages of the cell cycle, FtsK maintains its position in the stalk. However, after cytokinesis, it becomes diffuse in newborn swarmer cells. Due to the limited resolution of widefield fluorescence microscopy, it remains unclear whether the last FtsK complex in the stalk is positioned at the junction to the daughter cell, forming part of the divisome. Evidence for FtsK being part of the divisome comes from the ability of $FtsK_{HNE}$ to be recruited to the division site in *C. crescentus* (Fig. 2.24 C, p. 49). On the other hand, it is possible that FtsK is only recruited to the divisome in *H. neptunium* under certain conditions, e.g. when DNA is trapped at the closing septum, as known for SpoIIIE [224, 225].

In *H. neptunium*, the replicated chromosome has to traverse the stalk to reach the daughter cell compartment. FtsK's subcellular distribution tempted us to speculate about a potential role of FtsK in DNA transport through the stalk ("working model"). It was shown that the segregation of the *ori* region and other chromosomal loci through the stalk occurs in a directed manner and very rapidly (A. Jung, unpublished), suggesting the involvement of an active process, such as translocation by FtsK. Furthermore, the *ori* region is actively segregated to the stalked cell pole in the mother cell [200], facilitating the contact with the first FtsK complex. The generation of an FtsK deletion or depletion strain was not successful, emphasizing the essential role of FtsK in *H. neptunium*. The importance of the C-terminal region, harbouring the DNA pump, is further supported by the observation that a C-terminal fusion to GFP was not fully functional [193] and even a conditional mutant, missing only the C-terminal part, could not be generated. Remarkably, preliminary data of the cell cycle regulatory network of *H. neptunium* revealed that the expression of FtsK is at least slightly regulated by the cell cycle response regulator CtrA (see section 3.1). This emphasizes its putative essential function. In *C. crescentus*, the promotor region of *ftsK* contains a CtrA-binding motif as well, but it is not completely certain that the variations in the *ftsK* transcriptional levels over the course of the cell cycle are caused by CtrA-dependent regulation.

Experimental evidence for a role of FtsK in chromosome segregation through the stalk comes from analyses of an ATPase-deficient FtsK variant. Cells expressing $FtsK_{K487A}$ show morphological defects and anucleate cell compartments (Fig. 2.26, p. 52). However, this

phenotype is visible only in a fraction of the cell population, most likely because the effect of $FtsK_{K487A}$ is attenuated by the presence of the native protein. Furthermore, our "working model" is supported by the presence of anucleate cell compartments in a strain with putatively impaired FtsK expression ($TALE_{FtsK}$). This observation along with severe morphological and stalk biogenesis defects in this strain (Fig. 2.27, p. 53), suggests that FtsK is involved in DNA segregation through the stalk and that a perturbation in this process has severe consequences. However, the majority of the cell population has a wild type phenotype and a normal DNA distribution. Therefore, we hypothesize that either the expression level of FtsK is still high enough to allow normal chromosome segregation in most of the cells or that an FtsK-independent segregation mechanism exists. In this case, FtsK may have a redundant role or ensures the robustness of the process. Alternatively, it might be essential only under certain conditions, such as during dimer formation, which occurs in a minority of cells.

Consistent with our "working model" suggesting a role of FtsK in bulk chromosome segregation through the stalk, the distribution of FtsK-binding sites (KOPS) on the *H. neptunium* chromosome differs from other species like *C. crescentus* and *E. coli*, in which FtsK is only required during the late stages of chromosome segregation. Usually, KOPS motifs can be found throughout the chromosome mainly on the leading strand (leading strand skew), with a lower density of motifs near the origin region and a high density near the terminus region [153, 226, 227]. Interestingly, on the *H. neptunium* chromosome, the KOPS have the leading strand skew, too, but the motifs are evenly distributed between *ori* and *ter* [200], indicating that FtsK can be loaded onto the DNA nearly everywhere. Consequently, the translocation activity might not be focused on the terminus-proximal regions but on the vast majority of the DNA, as it would be required when FtsK mediates bulk chromosome segregation.

During late stages of the cell cycle in *E. coli* and *C. crescentus*, FtsK mediates the resolution of chromosome dimers by aligning the *dif* sites and directly activating the recombinase XerD at the division site [149, 158]. In *H. neptunium*, the terminus region was shown to be replicated and separated in the mother cell compartment (A. Jung, unpublished). Hence, dimer resolution (and decatenation) likely occurs in the mother cell body and not at the

division site. The involvement of a DNA translocase in this process is highly conserved across species, indicating that FtsK, as the sole known DNA translocase encoded in the *H. neptunium* genome, participates at least in the alignment of the *dif* sites, whereas the activation of the recombinase is less conserved and might be dispensable. Possibly, dimer resolution (and decatenation) occurs at the stalked mother cell pole in proximity to the first FtsK complex at the junction between the stalk and the mother cell, supported by the fact that the terminus region localizes near the stalked mother cell pole and is replicated there (A. Jung, unpublished).

As reported previously, FtsK has the ability to remove DNA-binding proteins from the translocated regions of the chromosome [159, 207]. Therefore, we assume that the majority of proteins binding to DNA in *H. neptunium*, are released during translocation through the stalk by FtsK. This assumption was reinforced by several experiments using the ParABS system from *Yersinia pestis* [228]. Most chromosomal loci labelled with this method lost their signal during translocation (A. Raßbach, A. Jung, unpublished). When the FROS system was applied, the signal of *ori*-proximal regions was largely persistent, whereas the signal of *ter*-proximal regions was lost again ([200] and A. Jung, unpublished). The underlying mechanisms are not completely clear, thus further evaluation is required. Possibly, the divisome is already more constricted when the *ter*-proximal regions pass the division site, leading to a removal of the respective proteins.It is conceivable that stripping off proteins from segregated DNA helps *H. neptunium* to establish an asymmetry between the mother cell and the daughter cell compartment in terms of DNA binding proteins. An unequal distribution of proteins is a common theme in dimorphic bacteria to allow different cell fates [229]. In contrast to cytoplasmic proteins, which might not that easily reach the daughter cell due to a longer distance they need to travel by diffusion, proteins bound to DNA could simply travel with the segregated DNA to the daughter cell. In order to prevent this, removal by FtsK might be an appropriate way to establish asymmetry. Once they are released, they would rather stay in the mother cell compartment due to the higher amount of DNA there.

Taken together, we could provide several lines of evidence that the FtsK homolog of *H. neptunium* is involved in DNA segregation through the stalk. Nevertheless, the final

proof is still missing and the role of FtsK in this and additional processes needs further investigation.

3.6 Concluding remarks and outlook

In the majority of bacteria, cell division seems to be a quite conserved process. However, extensive research showed that there are variations and adaptations to fit the individual needs of certain species. Therefore, we have started to investigate cell division in the stalked budding bacterium *H. neptunium*. The fascinating polyphyletic group of stalked budding bacteria deviates from the well-studied model organisms, such as *E. coli* and *C. crescentus* by their unique reproduction strategy and it will be very interesting to investigate the subcellular organization and molecular mechanisms underlying this mode of proliferation.

Here, we demonstrated that the cell division proteins FtsZ and FtsK exhibit an unusual subcellular localization in *H. neptunium*. Both proteins were not exclusively found at the division site. In the case of FtsZ, a second cluster remained at the mother stalked pole. The nature of the two clusters remains elusive. Nevertheless, in terms of biochemical properties, FtsZ behaves like its homologs. In the case of FtsK, the localization to the entire stalk could reflect its adapted function in chromosome segregation through the stalk. We presented several lines of evidence that FtsK is involved in this process, but the underlying mechanism this process needs further investigation. Furthermore, we gave proof that the role of MipZ in Z-ring positioning is not conserved across α-proteobacteria. In *H. neptunium*, MipZ seems to play only a minor or no role in this process. It will be interesting to analyze which function MipZ has in other species.

In summary, we could show that several highly conserved proteins behaved differently in *H. neptunium*, most probably due to an adaptation to the unique life style of *H. neptunium*. Thus, this work demonstrates how important it is to study conserved proteins in a variety of organisms and not to focus only on a few well-established model organisms. It will be interesting to investigate the mechanisms and regulatory pathways

involved in the asymmetric cell division of *H. neptunium* and identify the differences to well-known systems.

4 Material and Methods

4.1 Material

4.1.1 Source of chemicals and enzymes

Chemicals used in this study were obtained from Amersham (UK), Applichem (Germany), Becton Dickinson (USA), Carl-Roth (Germany), Difco (Spain), GE Healthcare (UK), Invitrogen (Germany), Kobe (Germany), Merck (Germany), Millipore (Germany), Perkin Elmer (USA), Peqlab (USA), Sigma-Aldrich (USA) or Fisher Scientific (USA).

Enzymes required for manipulation and cloning (T4 DNA ligase, phosphatase, restriction endonucleases) as well as size markers for DNA and proteins were purchased from Fermentas (Canada) and New England Biolabs (NEB; USA). For PCR reactions KOD Hot Start DNA Polymerase (Merck, Germany) or Biomix™ Red (Bioline, Germany) were used.

4.1.2 Buffers and Solutions

Standard buffers und solutions were prepared as described by Ausubel [230] and Sambrook [231]. Specific buffers and solutions are listed in the respective method section. All buffers und solutions were prepared using de-ionized water (Purelab Ultra water purification systems, ELGA, Germany) and autoclaved (20 min at 121 °C) or filter sterilized (pore size 0.22 µm, Sarstedt, Germany) when required.

4.1.3 Media

All media were sterilized by autoclaving at 121 °C and 2 bar for 20 min. Heat-sensitive additives such as antibiotics were filter sterilized (pore size 0.22 µm, Sarstedt, Germany) and added to the cooled-down medium (60 °C). For solid media, 1.5% (w/v) agar was added before autoclaving. All media additives are listed in tables 4.3 and 4.4.

Complex medium for *Escherichia coli*

LB (lysogeny broth)

tryptone	1.0 % (w/v)
yeast extract	0.5 % (w/v)
NaCl	1.0 % (w/v)

Complex medium for *Hyphomonas neptunium*

MB (marine broth)

peptone	0.5 % (w/v)
yeast extract	0.01 % (w/v)
Fe(III)	0.4 mM
NaCl	0.3 M
$MgCl_2$	62.0 mM
$MgSO_4$	27.0 mM
$CaCl_2$	16.0 mM
KCl	1.0 mM
Na_2CO_2	1.9 mM
KBr	0.7 mM
$SrCl_2$	0.2 M
H_3BO_3	0.4 M
Na-silicate	22.0 mM
NaF	57.0 mM
$(NH_4)NO_3$	20.0 mM
Na_2HPO_4	35.0 mM

The medium was boiled in the microwave before autoclaving. Subsequently, it was filter sterilized (pore size 0.22 µm, Sarstedt, Germany) to remove precipitates.

Complex medium for *Caulobacter crescentus*

PYE (*peptone yeast extract*)

Bacto™ peptone	0.2 % (w/v)
yeast extract	0,1 % (w/v)
$MgSO_4$	1 mM
$CaCl_2$	0.5 mM

Table 4.3: Antibiotics

Antibiotic	Final concentration [µg/µl]					
medium	*E. coli* liquid	*E. coli* solid	*H. neptunium* liquid	*H. neptunium* solid	*C. crescentus* liquid	*C. crescentus* solid
Kanamycin [50 mg/ml]	30	50	100	200	5	25
Rifampicin [10 mg/ml]	200	100	1	2	-	-
Ampicillin [20 mg/ml]	200	200	-	-	-	-
Chloramphenicol [10 mg/ml]	20	30	-	-	-	-

Table 4.4: Further media additives

Additive	Final concentration					
medium	*E. coli* liquid	*E. coli* solid	*H. neptunium* liquid	*H. neptunium* solid	*C. crescentus* liquid	*C. crescentus* solid
DAP [60 mM]	0.3 mM	0.3 mM	-	-	-	-
$ZnSO_4$ [1 M]	-	-	0.5 mM	0.5 mM	-	-
$CuSO_4$ [20 mM]	-	-	0.3 mM	0.3 mM	-	-
Glucose [20%]	0.5%	0.5%	-	-	-	-
IPTG [1 M]	0.5 mM	-	-	-	-	-
Xylose [20%]	-	-	-	-	0.3%	-

4.1.4 Oligonucleotides and Plasmids

Oligonucleotides were designed with Vector NTI Advance® 11.5 (Invitrogen, Germany) or GeneTool Lite 1.0 (BioTools Inc., USA) and synthesized by either Eurofins MWG Operon (Germany) or Sigma-Aldrich (USA).
In silico plasmid construction was performed using Vector NTI Advance® 11.5 (Invitrogen, Germany). All oligonucleotides (table 5.4) and plasmids (table 5.3) used in this study are listed in the appendix section.

4.1.5 Bacterial strains

All *H. neptunium* strains used in this study were derived from *H. neptunium* ATCC15444 (wild type). For general cloning purposes *E. coli* TOP10 (Invitrogen) was used as host strain. As donor strain during conjugation *E. coli* WM3064 was used. Protein overproduction was conducted in *E. coli* Rosetta™ (DE3)/pLysS. Additionally, *C. crescentus* CB15N (NA1000) was used for heterologous expression. All strains are listed in table 5.2 (appendix section).

4.2 Microbiological methods

4.2.1 Cultivation of *E. coli*

E. coli strains were grown aerobically in LB medium at 37 °C with shaking (220 rpm) or on LB-agar plates overnight. Cultures of *E. coli* WM3064 had to be supplemented with 300 µM DAP.

4.2.2 Cultivation of *H. neptunium*

H. neptunium cells were grown in MB medium at 28 °C in baffled flasks with constant agitation (220 rpm) under aerobic conditions for 1-2 days. On MB-agar plates, cells were incubated for 3-5 days.

4.2.3 Cultivation of *C. crescentus*

C. crescentus was grown aerobically at 28 °C in PYE with shaking at 220 rpm or on PYE-agar plates.

4.2.4 Storage

Cells of *E. coli*, *H. neptunium* and *C. crescentus* grown on solid media were stored at 4 °C for a maximum of two weeks. For long-term storage, stationary cultures were supplemented with 10% DMSO and frozen at -80 °C.

4.2.5 Measurement of cell density

The cell density of liquid cultures was measured spectrophotometrically (Ultrospec 10 photometer). The corresponding medium served as blank value.

4.2.6 Synchronization of *H. neptunium* cells

A stationary pre-culture of *H. neptunium* (10 ml) was diluted into 60 ml fresh MB medium and grown overnight to an OD_{600} of 0.6. Required equipment and solutions were pre-cooled to 4 °C and all following steps were performed on ice.

Cells were harvested at 3000x g, 4 °C for 15 min and resuspended in 10-20 ml sterile 1x PBS. Subsequently, the suspension was filtrated using a 1.2 µm pore size filter membrane (Millipore) and transferred to a new tube. Prior to the second filtration step, the filtration equipment was cleaned with sterile 1x PBS. Afterwards, the cells were filtrated using a 0.8 µm pore size filter membrane (Millipore). Swarmer cells were pellet by centrifugation at 3000x g, 4 °C for 15 min. The OD_{600} was adjusted to 0.3-0.4 by addition of pre-warmed MB medium. Cells were incubated at 28 °C and samples were taken at regular intervals.

4.3 Microscopic methods

All microscopic analyses were conducted using a Zeiss Axio Observer.Z1 microscope (Zeiss, Germany) equipped with a Zeiss Plan-Apochromat 100x/1.46 Oil DIC M27 objective and a pco.edge sCMOS camera (PCO, USA). For fluorescence detection a X-Cite® 120PC metal halide light source (EXFO, Canada) along with ET-DAPI, ET-YFP, ET-GFP and ET-TexasRed filter cubes (Chroma, USA) was used. Images were processed with Metamorph 7.7.5 (Universal Imaging Group), Photoshop CS6, and Illustrator CS6 (Adobe Systems).

4.3.1 Time-lapse microscopy

In order to visualize the localization of fluorescent protein fusions over the cell cycle, cells were grown to mid-exponential phase and immobilized on 1% MB-agarose pads. To avoid drying-out, the sample was sealed with VLAP (vaseline, lanolin and paraffin at a 1:1:1 ratio). Alternatively, cells were monitored in a B04A microfluidic plate (CellASIC™ Onix, Millipore, Germany). Flow rate of the medium was adjusted to 0.25 psi. Images were taken at the indicated time points.

4.3.2 Nucleoid staining

To image the nucleoid, cells were incubated with 1.5 μg/ml DAPI (4',6-diamidino-2-phenylindole) in the dark for 15 min at RT.

4.3.3 Nascent peptidoglycan staining

For visualizing newly synthesized peptidoglycan, the fluorescent stain HADA (hydroxyl-coumarin-carbonyl-amino-D-alanine) was used. Cells in mid-exponential phase were incubated with pre-warmed HADA (final concentration: 0.5 mM) with shaking at 28 °C for 9 min (5% of the generation time). Afterwards, 100% ice-cold EtOH was added to a final concentration of 70% and cells were incubated on ice for 20 min. Cells were washed

three times with 0.5 ml 1x PBS (18,000x g, 4 min), resuspended in 20-50 µl 1x PBS or MB, and imaged (DAPI channel).

4.3.4 Immunofluorescence microscopy

For immunofluorescence analysis, cells were grown to mid-exponential phase and fixed with 2.5% paraformaldehyde supplemented with 0.008% glutaraldehyde for 15 min. After incubation on ice for 40 min, cells were washed twice in 1-2 volumes 1x PBS (centrifugation step at 12,000x g for 1 min), resuspended in 1/5 volume GTE buffer (50 mM glucose, 20 mM Tris/HCl, pH 7.6, 10 mM EDTA), and transferred to poly-L-lysine coated 8-well slides (Thermo Scientific, USA). After 10 min incubation, the liquid was aspirated off and wells were dried. Subsequently, cells were blocked with 1% BSA in 1x PBS for 15 min and incubated with an α-FtsK antibody at dilutions of 1:50 or 1:100 for 1 h at RT in a humid chamber. Cells were washed ten times with 1x PBS and incubated with the secondary antibody Alexa-Fluor 594 goat anti-rabbit (Invitrogen, Germany) at a dilution of 1:200 for 1 h at RT in the dark. Prior to microscopic analysis, SlowFade® Antifade (Invitrogen, Germany) was applied to the cells.

4.3.5 Electron Microscopy

Electron microscopy was performed in collaboration with Dr. T. Heimerl (Philipps University Marburg, Department of Biology). Samples were prepared as described [108]. Briefly, proteins were pre-centrifuged for 10 min at 16,000x g and 4 °C. *H. neptunium* FtsZ (6 µM) and *C. crescentus* FtsZ (3 µM) were incubated in the absence or presence of 2 mM GTP for 15 min at 30 °C in buffer P (50 mM HEPES/NaOH, pH 7.2, 50 mM KCl, 10 mM $MgCl_2$). Aliquots (5 µl) were withdrawn and applied to glow-discharged carbon-coated grids. After 1 min, the grids were washed with one drop of distilled water, stained with 2% uranyl acetate for 1 min, and blotted to dryness. Images were taken using a JEOL 200kV JEM-2100 transmission electron microscope (JOEL, Germany) equipped with a 2k F214 FastScan CCD camera.

4.4 Molecular biological methods

4.4.1 Isolation of chromosomal and plasmid DNA

H. neptunium chromosomal DNA was prepared using the illustra™ bacteria genomic Prep Mini Spin Kit (GE Healthcare, UK) according to the manufacturer's instructions. Plasmid DNA was isolated using the GeneElute™ Plasmid MiniPrep Kit (Sigma-Aldrich; Germany) according to the manufacturer's instructions. The concentration of DNA was determined using a Nanodrop ND-1000 spectrophotometer (Nanodrop, USA).

4.4.2 Plasmid construction

A list of all plasmids used in this study (table 5.3) as well as their detailed construction (table 5.5) can be found in the appendix section.

Plasmids for the expression of C- or N-terminal gene fusions from an inducible promoter in *H. neptunium*

In order to generate plasmids that are integrated into the *H. neptunium* genome at the P_{zn} or P_{cu} locus by single homologous recombination, genes of interest were PCR amplified using specific oligonucleotides carrying recognition sites of restriction enzymes. The PCR product and the recipient vector, containing a fragment for homologous recombination at P_{zn}/P_{cu}, were treated with the respective restriction enzymes and ligated *in-frame* as described in section 4.4.10.

Plasmids for the generation of markerless deletions or insertions in *H. neptunium*

To obtain *in-frame* deletions of specific genes, the endogenous genes were replaced by fragments containing only the terminal 10 to 12 amino acids of the target gene using double homologous recombination. To this end, ~700 bp fragments up- and downstream of the target gene were PCR-amplified and fused in a second PCR reaction by overlap extention (overlap of 9 bp). The resulting PCR product and the pNPTS138 vector were treated with the respective restriction enzymes and ligated. The pNPTS138

vector is a suicide vector, carrying a kanamycin resistance cassette and the *sacB* gene for counterselection with sucrose. After transforming *H. neptunium* with a pNPTS138 derivative, positive clones were selected on MB-Kanamycin plates (first homologous recombination). These clones were re-streaked, grown in plain MB, and finally spread onto MB plates supplemented with 0.3% sucrose to select for cells that have lost the pNPTS138 derivative (second homologous recombination). These cells contained either the wild type genotype or the markerless deletion of the target gene. Cells were tested for kanamycin sensitivity and sucrose resistance in parallel. Additionally, deletion of the gene was verified by colony PCR.

To replace native genes with fusion genes, a similar protocol was used. First, a fluorescent protein gene was fused to the 5' end of the target gene. A ~700 bp fragment downstream of the gene was PCR-amplified and inserted downstream of the gene encoding the fluorescent protein fusion. This fragment was then cloned into the pNPTS138 vector, and the resulting plasmid was used as described above.

4.4.3 Preparation of chemically competent *E. coli* cells

Chemically competent *E. coli* cells were prepared after a modified protocol from Sambrook et al. [231]. Briefly, an overnight culture of *E. coli* TOP10 was diluted 1:100 in 500 ml LB medium and incubated to an OD_{600} of ~0.6. After 10 min incubation on ice, cells were harvested at 3000x g and 4 °C for 10 min. The cell pellet was resuspended in 30 ml ice-cold 0.1 M $CaCl_2$ and incubated on ice for 30 min. Subsequently, cells were centrifuged like before, resuspended in 8 ml ice-cold 0.1 M $CaCl_2$ supplemented with 15% (v/v) glycerol and snap-frozen in liquid nitrogen (150 µl aliquots). For further use, cells were stored at -80 °C.

Preparation of chemically competent *E. coli* WM3064 cells was performed analogously, but with addition of 300 µM DAP to the medium.

4.4.4 Transformation of chemically competent *E. coli* cells

***E. coli* TOP 10**

Competent cells were thawed on ice, mixed with 15 µl of the ligation reaction, and incubated on ice for 30 min. Afterwards, cells were heat-shocked at 42 °C for 90 s, placed on ice for another 5 min, and mixed with 500 µl LB medium. The cell suspension was incubated for 30-90 min at 37 °C with agitation and spread on LB-agar plates supplemented with appropriate antibiotics. Single colonies appeared usually after ~12 h incubation at 37 °C.

***E. coli* WM3064**

In order to transform *E. coli* WM3064 cells, the following modifications to the protocol described before were applied: LB media and plates contained 300 µM DAP. Instead of 15 µl of ligation reaction, 3 µl purified plasmid DNA was added to the competent cells and the incubation after the heat-shock was performed without shaking at 37 °C.

4.4.5 Transformation of *H. neptunium*

H. neptunium cells were transformed by conjugation using *E. coli* WM3064 (dap^-) as donor strain. To this end, *E. coli* (containing the plasmid of interest) and *H. neptunium* cultures were grown to stationary phase and harvested by centrifugation at 7,600x g for 2 min. The cell pellets were washed with 1 ml MB medium supplemented with 300 µM DAP each and finally resuspended in 100 µl MB medium containing 300 µM DAP. After mixing, the two cell suspensions were spotted onto a MB-agar plate containing 300 µM DAP but no antibiotics and incubated overnight at 28 °C. Cells were scraped off the plate and resuspended in 1 ml MB medium (without DAP). Cells were washed twice with 1 ml MB medium (centrifugation at 4,600x g for 2 min), resuspended in 1 ml MB medium, and plated in dilutions of 1:10 and 1:100 on selective MB-agar plates. Single colonies appeared usually after 5 days of incubation at 28 °C.

4.4.6 Preparation of electrocompetent *C. crescentus* cells

The preparation of electrocompetent *C. crescentus* cells was performed as described [232]. Briefly, *C. crescentus* was grown in 2x PYE to an OD_{600} of 1.0 and harvested by centrifugation (6,800x g, 4 °C, 10 min). Subsequently, cells were washed twice in 1 volume ice-cold 10% glycerol, resuspended in 1/10 volume ice-cold 10% glycerol, and centrifuged at 8,600x g for 10 min at 4 °C. Finally, the cell pellet was resuspended in 1/50 volume ice-cold 10% glycerol, aliquoted á 80 µl, and snap-frozen in liquid nitrogen.

4.4.7 Transformation of electrocompetent *C. crescentus* cells

Competent cells were thawed on ice, mixed with 3-8 µl purified plasmid, and transferred into pre-cooled electroporation cuvettes (0.1 cm, Bio-Rad, Germany). Electroporation was performed at 1.5 kV, 400 Ω and 25 µF in a GenePulser XCell™ (Bio-Rad, Germany). Following this, 900 µl ice-cold 2x PYE was added, cells were incubated 2-3 h at 28 °C, and finally plated on selective PYE-agar plates.

4.4.8 Polymerase chain reaction (PCR)

Amplification of specific DNA fragments was carried out using KOD Hot Start DNA polymerase (Merck, Germany). The reaction mix and the used program are listed in table 4.5 and 4.7. Successful amplification was verified by agarose gel electrophoresis (4.4.9). PCR products were either purified with the GeneElute™ PCR Clean-up Kit or with the GeneElute™ Gel Extraction Kit (both Sigma-Aldrich, Germany).

In order to verify plasmid uptake into *E. coli* cells or correct integration of DNA fragments into the chromosome of *H. neptunium*, colony PCR using BioMix™ Red (Bioline, Germany) was performed. The reaction mix is listed in table 4.6. In the case of *H. neptunium*, cells had to be boiled for 10 min at 95 °C in water before adding them to the PCR reaction mix.

Table 4.5: Reaction mix for KOD-PCR (50 µl)

reagent	volume [µl]
10x KOD buffer	5
dNTP mix	5
DMSO (5%)	2.5
$MgSO_4$	2
forward primer (100 µM)	0.35
reverse primer (100 µM)	0.35
chromosomal DNA	2
ddH_2O	31.8
KOD polymerase (1U/µl)	1

Table 4.6: Reaction mix for colony PCR (20 µl)

reagent	volume [µl]
BioMix™	10
DMSO (5%)	1
forward primer (100 µM)	0.1
reverse primer (100 µM)	0.1
DNA	2
ddH_2O	6.8

Table 4.7: PCR cycling parameters

step	temperature [°C]	time [min]	
1. initial denaturation	95	2	
2. denaturation	95	0.5	
3. primer annealing	65	0.5	25-35 cycles
4. elongation	72	0.5 pro kb	
5. final elongation	72	4	

4.4.9 Agarose gel electrophoresis

DNA samples were mixed with 10x loading dye (50% (v/v) glycerol, 0.2% bromophenol blue, 0.2% xylene cyanol FF, 0.2 M EDTA) and applied onto a 1% agarose gel containing 0.005% (v/v) ethidium bromide for visualization. Agarose gels were prepared in 0.5x TAE buffer (2.42 g/l Tris base, 0.57 ml/l glacial acetic acid, 0.19 g/l EDTA).

4.4.10 Restriction and ligation

For DNA digestion, 1-5 µg DNA was incubated with selected restriction endonucleases (NEB, USA; Fermentas, Canada) and the recommended buffer for 1-12 h at 37 °C. If necessary, 0.1 mg/ml bovine serum albumin (BSA, NEB, USA) was added to the mixture. To dephosphorylate 5' ends of plasmid backbones for cloning, DNA was additionally treated with alkaline phosphatase (SAP or fastAP, Fermentas, Canada). Digested DNA products were either purified with the GeneElute™ PCR Clean-up Kit or, after gel electrophoresis, with the GeneElute™ Gel Extraction Kit (both Sigma-Aldrich, Germany).
For DNA ligation, the DNA insert together with the recipient vector (molar ratio 3:1) was incubated with T4 DNA ligase in "rapid ligation buffer" (Fermentas, Canada) according to the manufacturer's instructions for 10-60 min at RT.

4.4.11 DNA sequencing

Sequencing of DNA products was performed by Eurofins MWG Operon (Germany). In general, 50-100 ng of plasmid DNA or PCR product was provided together with suitable oligonucleotides. Obtained sequences were analyzed with Vector NTI Advance® 11.5 (Invitrogen, Germany).

4.5 Biochemical methods

4.5.1 Protein detection (SDS-PAGE)

To separate proteins according to their mass, denaturing SDS polyacrylamide gels were used [233]. Protein samples were prepared as follows: Cells were collected by centrifugation at 18,000x g for 1 min. Next, cell pellets were resuspended in 2x SDS sample buffer (125 mM Tris base, 20% (v/v) glycerol, 2% (w/v) SDS, 200 mM DTT, 0.001% (w/v) bromophenol blue, pH 6.8) according to their optical density (100 µl buffer per 1 ml of suspension with an OD_{600} of 1) and heated at 95 °C for 10-15 min. Samples taken during biochemical assays (protein purification, Co-IP) were mixed with 2x SDS sample buffer in a ratio of 1:1 and heated at 95 °C for 10-15 min as well. Together with a molecular mass marker (PageRuler™ Prestained Protein Ladder; Fermentas, Canada), protein samples were loaded to an SDS gel consisting of a 5% stacking gel and an 11% resolving gel. For the composition of SDS gels, see table 4.8. The electrophoretic separation was carried out in 1x SDS running buffer (25 mM Tris base, 192 mM glycerol, 1% (w/v) SDS) at 15-30 MA per gel using the PerfectBlue™ Twin S system (Peqlab, USA).
To visualize the separated proteins, SDS gels were stained in Coomassie (40% methanol, 10% acetic acid glacial, 0.1% Coomassie Brilliant Blue R250) and destained (20% ethanol, 10% acetic acid glacial).

4.5.2 Immunoblot analysis

For immunoblot analysis, proteins were separated by SDS-PAGE as described before and transferred onto a polyvinylidene fluoride (PVDF) membrane (Millipore, USA) by semi-dry transfer. To this end, the membrane was first activated in 100% methanol for 15 sec, washed in H_2O for 2 min, and equilibrated in 1x Western transfer buffer (25 mM Tris base, 192 mM glycerol, 10% methanol) for 5 min. The transfer of the proteins onto the membrane was performed at 2 mA/cm^2 for 1.5-2 h using a PerfectBlue™ Semi-Dry-Electro blotter (Peqlab, USA). The membrane was then blocked with 2.5-5% non-fat milk in 1x TBST (10 mM Tris base, 150 mM NaCl, 0.1% (w/w) Tween 20, pH 7.5)

Table 4.8: Composition of an 11% resolving gel and a 5% stacking gel

component	5% stacking gel (2.5 ml)	11% resolving gel (5 ml)
ddH_2O	1.43 ml	1.9 ml
4x stacking buffer (0.5 M Tris base, 0.4% (w/v) SDS, pH 6.8)	625 µl	-
4x resolving buffer (1.5 M Tris base, 0.4% (w/v) SDS, pH 8.8)	-	1.25 ml
30% Rotiphorese® Acrylamide/Bis (29:1)	417 µl	1.9 ml
TEMED (N,N,N',N'-Tetramethylethylendiamine)	1.9 µl	3 µl
10 % (w/v) APS (Ammoniumperoxodisulfate)	25 µl	40 µl

overnight at 4 °C with gentle agitation. In order to detect proteins, the membrane was incubated with the primary antibody (table 4.9), diluted in 2.5-5% non-fat milk in 1x TBST, at RT for 1-2 h on a shaker. Before incubating the membrane with the secondary antibody for 1-2 h, it was washed three times in 1x TBST. As secondary antibody an α-rabbit horseradish peroxidase-coupled antibody (Perkin Elmer, USA) was used. The membrane was rinsed five times with 1x TBST and incubated with Western Lightning™ Chemiluminescence Reagent Plus (PerkinElmer, USA) according to the manufacturer's instructions for 1 min. Visualization of the signal was achieved by exposing the membrane to Amersham Hyperfilm™ ECL-Chemiluminescence films (GE Healthcare, UK) followed by development with a LAS-4000 Luminescent Image Analyzer (Fujifilm, Germany). Alternatively, the signal was visualized with the ChemiDoc™ MP Imaging System (Bio-Rad, USA).

Table 4.9: Primary antibodies used for immunoblot analysis

antibody	dilution	reference
α-GFP	1:10,000	Sigma-Aldrich, Germany
α-HA	1:8,000	Millipore, Germany
α-FtsZ	1:20,000	this study
α-FtsK	1:20,000	this study

4.5.3 Protein purification and antibody synthesis

In order to obtain **native FtsZ**, His_6-SUMO-FtsZ was overproduced and purified. To this end, plasmid pSE91 was transferred into *E. coli* Rosetta™ (DE3)/pLysS and cells were grown in 2x 750 ml LB medium supplemented with the respective antibiotics to an OD_{600} of ~1 at 37 °C with gentle agitation. By addition of 0.5 mM IPTG, protein overproduction was started and carried out by incubating the cells at 37 °C for 3 h with agitation. Cells were harvested at 7,500x g and 4 °C for 10 min, resuspended in 1/10 volume buffer BZ3 (50 mM Tris/HCl, pH 8.0, 300 mM KCl, 20 mM imidazole, 10% (v/v) glycerol), pelleted (8,600x g, 4 °C, 10 min), and snap-frozen in liquid nitrogen. For the purification, the pellet was resuspended in 12 ml buffer BZ3 containing 100 µg/ml PMSF and 10 U/ml DNaseI followed by cell lysis in a French Press (three passages at 16,000 psi). Cell debris was removed by centrifugation at 30,000x g and 4 °C for 30 min and the lysate was applied onto a HisTrap HP 5 ml column (GE Healthcare, UK) that had been equilibrated with 25 ml buffer BZ3 before. After washing the column with 25 ml buffer BZ3, the protein was eluted by applying 50 ml of a linear imidazole gradient (20-250 mM imidazole). Selected elution fractions were dialyzed against 3 l buffer CB (50 mM Tris/HCl, pH 8.0, 150 mM KCl, 10% (v/v) glycerol) overnight. To cleave off the His_6-SUMO tag, the protein was incubated with His_6-Ulp1 protease at a molar ratio of 1000:1 and 1 mM DTT for 2 h at 4 °C. After centrifugation at 13,000x g and 4 °C for 30 min, the cleavage reaction was applied onto a HisTrap HP 5 ml column equilibrated with buffer CB. The native FtsZ protein could be found in the flow-through fraction, whereas the His_6-SUMO tag and the His_6-Ulp1 protease are bound to the column. FtsZ was finally dialyzed against 3 l buffer A4 (50 mM HEPES/NaOH, pH 7.2, 50 mM KCl, 0.1 mM EDTA, 10% (v/v) glycerol) overnight, concentrated where necessary, snap-frozen in liquid nitrogen and stored at -80 °C until further use. For purification of FtsZ-His_6, plasmid pSE33 was transferred into *E. coli* Rosetta™ (DE3)/pLysS. Cells were grown in 4x 750 ml LB medium supplemented with the corresponding antibiotics to an OD_{600} of 1 at 37 °C. Expression was induced with 0.5 mM IPTG. After incubation for 3 h at 37 °C, cells were harvested by centrifugation (7,500x g, 10 min, 4 °C) and washed twice in buffer B1 (50 mM NaH_2PO_4, 300 mM NaCl, 10 mM imidazole, pH 8.0). After resuspension in buffer B2 (50mM NaH_2PO_4, 300 mM NaCl,

10 mM imidazole, 1 mM β-mercaptoethanol, pH 8.0) supplemented with 100 µg/ml PMSF and 10 U/ml DNase I, cells were lysed by 2-3 passages in a French press (16,000 psi). Cell debris was removed by centrifugation at 30,000x g and 4 °C for 30 min. The cleared lysate was applied onto a HisTrap HP 5 ml column (GE Healthcare, UK) that had been equilibrated with 5 volumes buffer B3 (50 mM NaH_2PO_4, 300 mM NaCl, 20 mM imidazole, 1 mM β-mercaptoethanol, pH 8.0). The column was washed with 5 volumes buffer B3. Subsequently, proteins were eluted with 10 volumes of a linear imidazole gradient (20-250 mM imidazole) using buffer B3 and B4 (50 mM NaH_2PO_4, 300 mM NaCl, 250 mM imidazole, pH 8.0). Selected elution fractions were dialyzed against 3 l buffer B6 (50 mM HEPES/NaOH, pH 7.2, 50 mM NaCl, 5 mM $MgCl_2$, 0.1 mM EDTA, 10% glycerol, 1 mM β-mercaptoethanol) overnight, snap-frozen, and stored at -80 °C until further use.

To purify **His_6-FtsK$_{\Delta 1\text{-}180}$**, plasmid pSE56 was transferred into *E. coli* Rosetta™ (DE3)pLysS and proceeded as described for FtsZ-His_6.

For antibody production, purified proteins were sent to Eurogentec (Belgium).

4.5.4 Crosslinking, Co-IP and mass spectrometry

For co-immunoprecipitation of FtsZ-HA, strains SE144 (P_{zn}::P_{zn}-*ftsZ-HA*) and the *H. neptunium* wild type were grown in 500 ml MB medium. Expression of FtsZ-HA was induced with 0.5 mM $ZnSO_4$ for 3 h. Proteins were crosslinked by addition of 0.6% para-formaldehyde (in 1x PBS) for 20 min at 37 °C. The reaction was stopped with 125 mM glycine (in ddH_2O) for 5 min at RT. Cells were harvested by centrifugation (8,600x g, 10 min, 4 °C) and washed twice with 250 ml wash buffer 1 (50 mM $NaPO_4$, pH 7.4, 5 mM $MgCl_2$) and once with 25 ml wash buffer 1. Cell pellets (~1 g) were snap-frozen in liquid nitrogen and stored at -80 °C. Pellets were thawed on ice, washed with 100 ml Co-IP buffer (20 mM HEPES/NaOH, pH 7.4, 100 mM NaCl, 20% glycerol, 0.5% Triton X-100), and resuspended finally in 15 ml Co-IP buffer. After addition of 10 mM $MgCl_2$, 5 µg/ml DNase I, 100 µg/ml PMSF, and 10 mg/ml lysozyme, the cell suspension was incubated on ice for 30 min, followed by 3-4 passages in a French press (16,000 psi). Cell debris was removed by centrifugation (30,000x g, 10 min, 4 °C). 2 ml of the cleared lysate were

mixed with 100 µl Ezview™ Red anti-HA affinity gel (Sigma-Aldrich, Germany), which had been equilibrated two times with Co-IP buffer before. The mixture was incubated for 2 h at 4 °C on a rotary shaker. After centrifugation (5,900x g, 2 min, 4 °C), the affinity gel-sample complexes were washed once with 750 µl Co-IP buffer, once with 750 µl wash buffer 2 (50 mM Tris/HCl, pH 8.0, 150 mM NaCl, 1 mM EDTA, 0.5% Triton X-100), and once with 750 µl wash buffer 3 (100 mM Tris/HCl, pH 8.0, 750 mM NaCl, 1 mM EDTA, 0.05% Triton X-100). Precipitated proteins were eluted with 100 µl SDS sample buffer without DTT and submitted to mass spectrometry analysis, performed in collaboration with Jörg Kahnt (Department of Ecophysiology, MPI Marburg).

4.5.5 Non-radioactive GTPase assay

The GTPase activity of purified proteins was measured by a phosphate assay based on ammonium molybdate [234]. Briefly, FtsZ proteins were pre-incubated for 10 min at 30 °C in buffer P (50 mM HEPES/NaOH, pH 7.2, 50 mM KCl, 10 mM $MgCl_2$). The reaction was started by addition of GTP (Jena Bioscience, Germany) to a final concentration of 2 mM. At the indicated time points, 150 µl samples were taken and mixed with 450 µl SolD. This solution is instable and has to be prepared freshly from 2 volumes SolA (12% (w/v) ascorbic acid dissolved in 1 M HCl) and 1 volume SolB (2% (w/v) ammonium molybdate tetrahydrate dissolved in H_2O). The mixture was incubated for 5 min at RT. After addition of 450 µl SolF (2% (w/v) sodium citrate, 2% (v/v) acetic acid dissolved in H_2O), the solution was incubated for 15 min at RT and finally measured spectrophotometrically at 655 nm. The amount of phosphate in the solution was calculated from a standard curve obtained with different concentrations of KH_2PO_4.

4.5.6 Polymerization assay

In order to evaluate the capability of purified FtsZ to form polymers, the protein was incubated with or without 2 mM GTP in buffer P (50 mM HEPES/NaOH, pH 7.2, 50 mM KCl, 10 mM $MgCl_2$) at 25 °C for 20 min. Afterwards, the solution was ultra-centrifuged

at 254,000x g and 25 °C for 15 min and the supernatant was removed. To visualize the polymers, pellet fractions were applied onto a SDS gel and stained with Coomassie blue.

4.5.7 Right angle light scattering

Experiments were performed at 25 °C with 10 µM $FtsZ_{HNE}$ or 10 µM $FtsZ_{CC}$, in buffer P (50 mM HEPES/NaOH, pH 7.2, 50 mM KCl, 10 mM $MgCl_2$). The excitation and emission wavelength of the temperature-controlled ISS PC1 spectrofluorometer (ISS Inc., USA) were set to 350 nm. The filamentation was started after 100 s by addition of 2 mM GTP and followed for 500 s.

4.5.8 Bioinformatic and statistical methods

All *H. neptunium* nucleotide and amino acid sequences were obtained from NCBI (`http://www.ncbi.nlm.nih.gov/`). Homologous proteins were identified using the NCBI Blastp algorithm. Conserved protein domains were identified with the help of the SMART (`http://smart.embl-heidelberg.de/`) or Pfam (`http://pfam.xfam.org/search`) search. Transmembrane domains and signal sequences were predicted using TMHMM and SignalP (both on `http://expasy.org`). Protein sequence alignments were generated with ClustalW2 (`http://www.ebi.ac.uk/Tools/msa/clustalw2/`) and processed with Jalview 2.8 [235]. For statistical analyses Origin 6.1 (OriginLab, USA) and Boxplot Webtool (`http://boxplot.tyerslab.com/`) was used. Demographs were generated by measuring the fluorescence intensity profiles with ImageJ 1.47v. The data were then processed in R (version 3.1.1.) using the cell profiles script (`http://github.com/tacameron/Cell-Profiles`) [180]. Immunoblots were analyzed with Image Lab 5.0 (Bio-Rad, USA).

5 Appendix

Table 5.1: Homologs of *C. crescentus* cell division proteins identified in *H. neptunium* by BLAST analysis

Protein	*H. neptunium*	*C. crescentus*
FtsZ	HNE_0390	CCNA_02623
MipZ	HNE_1128	CCNA_02246
FzlA	HNE_3104	CCNA_03754
FzlC	HNE_3371	CCNA_00099
ZapA	HNE_3457	CCNA_03356
FtsA	HNE_0391	CCNA_02624
FtsE	HNE_3390	CCNA_02299
FtsX	HNE_3391	CCNA_02300
FtsK	HNE_3541	CCNA_03819
FtsQ	HNE_0392	CCNA_02625
FtsL	HNE_3031	CCNA_02644
FtsB	HNE_1978	CCNA_01797
FtsI	HNE_3030	CCNA_02643
FtsW	HNE_3025	CCNA_02635
FtsN	HNE_2049	CCNA_02086
TolA	HNE_0153	CCNA_03339
TolQ	HNE_0151	CCNA_03341
TolR	HNE_0152	CCNA_03340
TolB	HNE_0154	CCNA_03338
Pal	HNE_0155	CCNA_03337
AmiC	HNE_0674	CCNA_01952
DipM	-	CCNA_02075

Table 5.2: Used strains

Strain	Genotype	Reference/Construction
ATCC15444	*H. neptunium* wild type strain	American Type Culture Collection
WS14	ATCC15444 Δ*hfsB*	[179]
CB15N	synchronizable derivative of wild type *C. crescentus*	[236]
TOP10	F- *mcrA* Δ(*mrr-hsdRMS-mcrBC*) ϕ80*lacZ*ΔM15 Δ*lacX74 nupG recA1 araD139* Δ(ara-leu)7697 *galE15 galK16 rpsL*(Str^R) *endA1* λ-	Invitrogen
WM3064	*thrB1004 pro thi rpsL hsdS lacZ*ΔM15 *RP4-1360* Δ(*araBAD)567* Δ*dapA1341*::[*erm pir* (wt)]	W. Metcalf, University of Illinois
Rosetta™ (DE3) pLysS	F *ompT hsdSB*(*rB- mB-*) *gal dcm* (DE3) pLysSRARE2 (Cam^R	Novagen
AR46	ATCC15444 Δ*HNE0708*	[185]
EC205	ATCC15444 Δ*bacAB*	E. Cserti (unpublished)
WS09	ATCC15444 *ftsK*::*ftsK-venus*	[179]
JZ13	ATCC15444 P_{zn}::P_{zn}-*venus-tolQ*	[237]
JZ28	ATCC15444 *ftsQ*::*ftsQ-mCherry*	[237]
JZ29	ATCC15444 *ftsE*::*venus-ftsE*	[237]
JZ49	ATCC15444 *ftsA*::*venus-ftsA*	J. Zimmer (this study) Replacement of *ftsA* with *venus-ftsA* in ATCC15444 using pJZ26

Table 5.2: used strains: continued

Strain	Genotype	Reference/Construction
JZ50	ATCC15444 *fzlA*::*venus-fzlA*	J. Zimmer (this study) Replacement of *fzlA* with *venus-fzlA* in ATCC15444 using pJZ28
JZ51	ATCC15444 *ftsW*::*venus-ftsW*	J. Zimmer (this study) Replacement of *ftsW* with *venus-ftsW* in ATCC15444 using pJZ27
SE38	WS14 P_{zn}::P_{zn}-*gfp-zapA*	[238]
SE71	ATCC15444 P_{zn}::P_{zn}-*venus-ftsK*	this study Integration of pSE23 in ATCC15444
SE74	ATCC15444 P_{zn}::P_{zn}-*ftsZ-venus*	[238]
SE76	ATCC15444 P_{zn}::P_{zn}-*gfp-ftsA* [238]	[238]
SE77	ATCC15444 P_{zn}::P_{zn}-*venus-ftsN*	[238]
SE89	Rosetta™ (DE3) pLysS carrying pSE33	[238]
SE94	ATCC15444 P_{zn}::P_{zn}-*ftsZ*	[238]
SE96	ATCC15444 P_{zn}::P_{zn}-*ftsN*	[238]
SE97	ATCC15444 Δ*ftsZ* P_{zn}::P_{zn}-*ftsZ*	this study Deletion of *ftsZ* in SE94 using pSE38
SE99	ATCC15444 Δ*ftsN* P_{zn}::P_{zn}-*ftsN*	this study Deletion of *ftsN* in SE96 using pSE40
SE104	ATCC15444 P_{zn}::P_{zn}-*ftsA-venus*	this study Integration of pSE24 in ATCC15444
SE106	ATCC15444 P_{zn}::P_{zn}-*mipZ-venus*	this study Integration of pSE44 in ATCC15444

Table 5.2: used strains: continued

Strain	Genotype	Reference/Construction
SE113	ATCC15444 Δ*mipZ* P_{zn}::P_{zn}-*ftsZ-venus*	this study Integration of pSE14 in SE124
SE124	ATCC15444 Δ*mipZ*	this study Deletion of *mipZ* in ATCC15444 using pAR24
SE133	Rosetta™ (DE3) pLysS carrying pSE56	this study
SE141	ATCC15444 Δ*ftsN* P_{zn}::P_{zn}-*ftsN* P_{cu}::P_{cu}-*ftsZ-venus*	this study Integration of pSE58 in SE97
SE144	ATCC15444 P_{zn}::P_{zn}-*ftsZ-HA*	this study Integration of pSE63 in ATCC15444
SE147	ATCC15444 Δ*ftsZ* P_{zn}::P_{zn}-*ftsZ* P_{cu}::P_{cu}-*ftsK-venus*	this study Integration of pSE59 in SE97
SE148	ATCC15444 Δ*ftsN* P_{zn}::P_{zn}-*ftsN* P_{cu}::P_{cu}-*ftsK-venus*	this study Integration of pSE59 in SE99
SE150	ATCC15444 P_{zn}::P_{zn}-$ftsK_{aa1\text{-}185}$-*venus*	this study Integration of pSE57 in ATCC15444
SE151	ATCC15444 P_{zn}::P_{zn}-*ftsK-venus*	this study Integration of pSE54 in ATCC15444
SE152	ATCC15444 P_{zn}::P_{zn}-*venus-fzlC*	this study Integration of pSE64 in ATCC15444
SE156	ATCC15444 P_{zn}::P_{zn}-$ftsK_{K487A}$	this study Integration of pSE67 in ATCC15444
SE157	ATCC15444 P_{zn}::P_{zn}-*ftsZ'-venus-'ftsZ*	this study Integration of pSE69 in ATCC15444

Table 5.2: used strains: continued

Strain	Genotype	Reference/Construction
SE158	ATCC15444 Δ*HNE0708* P_{zn}::P_{zn}-*ftsZ*-*venus*	this study Integration of pSE14 in AR46
SE159	ATCC15444 Δ*HNE0708* P_{zn}::P_{zn}-*ftsK*-*venus*	this study Integration of pSE54 in AR46
SE161	ATCC15444 *ftsI*::*venus-ftsI*	this study Replacement of *ftsI* with *venus-ftsI* in ATCC15444 using pSE68
SE170	ATCC15444 Δ*mipZ* P_{zn}::P_{zn}-$mipZ_{D62A}$	this study Integration of pSE75 in SE124
SE174	ATCC15444 Δ*bacAB* P_{zn}::P_{zn}-*ftsZ*-*venus*	this study Integration of pSE14 in EC205
SE175	ATCC15444 Δ*bacAB* P_{zn}::P_{zn}-*ftsK*-*venus*	this study Integration of pSE54 in EC205
SE181	ATCC15444 *fzlC*::*venus-fzlC*	this study Replacement of *fzlC* with *venus-fzlC* in ATCC15444 using pSE76
SE194	Rosetta™ (DE3) pLysS carrying pSE91	this study
SE195	CB15N P_{xyl}::P_{xyl}-*ftsK*-*venus*	this study Integration of pSE93 in CB15N
SE197	ATCC15444 P_{zn}::P_{zn}-$TALE_{ftsK}$	this study Integration of pSE94 in ATCC15444
SE203	ATCC15444 *ftsN*::*venus-ftsN*	this study Replacement of *ftsN* with *venus-ftsN* in ATCC15444 using pSE96

Table 5.3: Used plasmids

Plasmid	Genotype/description	Reference/Source
pCCHYC-2	pXCHYC-2-based, integrating vector for constructing C-terminal fusions to mCherry under the control of P_{cu}, Kan^R	[192]
pET21a(+)	Vector for overexpression of C-terminally His_6-tagged proteins, Amp^R	Novagen
pET28a(+)	Vector for overexpression of N-terminally His_6-tagged proteins, Kan^R	Novagen
pNPTS138	*sacB*-containing suicide vector for double homologous recombination	M. R. K. Alley, unpublished
pXCHYC-2	Integrating plasmid for constructing C-terminal fusions to mCherry under the control of P_{xyl}, Kan^R	[239]
pXCHYN-2	Integrating plasmid for constructing N-terminal fusions to mCherry under the control of P_{xyl}, Kan^R	[239]
pXCFPC-2	Integrating plasmid for constructing C-terminal fusions to CFP under the control of P_{xyl}, Kan^R	[239]
pXCFPN-2	Integrating plasmid for constructing N-terminal fusions to CFP under the control of P_{xyl}, Kan^R	[239]
pXGFPC-2	Integrating plasmid for constructing C-terminal fusions to GFP under the control of P_{xyl}, Kan^R	[239]
pXGFPN-2	Integrating plasmid for constructing N-terminal fusions to GFP under the control of P_{xyl}, Kan^R	[239]
pXVENC-2	Integrating plasmid for constructing C-terminal fusions to Venus under the control of P_{xyl}, Kan^R	[239]
pXVENN-2	Integrating plasmid for constructing N-terminal fusions to Venus under the control of P_{xyl}, Kan^R	[239]

Table 5.3: used plasmids: continued

Strain	Genotype/description	Reference/Source
14AEDVYC	plasmid carrying $TALE_{FtsK}$	Life Technologies, USA
pAR24	pNPTS138 derivative for generating an *in-frame* deletion in *mipZ*	[185]
pTB146	Vector for overexpression of N-terminally His_6-SUMO-tagged proteins, Amp^R	[240]
pKH8	Integrating vector for constructing C-terminal fusions to mCherry under the control of P_{zn}, Rif^R	[241]
pJZ07	pSE51 derivative carrying *ftsE*	[237]
pJZ09	pSE51 derivative carrying *tolQ*	[237]
pJZ16	pNPTS138 derivative for replacing native *ftsQ* with *ftsQ-mCherry*	[237]
pJZ17	pNPTS138 derivative for replacing native *ftsE* with *venus-ftsE*	[237]
pJZ26	pNPTS138 derivative for replacing native *ftsA* with *venus-ftsA*	J. Zimmer (this study)
pJZ27	pNPTS138 derivative for replacing native *ftsW* with *venus-ftsW*	J. Zimmer (this study)
pJZ28	pNPTS138 derivative for replacing native *fzlA* with *venus-fzlA*	J. Zimmer (this study)
pSE04 (pZGFPC-2)	pXGFPC-2-based, integrating vector for constructing C-terminal fusions to GFP under the control of P_{zn}, Kan^R	[178]
pSE14	pSE31 derivative carrying *ftsZ-venus*	[238]

Table 5.3: used plasmids: continued

Strain	Genotype/description	Reference/Source
pSE16	pXGFPN-2-based, integrating vector for constructing N-terminal fusions to GFP under the control of P_{zn}(2), Kan^R	[238]
pSE23	pSE32 derivative carrying *venus-ftsK*	this study
pSE24	pSE31 derivative carrying *ftsA-venus*	this study
pSE25	pSE32 derivative carrying *venus-ftsI*	[238]
pSE26	pSE32 derivative carrying *venus-ftsN*	[238]
pSE27 (pZGFPN-2)	pXGFPN-2-based, integrating vector for constructing N-terminal fusions to GFP under the control of P_{zn}, Kan^R	[178]
pSE28 (pZCHYC-2)	pXCHYC-2-based, integrating vector for constructing C-terminal fusions to mCherry unter the control of P_{zn}, Kan^R	[178]
pSE31	pXVENC-2 -based, integrating vector for constructing C-terminal fusion to Venus under the control of P_{zn}(2), Kan^R	[238]
pSE32	pXVENN-2 -based, integrating vector for constructing N-terminal fusion to Venus under the control of P_{zn}(2), Kan^R	[238]
pSE33	pET21a(+) derivative carrying *ftsZ*	[238]
pSE35	pKH8 derivative carrying *ftsZ*	[238]
pSE37	pKH8 derivative carrying *ftsN*	[238]
pSE38	pNPTS138 derivative for generating an *in-frame* deletion in *ftsZ*	[238]

Table 5.3: used plasmids: continued

Strain	Genotype/description	Reference/Source
pSE40	pNPTS138 derivative for generating an *in-frame* deletion in *ftsN*	[238]
pSE44	pSE31 derivative carrying *mipZ-venus*	this study
pSE49 (pZCHYN-2)	pXCHYN-2-based, integrating vector for constructing N-terminal fusions to mCherry under the control of P_{zn}, Kan^R	[178]
pSE50 (pZVENC-2)	pXVENC-2-based, integrating vector for constructing C-terminal fusions to Venus under the control of P_{zn}, Kan^R	[178]
pSE51 (pZVENN-2)	pXVENN-2-based, integrating vector for constructing N-terminal fusions to Venus under the control of P_{zn}, Kan^R	[178]
pSE52 (pZCFPC-2)	pXCFPC-2-based, integrating vector for constructing C-terminal fusions to CFP under the control of P_{zn}, Kan^R	[178]
pSE53 (pZCFPN-2)	pXCFPN-2-based, integrating vector for constructing N-terminal fusions to CFP under the control of P_{zn}, Kan^R	[178]
pSE54	pSE50 derivative carrying *ftsK*	this study
pSE56	pET28a(+) derivative carrying $ftsK_{aa1\text{-}180}$	this study
pSE57	pSE50 derivative carrying $ftsK_{\Delta aa186\text{-}837}$	this study
pSE58	pCCHYC-2 derivative carrying *ftsZ-venus*	this study
pSE59	pCCHYC-2 derivative carrying *ftsK-venus*	this study
pSE63	pSE50 derivative carrying *ftsZ-HA*	this study

Table 5.3: used plasmids: continued

Strain	Genotype/description	Reference/Source
pSE64	pSE32 derivative carrying *venus-fzlC*	this study
pSE67	pSE50 derivative carrying $ftsK_{K487A}$	this study
pSE68	pNPTS138 derivative for replacing native *ftsI* with *venus-ftsI*	this study
pSE69	pSE50 derivative carrying the *ftsZ* sandwich fusion	this study
pSE75	pSE52 derivative carrying $mipZ_{D62A}$	this study
pSE76	pNPTS138 derivative for replacing native *fzlC* with *venus-fzlC*	this study
pSE84	pET21a(+) derivative carrying *ftsZ* (with stop codon)	this study
pSE91	pTB146 derivative carrying *ftsZ*	this study
pSE93	pXVENC-2 derivative carrying *ftsK*	this study
pSE94	pSE53 derivative carrying $TALE_{ftsK}$	this study
pSE96	pNPTS138 derivative for replacing native *ftsN* with *venus-ftsN*	this study

Table 5.4: Used oligonucleotides

Name	Sequence (5' - 3')
RecUni-1	atgccgtttgtgatggcttccatgtcg
M13for	gccagggttttcccagtcacga
M13rev	gagcggataacaatttcacacagg
eGYC-down	gctgctgcccgacaaccactacctgag
eGYC-up	cttgccgtaggtggcatcgccctcg
mCherry-up	ctcgccctcgccctcgatctcgaac
mCherry-down	ggcgcctacaacgtcaacatcaagttgg

Table 5.4: used oligonucleotides: continued

Name	Sequence (5' - 3')
REV-uni	ggggatgtgctgcaaggcgattaagttg
pET-for	cacgatgcgtccggcgtagaggatc
pET-rev	cctttcagcaaaaaacccctcaagacccg
RecZn-2	aggcaaccagcacgaacgccagc
P2372_check_fwd	cgcgggcgatgttgaggaagttctg
pCop1486_out_for	cgaagtccgccgtggccgag
pCop1486_check_for	ccccttatcatccagaccagctacg
pCop1486_check_rev	ggcttttgatttttgacgtcgag
P_{xyl}-for	tgtcggcggcttctagcatggaccg
oAR188	gcggcatatgcccgctgacggcgtcgctcat
oAR189	aggtaccgaagtcgatgctggcgccggcaagc
oJZ48	atggatccgccattgagaaagaccgaaacagcg
oJZ59	gtttgccatggtaccatgcatattaattaaggcgcc
oJZ60	gcgcacctgatggtgagcaagggcgaggagctg
oJZ61	catggtaccatggcaaacctctcggcaaaacgc
oJZ62	gctcaccatcaggtgcgctcaccggcggg
oJZ63	ataagcttctggatgggcgggtcgatgtc
oJZ64	ataagcttgccaaggggccgcaaaaggtg
oJZ65	gctcaccatgcggtcaccttgaggctcgcc
oJZ66	atagctcacggtaccatgcatattaattaaggcgcc
oJZ67	ggtgaccgcatggtgagcaagggcgaggagctg
oJZ68	catggtaccgtgagctatacggccaacgcaccg
oJZ69	atggatccgtcgagctggtagctgtcgagtggc
oJZ70	ataagcttcgccctggacaataaggtcgcc
oJZ71	gctcaccatgaattatactgtggataacatgcg
oJZ72	tcgcagcatggtaccatgcatattaattaaggcgcc
oJZ73	gtataattcatggtgagcaagggcgaggagctg
oJZ74	catggtaccatgctgcgactgtatcactggcccc
oJZ75	atggatccccgttcttttagccgggctgcg
oKH34	atttccactggatgggcagcaaaac
oSE15	cgcgggcgatgttgaggaagttctg
oSE16	aattaacatatgacccaagaactcagacccaaaatcg

Table 5.4: used oligonucleotides: continued

Name	Sequence (5' - 3')
oSE17	atgagctccgttattggcggaccggcgcag
oSE18	aattaacatatgacagattacgccagccgcgacac
oSE19	atgagctccagctgcgctggccttgccgttg
oSE28	caccggcatcggcctctattgcg
oSE29	ttccttgatgcggccacggatgc
oSE30	ccttgccggcgaccagcatcagg
oSE37	aacaccatgtgggcgccttcaagatggaggc
oSE38	ggcgcccacatggtgttcatcgccgcgggcatg
oSE39	atgagctcgcatgacagattacgccagccgcgacac
oSE40	aattagctagcttaagctgcgctggccttgccgttg
pSE41	aattaacatatggcaaacctctcggcaaaacgcctcg
pSE42	atgagctccgaaattttccttcagccagcgcagcg
oSE47	atggtacctcagttattggcggaccggcg
oSE48	aattaacatatgagccgatcggacatggcaggcc
oSE49	atggtaccttatcccgtcaccacgatgcaatttg
oSE50	atgagctcttaagctgcgctggccttgccgttg
oSE51	aattctgcaggtggccagcatgtcaccgcagacc
oSE52	gaaggcgggaacgacgattttgggtctgagttc
oSE53	atcgtcgttcccgccttcctgcgccggtccg
oSE54	atggatccgcttggggccgtcaataacttcaac
oSE55	aattctgcaggaagcccaggtcgccgcgctctc
oSE56	tgccccggagttttcgcggcctgccatgtcc
oSE57	cgcgaaaactccggggcaaattgcatcgtggt
oSE58	atggatcctcatgaccttggagaccgtggcg
oSE63	cgggccttggcacgctgatcgag
oSE64	tgggaaaccctcgaaggcctcgtc
oSE66	gcaacacatcgcagcccgccacg
oSE67	gcaacacatcgcagcccgccacg
oSE73	aattaacatatgggccgccgcgatgcccagctg
oSE74	atggatccttaagctgcgctggccttgccgttg
oSE75	atgagctccctgggcatcgcggcggccaaag
oSE77	atgagctcttaagcgtagtctgggacgtcgtatgggtagttattggcggaccggcgcag

Table 5.4: used oligonucleotides: continued

Name	Sequence (5' - 3')
oSE78	atggtaccttggccgagagcgagtctgatttc
oSE79	atgagctctcaggcgggcgtttcgcggatg
oSE82	cggttcgggtgcatcggtcggcgtcaacg
oSE83	gccgaccgatgcacccgaaccggtggt
oSE84	caccatgctcgatccgctctcggcgcgcgagcgggcgagg
oSE85	gccgagagcggatcgagcatggtgagcaagggcgaggagc
oSE86	ctgcatacccggtgcaccagacttgtacagctcgtccatgccg
oSE87	tacaagtctggtgcaccgggtatgcagctccagcttggccttg
oSE88	aattaaaagcttgcagagcgcatattgaagcccggc
oSE89	cttgctcaccatctgggcgcctccgcagg
oSE90	ggcgcccagatggtgagcaagggcgaggagctg
oSE91	atggatccaggcgtatcgctggcgcggttgg
oSE92	ggccgtatccgcgtctccgtggtg
oSE93	gcggcggttgtcgaggaagctgt
oSE94	ggggctggccgacctgaaaccg
oSE95	tcattgatctcgcagtccgccagcgctc
oSE96	gcgctggcggactgcgagatcaatgac
oSE97	atggtacctcagaagtcgatgctggcgccggca
oSE98	aattaaaagctttatttcgctttagggagaggggatg
oSE99	cttgctcaccatggctggacctatccccgaactctg
oSE100	ggtccagccatggtgagcaagggcgaggagctg
oSE101	atggatccggccgccatcgggcaggatctg
oSE102	gcggaaaattcccataccggacag
oSE108	atgagctctcagttattggcggaccggcg
oSE116	atggatcctcagttattggcggaccggcg
oSE117	atgctcttcaggtatgacccaagaactcagacccaaaatc
oSE118	aattaacatatggacctgagaacactgggatattc
oSE119	atggtaccttactgcagaatcctatcccatctc
oSE120	gacaggagcccctctgaacc
oSE121	gacagctgggccacaatgct
oSE122	gttcagaggggctcctgtcaggg
oSE124	aattaaaagcttcgaccagttcgccggcccagaag

Table 5.4: used oligonucleotides: continued

Name	Sequence (5' - 3')
oSE125	gctcaccatggaagaactccttggaatcaatcac
oSE126	agttcttccatggtgagcaagggcgaggagctg
oSE127	atggatccacgcggagacggtagaagacacc
oSE128	ccatcaggatcacgccccacgga

Table 5.5: Construction of plasmids

Plasmid	Construction
pJZ26	Amplification of ~700 bp upstream of *ftsA* from ATCC15444 chrom. DNA using oligos oJZ62 and oJZ63. Amplification of *venus* from pJZ07 using oligos oJZ59 and oJZ60. Amplification of the first ~700 bp of *ftsA* from ATCC15444 chrom. DNA using oligos oJZ61 and oJZ48. Fusion of the three PCR-products by overlap-extension PCR,restriction with HindIII BamHI, and ligation into pNPTS138 cut with HindIII BamHI.
pJZ27	Amplification of ~700 bp upstream of *ftsW* from ATCC15444 chrom. DNA using oligos oJZ64 and oJZ65. Amplification of *venus* from pJZ07 using oligos oJZ66 and oJZ67. Amplification of the first ~700 bp of *ftsW* from ATCC15444 chrom. DNA using oligos oJZ68 and oJZ69. Fusion of the three PCR-products by overlap-extension PCR, restriction with HindIII BamHI, and ligation into pNPTS138 cut with HindIII BamHI.
pJZ28	Amplification of ~700 bp upstream of *fzlA* from ATCC15444 chrom. DNA using oligos oJZ70 and oJZ71. Amplification of *venus* from pJZ07 using oligos oJZ72 and oJZ73. Amplification of the first ~700 bp of *fzlA* from ATCC15444 chrom. DNA using oligos oJZ74 and oJZ75. Fusion of the three PCR-products by overlap-extension PCR, restriction with HindIII BamHI, and ligation into pNPTS138 cut with HindIII BamHI.
pSE23	Amplification of *ftsK* from ATCC15444 chrom. DNA using oligos oSE39 and oSE40, restriction with SacI NheI, and ligation into pSE32 cut with SacI NheI.

Table 5.5: construction of plasmids: continued

Plasmid	Construction
pSE24	Amplification of *ftsA* from ATCC15444 chrom. DNA using oligos oSE41 and oSE42, restriction with SacI NheI, and ligation into pSE31 cut with SacI NheI.
pSE44	Amplification of *mipZ* from ATCC15444 chrom. DNA using oligos oAR188 and oAR189, restriction with NdeI KpnI, and ligation into pSE31 cut with NdeI KpnI.
pSE54	Amplification of *ftsK* from ATCC15444 chrom. DNA using oligos oSE18 and oSE19, digestion with NdeI SacI, and ligation into pSE50 cut with NdeI SacI.
pSE56	Amplification of $ftsK_{\text{aa181-837}}$ from ATCC15444 chrom. DNA using oligos oSE73 and oSE74, digestion with NdeI BamHI, and ligation into pET28a(+) cut with NdeI BamHI.
pSE57	Amplification of $ftsK_{\text{aa1-185}}$ from ATCC15444 chrom. DNA using oligos oSE18 and oSE75, digestion with NdeI SacI, and ligation into pSE50 cut with NdeI SacI.
pSE58	Restriction of pSE14 with NdeI NheI and isolation of the *ftsZ-venus* fragment. Restriction of pCCHYC-2 with NdeI NheI, isolation of the vector backbone, and ligation with *ftsZ-venus*.
pSE59	Restriction of pSE54 with NdeI NheI and isolation of the *ftsK-venus* fragment. Restriction of pCCHYC-2 with NdeI NheI, isolation of the vector backbone, and ligation with *ftsK-venus*.
pSE63	Amplification of *ftsZ-HA* from pSE14 plasmid DNA using oligos oSE16 and oSE77, digestion with NdeI SacI, and ligation into pSE50 cut with NdeI SacI.
pSE64	Amplification of *fzlC* from ATCC15444 chrom. DNA using oligos oSE78 and oSE79, digestion with KpnI SacI, and ligation into pSE32 cut with KpnI SacI.
pSE67	Amplification of the 5' part of *ftsK* from ATCC15444 chrom. DNA using oligos oSE18 and oSE83 (carries mutation). Amplification of the 3' part of *ftsK* from ATCC15444 chrom. DNA using oligos oSE82 (carries mutation) and oSE50. Fusion of the two *ftsK* parts by overlap-extension PCR, restriction with NdeI SacI, and ligation into pSE50 cut with NdeI SacI.

Table 5.5: construction of plasmids: continued

Plasmid	Construction
pSE68	Amplification of ~700 bp upstream of *ftsI* from ATCC15444 chrom. DNA using oligos oSE88 and oSE89. Amplification of *venus-ftsI'* from pSE25 plasmid DNA using oligos oSE90 and oSE91. Fusion of the two PCR-products by overlap-extension PCR, digestion with HindIII BamHI, and ligation into pNPTS138 cut with HindIII BamHI.
pSE69	Amplification of the 5' part of $ftsZ_{aa1\text{-}51}$ from pSE35 plasmid DNA using oligos oSE16 and oSE84. Amplification of *venus* from pSE50 using oligos oSE85 and oSE86. Amplification of 3' part of $ftsZ_{aa52\text{-}xy}$ from pSE35 plasmid DNA using oligos oSE87 and oSE47. Fusion of the three PCR-products by overlap-extension PCR, restriction with NdeI KpnI, and ligation into pSE50 cut with NdeI KpnI.
pSE75	Amplification of the 5' part of *mipZ* from pSE44 plasmid DNA using oligos oAR188 and oSE96 (carries mutation). Amplification of the 3' part of *mipZ* from pSE44 plasmid DNA using oligos oSE95 (carries mutation) and oSE97. Fusion of the two *mipZ* parts by overlap-extension PCR, restriction with NdeI KpnI, and ligation into pSE52 cut with NdeI KpnI.
pSE76	Amplification of ~700 bp upstream of *fzlC* from ATCC15444 chrom. DNA using oligos oSE98 and oSE99. Amplification of *venus-fzlC'* from pSE64 plasmid DNA using oligos oSE100 and oSE101. Fusion of the two PCR-products by overlap-extension PCR, digestion with HindIII BamHI, and ligation into pNPTS138 cut with HindIII BamHI.
pSE84	Amplification of *ftsZ* from pSE58 plasmid DNA using oligos oSE16 and oSE108, restriction with NdeI SacI, and ligation into pET21a(+) cut with NdeI SacI.
pSE91	Amplification of *ftsZ* from pSE84 plasmid DNA using oligos oSE117 and oSE116, digestion with SapI BamHI, and ligation into pTB146 cut with SapI BamHI.
pSE93	Restriction of pSE54 with NdeI NheI and isolation of the *ftsK-venus* fragment. Restriction of pXVENC-2 with NdeI NheI, isolation of the vector backbone, and ligation with *ftsK-venus*.

Table 5.5: construction of plasmids: continued

Plasmid	Construction
pSE94	Amplification of $TALE_{\mathrm{ftsK}}$ from 14AEDVYC plasmid DNA using oligos oSE118 and oSE119, restriction with NdeI KpnI, and ligation into pSE53 cut with NdeI KpnI.
pSE96	Amplification of ~700 bp upstream of *ftsN* from ATCC15444 chrom. DNA using oligos oSE124 and oSE125. Amplification of *venus-ftsN'* from pSE26 plasmid DNA using oligos oSE126 and oSE127. Fusion of the two PCR-products by overlap-extension PCR, digestion with HindIII BamHI, and ligation into pNPTS138 cut with HindIII BamHI.

6 References

[1] **Rothfield, L.**, **Justice, S.**, **Garcia-Lara, J.** (1999) Bacterial cell division. *Annu Rev Genet* **33**:423–48.

[2] **Vaughan, S.**, **Wickstead, B.**, **Gull, K.**, **Addinall, S.G.** (2004) Molecular evolution of FtsZ protein sequences encoded within the genomes of archaea, bacteria, and eukaryota. *J Mol Evol* **58**(1):19–29.

[3] **Loewe, J.**, **Amos, L.A.** (1998) Crystal structure of the bacterial cell-division protein FtsZ. *Nature* **391**(6663):203–6.

[4] **Erickson, H.P.** (1995) FtsZ, a prokaryotic homolog of tubulin? *Cell* **80**(3):367–70.

[5] **Huang, K.H.**, **Durand-Heredia, J.**, **Janakiraman, A.** (2013) FtsZ ring stability: of bundles, tubules, crosslinks, and curves. *J Bacteriol* **195**(9):1859–68.

[6] **Stricker, J.**, **Maddox, P.**, **Salmon, E.D.**, **Erickson, H.P.** (2002) Rapid assembly dynamics of the *Escherichia coli* FtsZ-ring demonstrated by fluorescence recovery after photobleaching. *Proc Natl Acad Sci U S A* **99**(5):3171–5.

[7] **Anderson, D.E.**, **Gueiros-Filho, F.J.**, **Erickson, H.P.** (2004) Assembly dynamics of FtsZ rings in *Bacillus subtilis* and *Escherichia coli* and effects of FtsZ-regulating proteins. *J Bacteriol* **186**(17):5775–81.

[8] **Natale, P.**, **Pazos, M.**, **Vicente, M.** (2013) The *Escherichia coli* divisome: born to divide. *Environ Microbiol* **15**(12):3169–82.

[9] **Rico, A.I.**, **Krupka, M.**, **Vicente, M.** (2013) In the beginning, *Escherichia coli* assembled the proto-ring: an initial phase of division. *J Biol Chem* **288**(29):20830–6.

[10] **Fu, G.**, **Huang, T.**, **Buss, J.**, **Coltharp, C.**, **Hensel, Z.**, **Xiao, J.** (2010) In vivo structure of the *E. coli* FtsZ-ring revealed by photoactivated localization microscopy (PALM). *PLoS One* **5**(9):e12682.

[11] **Jennings, P.C.**, **Cox, G.C.**, **Monahan, L.G.**, **Harry, E.J.** (2011) Super-resolution imaging of the bacterial cytokinetic protein FtsZ. *Micron* **42**(4):336–41.

[12] **Li, Z.**, **Trimble, M.J.**, **Brun, Y.V.**, **Jensen, G.J.** (2007) The structure of FtsZ filaments in vivo suggests a force-generating role in cell division. *EMBO J* **26**(22):4694–708.

[13] **Milam, S.L.**, **Osawa, M.**, **Erickson, H.P.** (2012) Negative-stain electron microscopy of inside-out FtsZ rings reconstituted on artificial membrane tubules show ribbons of protofilaments. *Biophys J* **103**(1):59–68.

[14] **Gueiros-Filho, F.J.**, **Losick, R.** (2002) A widely conserved bacterial cell division protein that promotes assembly of the tubulin-like protein FtsZ. *Genes Dev* **16**(19):2544–56.

[15] **Mateos-Gil, P.**, **Márquez, I.**, **López-Navajas, P.**, **Jiménez, M.**, **Vicente, M.**, **Mingorance, J.**, **Rivas, G.**, **Vélez, M.** (2012) FtsZ polymers bound to lipid bilayers through

ZipA form dynamic two dimensional networks. *Biochim Biophys Acta* **1818**(3):806–13.

[16] **Szwedziak, P.**, **Wang, Q.**, **Bharat, T.A.M.**, **Tsim, M.**, **Löwe, J.** (2014) Architecture of the ring formed by the tubulin homologue FtsZ in bacterial cell division. *Elife* **3**:e04601.

[17] **Jimenez, M.**, **Martos, A.**, **Vicente, M.**, **Rivas, G.** (2011) Reconstitution and organization of *Escherichia coli* proto-ring elements (FtsZ and FtsA) inside giant unilamellar vesicles obtained from bacterial inner membranes. *J Biol Chem* **286**(13):11236–41.

[18] **Osawa, M.**, **Anderson, D.E.**, **Erickson, H.P.** (2008) Reconstitution of contractile FtsZ rings in liposomes. *Science* **320**(5877):792–4.

[19] **Osawa, M.**, **Anderson, D.E.**, **Erickson, H.P.** (2009) Curved FtsZ protofilaments generate bending forces on liposome membranes. *EMBO J* **28**(22):3476–84.

[20] **Osawa, M.**, **Erickson, H.P.** (2011) Inside-out Z rings–constriction with and without GTP hydrolysis. *Mol Microbiol* **81**(2):571–9.

[21] **Meier, E.L.**, **Goley, E.D.** (2014) Form and function of the bacterial cytokinetic ring. *Curr Opin Cell Biol* **26**:19–27.

[22] **Söderström, B.**, **Skoog, K.**, **Blom, H.**, **Weiss, D.S.**, **von Heijne, G.**, **Daley, D.O.** (2014) Disassembly of the divisome in *Escherichia coli*: evidence that FtsZ dissociates before compartmentalization. *Mol Microbiol* **92**(1):1–9.

[23] **Haney, S.A.**, **Glasfeld, E.**, **Hale, C.**, **Keeney, D.**, **He, Z.**, **de Boer, P.** (2001) Genetic analysis of the *Escherichia coli* FtsZ-ZipA interaction in the yeast two-hybrid system. Characterization of FtsZ residues essential for the interactions with ZipA and with FtsA. *J Biol Chem* **276**(15):11980–7.

[24] **Hale, C.A.**, **de Boer, P.A.** (1997) Direct binding of FtsZ to ZipA, an essential component of the septal ring structure that mediates cell division in *E. coli*. *Cell* **88**(2):175–85.

[25] **Hale, C.A.**, **de Boer, P.A.J.** (2002) ZipA is required for recruitment of FtsK, FtsQ, FtsL, and FtsN to the septal ring in *Escherichia coli*. *Journal of Bacteriology* **184**(9):2552–2556.

[26] **RayChaudhuri, D.** (1999) ZipA is a MAP-Tau homolog and is essential for structural integrity of the cytokinetic FtsZ ring during bacterial cell division. *EMBO J* **18**(9):2372–83.

[27] **Pichoff, S.**, **Lutkenhaus, J.** (2005) Tethering the Z ring to the membrane through a conserved membrane targeting sequence in FtsA. *Mol Microbiol* **55**(6):1722–34.

[28] **van den Ent, F.**, **Loewe, J.** (2000) Crystal structure of the cell division protein FtsA from *Thermotoga maritima*. *EMBO J* **19**(20):5300–7.

[29] **Geissler, B.**, **Elraheb, D.**, **Margolin, W.** (2003) A gain-of-function mutation in *ftsA* bypasses the requirement for the essential cell division gene *zipA* in *Escherichia coli*. *Proc Natl Acad Sci U S A* **100**(7):4197–202.

[30] **Goley, E.D.**, **Yeh, Y.C.**, **Hong, S.H.**, **Fero, M.J.**, **Abeliuk, E.**, **McAdams, H.H.**, **Shapiro, L.** (2011) Assembly of the *Caulobacter* cell division machine. *Mol Microbiol* **80**(6):1680–98.

[31] **Möll, A.**, **Thanbichler, M.** (2009) FtsN-like proteins are conserved components of the cell division machinery in proteobacteria. *Mol Microbiol* **72**(4):1037–53.

[32] **Corbin, B.D.**, **Wang, Y.**, **Beuria, T.K.**, **Margolin, W.** (2007) Interaction between cell division proteins FtsE and FtsZ. *J Bacteriol* **189**(8):3026–35.

[33] **Schmidt, K.L.**, **Peterson, N.D.**, **Kustusch, R.J.**, **Wissel, M.C.**, **Graham, B.**, **Phillips, G.J.**, **Weiss, D.S.** (2004) A predicted ABC transporter, FtsEX, is needed for cell division in *Escherichia coli*. *J Bacteriol* **186**(3):785–93.

[34] **Yang, D.C.**, **Peters, N.T.**, **Parzych, K.R.**, **Uehara, T.**, **Markovski, M.**, **Bernhardt, T.G.** (2011) An ATP-binding cassette transporter-like complex governs cell-wall hydrolysis at the bacterial cytokinetic ring. *Proc Natl Acad Sci U S A* **108**(45):E1052–60.

[35] **Garti-Levi, S.**, **Hazan, R.**, **Kain, J.**, **Fujita, M.**, **Ben-Yehuda, S.** (2008) The FtsEX ABC transporter directs cellular differentiation in *Bacillus subtilis*. *Mol Microbiol* **69**(4):1018–28.

[36] **Durand-Heredia, J.**, **Rivkin, E.**, **Fan, G.**, **Morales, J.**, **Janakiraman, A.** (2012) Identification of ZapD as a cell division factor that promotes the assembly of FtsZ in *Escherichia coli*. *J Bacteriol* **194**(12):3189–98.

[37] **Durand-Heredia, J.M.**, **Yu, H.H.**, **De Carlo, S.**, **Lesser, C.F.**, **Janakiraman, A.** (2011) Identification and characterization of ZapC, a stabilizer of the FtsZ ring in *Escherichia coli*. *J Bacteriol* **193**(6):1405–13.

[38] **Ebersbach, G.**, **Galli, E.**, **Moller-Jensen, J.**, **Loewe, J.**, **Gerdes, K.** (2008) Novel coiled-coil cell division factor ZapB stimulates Z ring assembly and cell division. *Mol Microbiol* **68**(3):720–35.

[39] **Hale, C.A.**, **Shiomi, D.**, **Liu, B.**, **Bernhardt, T.G.**, **Margolin, W.**, **Niki, H.**, **de Boer, P.A.** (2011) Identification of *Escherichia coli* ZapC (YcbW) as a component of the division apparatus that binds and bundles FtsZ polymers. *J Bacteriol* **193**(6):1393–404.

[40] **Espeli, O.**, **Borne, R.**, **Dupaigne, P.**, **Thiel, A.**, **Gigant, E.**, **Mercier, R.**, **Boccard, F.** (2012) A MatP-divisome interaction coordinates chromosome segregation with cell division in *E. coli*. *EMBO J* **31**(14):3198–211.

[41] **Goley, E.D.**, **Dye, N.A.**, **Werner, J.N.**, **Gitai, Z.**, **Shapiro, L.** (2010) Imaging-based identification of a critical regulator of FtsZ protofilament curvature in *Caulobacter*. *Mol Cell* **39**(6):975–87.

[42] **Guendogdu, M.E.**, **Kawai, Y.**, **Pavlendova, N.**, **Ogasawara, N.**, **Errington, J.**, **Scheffers, D.J.**, **Hamoen, L.W.** (2011) Large ring polymers align FtsZ polymers for normal septum formation. *EMBO J* **30**(3):617–26.

[43] **Haeusser, D.P.**, **Schwartz, R.L.**, **Smith, A.M.**, **Oates, M.E.**, **Levin, P.A.** (2004) EzrA prevents aberrant cell division by modulating assembly of the cytoskeletal protein FtsZ. *Mol Microbiol* **52**(3):801–14.

[44] **Claessen, D.**, **Emmins, R.**, **Hamoen, L.W.**, **Daniel, R.A.**, **Errington, J.**, **Edwards, D.H.** (2008) Control of the cell elongation-division cycle by shuttling of PBP1 protein in *Bacillus subtilis*. *Mol Microbiol* **68**(4):1029–46.

[45] **Steele, V.R.**, **Bottomley, A.L.**, **Garcia-Lara, J.**, **Kasturiarachchi, J.**, **Foster, S.J.** (2011) Multiple essential roles for EzrA in cell division of *Staphylococcus aureus*. *Mol Microbiol* **80**(2):542–55.

[46] **Buddelmeijer, N.**, **Beckwith, J.** (2004) A complex of the *Escherichia coli* cell division proteins FtsL, FtsB and FtsQ forms independently of its localization to the septal region. *Mol Microbiol* **52**(5):1315–27.

[47] **Gonzalez, M.D.**, **Akbay, E.A.**, **Boyd, D.**, **Beckwith, J.** (2010) Multiple interaction domains in FtsL, a protein component of the widely conserved bacterial FtsLBQ cell division complex. *J Bacteriol* **192**(11):2757–68.

[48] **Di Lallo, G.**, **Fagioli, M.**, **Barionovi, D.**, **Ghelardini, P.**, **Paolozzi, L.** (2003) Use of a two-hybrid assay to study the assembly of a complex multicomponent protein machinery: bacterial septosome differentiation. *Microbiology* **149**(Pt 12):3353–9.

[49] **D'Ulisse, V.**, **Fagioli, M.**, **Ghelardini, P.**, **Paolozzi, L.** (2007) Three functional subdomains of the *Escherichia coli* FtsQ protein are involved in its interaction with the other division proteins. *Microbiology* **153**(Pt 1):124–38.

[50] **Karimova, G.**, **Dautin, N.**, **Ladant, D.** (2005) Interaction network among *Escherichia coli* membrane proteins involved in cell division as revealed by bacterial two-hybrid analysis. *J Bacteriol* **187**(7):2233–43.

[51] **Busiek, K.K.**, **Margolin, W.** (2014) A role for FtsA in SPOR-independent localization of the essential *Escherichia coli* cell division protein FtsN. *Mol Microbiol* **92**(6):1212–26.

[52] **Liu, B.**, **Persons, L.**, **Lee, L.**, **de Boer, P.A.** (2014) Roles for both FtsA and the FtsBLQ subcomplex in FtsN-stimulated cell constriction in *Escherichia coli*. *Mol Microbiol* .

[53] **Pichoff, S.**, **Du, S.**, **Lutkenhaus, J.** (2014) The bypass of ZipA by overexpression of FtsN requires a previously unknown conserved FtsN motif essential for FtsA-FtsN interaction supporting a model in which FtsA monomers recruit late cell division proteins to the Z ring. *Mol Microbiol* .

[54] **Tsang, M.J.**, **Bernhardt, T.G.** (2014) A role for the FtsQLB complex in cytokinetic ring activation revealed by an ftsL allele that accelerates division. *Mol Microbiol* .

[55] **Botta, G.A.**, **Park, J.T.** (1981) Evidence for involvement of penicillin-binding protein 3 in murein synthesis during septation but not during cell elongation. *J Bacteriol* **145**(1):333–40.

[56] **Costa, T.**, **Priyadarshini, R.**, **Jacobs-Wagner, C.** (2008) Localization of PBP3 in *Caulobacter crescentus* is highly dynamic and largely relies on its functional transpeptidase domain. *Mol Microbiol* **70**(3):634–51.

[57] **Boyle, D.S.**, **Khattar, M.M.**, **Addinall, S.G.**, **Lutkenhaus, J.**, **Donachie, W.D.** (1997) FtsW is an essential cell-division gene in *Escherichia coli*. *Mol Microbiol* **24**(6):1263–73.

[58] **Mohammadi, T.**, **van Dam, V.**, **Sijbrandi, R.**, **Vernet, T.**, **Zapun, A.**, **Bouhss, A.**, **Diepeveen-de Bruin, M.**, **Nguyen-Disteche, M.**, **de Kruijff, B.**, **Breukink, E.** (2011) Identification of FtsW as a transporter of lipid-linked cell wall precursors across the membrane. *EMBO J* **30**(8):1425–32.

[59] **Fraipont, C.**, **Alexeeva, S.**, **Wolf, B.**, **van der Ploeg, R.**, **Schloesser, M.**, **den Blaauwen, T.**, **Nguyen-Disteche, M.** (2011) The integral membrane FtsW protein and peptidoglycan synthase PBP3 form a subcomplex in *Escherichia coli*. *Microbiology* **157**(Pt 1):251–9.

[60] **Mercer, K.L.**, **Weiss, D.S.** (2002) The *Escherichia coli* cell division protein FtsW is required to recruit its cognate transpeptidase, FtsI (PBP3), to the division site. *J Bacteriol* **184**(4):904–12.

[61] **Sham, L.T.**, **Butler, E.K.**, **Lebar, M.D.**, **Kahne, D.**, **Bernhardt, T.G.**, **Ruiz, N.** (2014) Bacterial cell wall. MurJ is the flippase of lipid-linked precursors for peptidoglycan biogenesis. *Science* **345**(6193):220–2.

[62] **Gerding, M.A.**, **Liu, B.**, **Bendezu, F.O.**, **Hale, C.A.**, **Bernhardt, T.G.**, **de Boer, P.A.** (2009) Self-enhanced accumulation of FtsN at Division Sites and Roles for Other Proteins with a SPOR domain (DamX, DedD, and RlpA) in *Escherichia coli* cell constriction. *J Bacteriol* **191**(24):7383–401.

[63] **Müller, P.**, **Ewers, C.**, **Bertsche, U.**, **Anstett, M.**, **Kallis, T.**, **Breukink, E.**, **Fraipont, C.**, **Terrak, M.**, **Nguyen-Disteche, M.**, **Vollmer, W.** (2007) The essential cell division protein FtsN interacts with the murein (peptidoglycan) synthase PBP1B in *Escherichia coli*. *J Biol Chem* **282**(50):36394–402.

[64] **Typas, A.**, **Banzhaf, M.**, **Gross, C.A.**, **Vollmer, W.** (2012) From the regulation of peptidoglycan synthesis to bacterial growth and morphology. *Nat Rev Microbiol* **10**(2):123–36.

[65] **Gerding, M.A.**, **Ogata, Y.**, **Pecora, N.D.**, **Niki, H.**, **de Boer, P.A.** (2007) The trans-envelope Tol-Pal complex is part of the cell division machinery and required for proper outer-membrane invagination during cell constriction in *E. coli*. *Mol Microbiol* **63**(4):1008–25.

[66] **Yeh, Y.C.**, **Comolli, L.R.**, **Downing, K.H.**, **Shapiro, L.**, **McAdams, H.H.** (2010) The *Caulobacter* Tol-Pal complex is essential for outer membrane integrity and the positioning of a polar localization factor. *J Bacteriol* **192**(19):4847–58.

[67] **Paradis-Bleau, C.**, **Markovski, M.**, **Uehara, T.**, **Lupoli, T.J.**, **Walker, S.**, **Kahne, D.E.**, **Bernhardt, T.G.** (2010) Lipoprotein cofactors located in the outer membrane activate bacterial cell wall polymerases. *Cell* **143**(7):1110–20.

[68] **Typas, A.**, **Banzhaf, M.**, **van den Berg van Saparoea, B.**, **Verheul, J.**, **Biboy, J.**, **Nichols, R.J.**, **Zietek, M.**, **Beilharz, K.**, **Kannenberg, K.**, **von Rechenberg, M.**, **Breukink, E.**, **den Blaauwen, T.**, **Gross, C.A.**, **Vollmer, W.** (2010) Regulation of peptidoglycan synthesis by outer-membrane proteins. *Cell* **143**(7):1097–109.

[69] **Goley, E.D.**, **Comolli, L.R.**, **Fero, K.E.**, **Downing, K.H.**, **Shapiro, L.** (2010) DipM links peptidoglycan remodelling to outer membrane organization in *Caulobacter*. *Mol Microbiol* **77**(1):56–73.

[70] **Möll, A.**, **Schlimpert, S.**, **Briegel, A.**, **Jensen, G.J.**, **Thanbichler, M.** (2010) DipM, a new factor required for peptidoglycan remodelling during cell division in *Caulobacter crescentus*. *Mol Microbiol* **77**(1):90–107.

[71] **Poggio, S.**, **Takacs, C.N.**, **Vollmer, W.**, **Jacobs-Wagner, C.** (2010) A protein critical for cell constriction in the Gram-negative bacterium emphCaulobacter crescentus localizes at the division site through its peptidoglycan-binding LysM domains. *Mol Microbiol* **77**(1):74–89.

[72] **Rogers, H.J.**, **Perkins, H.R.**, **Ward, J.B.** (1980) Microbial cell walls and membranes. Chapman and Hall. Springer Science & Business Media, London.

[73] **Matsuhashi, M.**, **Wachi, M.**, **Ishino, F.** (1990) Machinery for cell growth and division: penicillin-binding proteins and other proteins. *Res Microbiol* **141**(1):89–103.

[74] **Spratt, B.G.** (1975) Distinct penicillin binding proteins involved in the division, elongation, and shape of *Escherichia coli* K12. *Proc Natl Acad Sci U S A* **72**(8):2999–3003.

[75] **Höltje, J.V.** (1995) From growth to autolysis: the murein hydrolases in *Escherichia coli*. *Arch Microbiol* **164**(4):243–54.

[76] **den Blaauwen, T.**, **de Pedro, M.A.**, **Nguyen-Disteche, M.**, **Ayala, J.A.** (2008) Morphogenesis of rod-shaped sacculi. *FEMS Microbiol Rev* **32**(2):321–44.

[77] **Daniel, R.A.**, **Errington, J.** (2003) Control of cell morphogenesis in bacteria: two distinct ways to make a rod-shaped cell. *Cell* **113**(6):767–76.

[78] **Doi, M.**, **Wachi, M.**, **Ishino, F.**, **Tomioka, S.**, **Ito, M.**, **Sakagami, Y.**, **Suzuki, A.**, **Matsuhashi, M.** (1988) Determinations of the DNA sequence of the mreB gene and of the gene products of the mre region that function in formation of the rod shape of *Escherichia coli* cells. *J Bacteriol* **170**(10):4619–24.

[79] **Aaron, M.**, **Charbon, G.**, **Lam, H.**, **Schwarz, H.**, **Vollmer, W.**, **Jacobs-Wagner, C.** (2007) The tubulin homologue FtsZ contributes to cell elongation by guiding cell wall precursor synthesis in *Caulobacter crescentus*. *Mol Microbiol* **64**(4):938–52.

[80] **Vollmer, W.**, **Bertsche, U.** (2008) Murein (peptidoglycan) structure, architecture and biosynthesis in *Escherichia coli*. *Biochim Biophys Acta* **1778**(9):1714–34.

[81] **de Pedro, M.A.**, **Quintela, J.C.**, **Holtje, J.V.**, **Schwarz, H.** (1997) Murein segregation in *Escherichia coli*. *J Bacteriol* **179**(9):2823–34.

[82] **Bramkamp, M.** (2015) Following the equator: division site selection in *Streptococcus pneumoniae*. *Trends Microbiol* **23**(3):121–2.

[83] **Monahan, L.G.**, **Harry, E.J.** (2013) Identifying how bacterial cells find their middle: a new perspective. *Mol Microbiol* **87**(2):231–4.

[84] **de Boer, P.A.**, **Crossley, R.E.**, **Rothfield, L.I.** (1989) A division inhibitor and a topological specificity factor coded for by the minicell locus determine proper placement of the division septum in *E. coli*. *Cell* **56**(4):641–9.

[85] **de Boer, P.A.**, **Crossley, R.E.**, **Rothfield, L.I.** (1990) Central role for the *Escherichia coli minC* gene product in two different cell division-inhibition systems. *Proc Natl Acad Sci U S A* **87**(3):1129–33.

[86] **Hu, Z.**, **Mukherjee, A.**, **Pichoff, S.**, **Lutkenhaus, J.** (1999) The MinC component of the division site selection system in *Escherichia coli* interacts with FtsZ to prevent polymerization. *Proc Natl Acad Sci U S A* **96**(26):14819–24.

[87] **Hu, Z.**, **Lutkenhaus, J.** (2000) Analysis of MinC reveals two independent domains involved in interaction with MinD and FtsZ. *J Bacteriol* **182**(14):3965–71.

[88] **Shen, B.**, **Lutkenhaus, J.** (2010) Examination of the interaction between FtsZ and MinCN in *E. coli* suggests how MinC disrupts Z rings. *Mol Microbiol* **75**(5):1285–98.

[89] **Cordell, S.C.**, **Loewe, J.** (2001) Crystal structure of the bacterial cell division regulator MinD. *FEBS Lett* **492**(1-2):160–5.

[90] **de Boer, P.A.**, **Crossley, R.E.**, **Hand, A.R.**, **Rothfield, L.I.** (1991) The MinD protein is a membrane ATPase required for the correct placement of the *Escherichia coli division site*. *EMBO J* **10**(13):4371–80.

[91] **Szeto, T.H.**, **Rowland, S.L.**, **Habrukowich, C.L.**, **King, G.F.** (2003) The MinD membrane targeting sequence is a transplantable lipid-binding helix. *J Biol Chem* **278**(41):40050–6.

[92] **Hu, Z.**, **Lutkenhaus, J.** (2001) Topological regulation of cell division in *E. coli*. Spatiotemporal oscillation of MinD requires stimulation of its ATPase by MinE and phospholipid. *Mol Cell* **7**(6):1337–43.

[93] **Raskin, D.M.**, **de Boer, P.A.** (1999) Rapid pole-to-pole oscillation of a protein required for directing division to the middle of *Escherichia coli*. *Proc Natl Acad Sci U S A* **96**(9):4971–6.

[94] **Cha, J.H.**, **Stewart, G.C.** (1997) The divIVA minicell locus of *Bacillus subtilis*. *J Bacteriol* **179**(5):1671–83.

[95] **Edwards, D.H.**, **Errington, J.** (1997) The *Bacillus subtilis* DivIVA protein targets to the division septum and controls the site specificity of cell division. *Mol Microbiol* **24**(5):905–15.

[96] **Edwards, D.H.**, **Thomaides, H.B.**, **Errington, J.** (2000) Promiscuous targeting of *Bacillus subtilis* cell division protein DivIVA to division sites in Escherichia coli and fission yeast. *EMBO J* **19**(11):2719–27.

[97] **Bramkamp, M.**, **Emmins, R.**, **Weston, L.**, **Donovan, C.**, **Daniel, R.A.**, **Errington, J.** (2008) A novel component of the division-site selection system of *Bacillus subtilis* and a new mode of action for the division inhibitor MinCD. *Mol Microbiol* **70**(6):1556–69.

[98] **Patrick, J.E.**, **Kearns, D.B.** (2008) MinJ (YvjD) is a topological determinant of cell division in *Bacillus subtilis*. *Mol Microbiol* **70**(5):1166–79.

[99] **Bramkamp, M.**, **van Baarle, S.** (2009) Division site selection in rod-shaped bacteria. *Curr Opin Microbiol* **12**(6):683–8.

[100] **Gregory, J.A.**, **Becker, E.C.**, **Pogliano, K.** (2008) *Bacillus subtilis* MinC destabilizes FtsZ-rings at new cell poles and contributes to the timing of cell division. *Genes Dev* **22**(24):3475–88.

[101] **van Baarle, S.**, **Bramkamp, M.** (2010) The MinCDJ system in *Bacillus subtilis* prevents minicell formation by promoting divisome disassembly. *PLoS One* **5**(3):e9850.

[102] **Bernhardt, T.G.**, **de Boer, P.A.** (2005) SlmA, a nucleoid-associated, FtsZ binding protein required for blocking septal ring assembly over chromosomes in *E. coli*. *Mol Cell* **18**(5):555–64.

[103] **Wu, L.J.**, **Errington, J.** (2004) Coordination of cell division and chromosome segregation by a nucleoid occlusion protein in *Bacillus subtilis*. *Cell* **117**(7):915–25.

[104] **Cho, H.**, **McManus, H.R.**, **Dove, S.L.**, **Bernhardt, T.G.** (2011) Nucleoid occlusion factor SlmA is a DNA-activated FtsZ polymerization antagonist. *Proc Natl Acad Sci U S A* **108**(9):3773–8.

[105] **Wu, L.J.**, **Ishikawa, S.**, **Kawai, Y.**, **Oshima, T.**, **Ogasawara, N.**, **Errington, J.** (2009) Noc protein binds to specific DNA sequences to coordinate cell division with chromosome segregation. *EMBO J* **28**(13):1940–52.

[106] **Tonthat, N.K.**, **Arold, S.T.**, **Pickering, B.F.**, **Van Dyke, M.W.**, **Liang, S.**, **Lu, Y.**, **Beuria, T.K.**, **Margolin, W.**, **Schumacher, M.A.** (2011) Molecular mechanism by which the nucleoid occlusion factor, SlmA, keeps cytokinesis in check. *EMBO J* **30**(1):154–64.

[107] **Cho, H.**, **Bernhardt, T.G.** (2013) Identification of the SlmA Active Site Responsible for Blocking Bacterial Cytokinetic Ring Assembly over the Chromosome. *PLoS Genet* **9**(2):e1003304.

[108] **Du, S.**, **Lutkenhaus, J.** (2014) SlmA antagonism of FtsZ assembly employs a two-pronged mechanism like MinCD. *PLoS Genet* **10**(7):e1004460.

[109] **Wu, L.J.**, **Errington, J.** (2012) Nucleoid occlusion and bacterial cell division. *Nat Rev Microbiol* **10**(1):8–12.

[110] **Adams, D.W.**, **Wu, L.J.**, **Errington, J.** (2015) Nucleoid occlusion protein Noc recruits DNA to the bacterial cell membrane. *EMBO J* **34**(4):491–501.

[111] **Rodrigues, C.D.**, **Harry, E.J.** (2012) The Min system and nucleoid occlusion are not required for identifying the division site in *Bacillus subtilis* but ensure its efficient utilization. *PLoS Genet* **8**(3):e1002561.

[112] **Bailey, M.W.**, **Bisicchia, P.**, **Warren, B.T.**, **Sherratt, D.J.**, **Mannik, J.** (2014) Evidence for divisome localization mechanisms independent of the Min system and SlmA in *Escherichia coli*. *PLoS Genet* **10**(8):e1004504.

[113] **Cambridge, J.**, **Blinkova, A.**, **Magnan, D.**, **Bates, D.**, **Walker, J.R.** (2014) A replication-inhibited unsegregated nucleoid at mid-cell blocks Z-ring formation and cell division independently of SOS and the SlmA nucleoid occlusion protein in *Escherichia coli*. *J Bacteriol* **196**(1):36–49.

[114] **Kiekebusch, D.**, **Michie, K.A.**, **Essen, L.O.**, **Loewe, J.**, **Thanbichler, M.** (2012) Localized dimerization and nucleoid binding drive gradient formation by the bacterial cell division inhibitor MipZ. *Mol Cell* **46**(3):245–59.

[115] **Thanbichler, M.**, **Shapiro, L.** (2006) MipZ, a spatial regulator coordinating chromosome segregation with cell division in *Caulobacter*. *Cell* **126**(1):147–62.

[116] **Willemse, J.**, **Borst, J.W.**, **de Waal, E.**, **Bisseling, T.**, **van Wezel, G.P.** (2011) Positive control of cell division: FtsZ is recruited by SsgB during sporulation of *Streptomyces*. *Genes Dev* **25**(1):89–99.

[117] **Treuner-Lange, A.**, **Aguiluz, K.**, **van der Does, C.**, **Gomez-Santos, N.**, **Harms, A.**, **Schumacher, D.**, **Lenz, P.**, **Hoppert, M.**, **Kahnt, J.**, **Munoz-Dorado, J.**, **Sogaard-Andersen, L.** (2013) PomZ, a ParA-like protein, regulates Z-ring formation and cell division in *Myxococcus xanthus*. *Mol Microbiol* **87**(2):235–53.

[118] **Fleurie, A.**, **Lesterlin, C.**, **Manuse, S.**, **Zhao, C.**, **Cluzel, C.**, **Lavergne, J.P.**, **Franz-Wachtel, M.**, **Macek, B.**, **Combet, C.**, **Kuru, E.**, **VanNieuwenhze, M.S.**, **Brun, Y.V.**, **Sherratt, D.**, **Grangeasse, C.** (2014) MapZ marks the division sites and positions FtsZ rings in *Streptococcus pneumoniae*. *Nature* **516**(7530):259–62.

[119] **Holeckova, N.**, **Doubravova, L.**, **Massidda, O.**, **Molle, V.**, **Buriankova, K.**, **Benada, O.**, **Kofronova, O.**, **Ulrych, A.**, **Branny, P.** (2014) LocZ Is a New Cell Division Protein Involved in Proper Septum Placement in *Streptococcus pneumoniae*. *MBio* **6**(1).

[120] **Webb, C.D.**, **Graumann, P.L.**, **Kahana, J.A.**, **Teleman, A.A.**, **Silver, P.A.**, **Losick, R.** (1998) Use of time-lapse microscopy to visualize rapid movement of the replication origin region of the chromosome during the cell cycle in *Bacillus subtilis*. *Mol Microbiol* **28**(5):883–92.

[121] **Gordon, G.S.**, **Sitnikov, D.**, **Webb, C.D.**, **Teleman, A.**, **Straight, A.**, **Losick, R.**, **Murray, A.W.**, **Wright, A.** (1997) Chromosome and low copy plasmid segregation in *E. coli*: visual evidence for distinct mechanisms. *Cell* **90**(6):1113–21.

[122] **Jensen, R.B.**, **Shapiro, L.** (1999) Chromosome segregation during the prokaryotic cell division cycle. *Curr Opin Cell Biol* **11**(6):726–31.

[123] **Livny, J.**, **Yamaichi, Y.**, **Waldor, M.K.** (2007) Distribution of centromere-like parS sites in bacteria: insights from comparative genomics. *J Bacteriol* **189**(23):8693–703.

[124] **Ireton, K.**, **Gunther, N.W.t.**, **Grossman, A.D.** (1994) spo0J is required for normal chromosome segregation as well as the initiation of sporulation in *Bacillus subtilis*. *J Bacteriol* **176**(17):5320–9.

[125] **Heidelberg, J.F.**, **Eisen, J.A.**, **Nelson, W.C.**, **Clayton, R.A.**, **Gwinn, M.L.**, **Dodson, R.J.**, **Haft, D.H.**, **Hickey, E.K.**, **Peterson, J.D.**, **Umayam, L.**, **Gill, S.R.**, **Nelson, K.E.**, **Read, T.D.**, **Tettelin, H.**, **Richardson, D.**, **Ermolaeva, M.D.**, **Vamathevan, J.**, **Bass, S.**, **Qin, H.**, **Dragoi, I.**, **Sellers, P.**, **McDonald, L.**, **Utterback, T.**, **Fleishmann, R.D.**, **Nierman, W.C.**, **White, O.**, **Salzberg, S.L.**, **Smith, H.O.**, **Colwell, R.R.**, **Mekalanos, J.J.**, **Venter, J.C.**, **Fraser, C.M.** (2000) DNA sequence of both chromosomes of the cholera pathogen *Vibrio cholerae*. *Nature* **406**(6795):477–83.

[126] **Mohl, D.A.**, **Gober, J.W.** (1997) Cell cycle-dependent polar localization of chromosome partitioning proteins in *Caulobacter crescentus*. *Cell* **88**(5):675–84.

[127] **Mohl, D.A.**, **Easter, J., J.**, **Gober, J.W.** (2001) The chromosome partitioning protein, ParB, is required for cytokinesis in *Caulobacter crescentus*. *Mol Microbiol* **42**(3):741–55.

[128] **Ebersbach, G.**, **Gerdes, K.** (2005) Plasmid segregation mechanisms. *Annu Rev Genet* **39**:453–79.

[129] **Banigan, E.J.**, **Gelbart, M.A.**, **Gitai, Z.**, **Wingreen, N.S.**, **Liu, A.J.** (2011) Filament depolymerization can explain chromosome pulling during bacterial mitosis. *PLoS Comput Biol* **7**(9):e1002145.

[130] **Ptacin, J.L.**, **Shapiro, L.** (2010) Initiating bacterial mitosis: understanding the mechanism of ParA-mediated chromosome segregation. *Cell Cycle* **9**(20):4033–4.

[131] **Ringgaard, S.**, **van Zon, J.**, **Howard, M.**, **Gerdes, K.** (2009) Movement and equipositioning of plasmids by ParA filament disassembly. *Proc Natl Acad Sci U S A* **106**(46):19369–74.

[132] **Hwang, L.C.**, **Vecchiarelli, A.G.**, **Han, Y.W.**, **Mizuuchi, M.**, **Harada, Y.**, **Funnell, B.E.**, **Mizuuchi, K.** (2013) ParA-mediated plasmid partition driven by protein pattern self-organization. *EMBO J* **32**(9):1238–49.

[133] **Vecchiarelli, A.G.**, **Han, Y.W.**, **Tan, X.**, **Mizuuchi, M.**, **Ghirlando, R.**, **Biertumpfel, C.**, **Funnell, B.E.**, **Mizuuchi, K.** (2010) ATP control of dynamic P1 ParA-DNA interactions: a key role for the nucleoid in plasmid partition. *Mol Microbiol* **78**(1):78–91.

[134] **Vecchiarelli, A.G.**, **Hwang, L.C.**, **Mizuuchi, K.** (2013) Cell-free study of F plasmid partition provides evidence for cargo transport by a diffusion-ratchet mechanism. *Proc Natl Acad Sci U S A* **110**(15):E1390–7.

[135] **Lim, H.C.**, **Surovtsev, I.V.**, **Beltran, B.G.**, **Huang, F.**, **Bewersdorf, J.**, **Jacobs-Wagner, C.** (2014) Evidence for a DNA-relay mechanism in ParABS-mediated chromosome segregation. *Elife* **3**:e02758.

[136] **Wang, X.**, **Montero Llopis, P.**, **Rudner, D.Z.** (2013) Organization and segregation of bacterial chromosomes. *Nat Rev Genet* **14**(3):191–203.

[137] **Bowman, G.R.**, **Comolli, L.R.**, **Zhu, J.**, **Eckart, M.**, **Koenig, M.**, **Downing, K.H.**, **Moerner, W.E.**, **Earnest, T.**, **Shapiro, L.** (2008) A polymeric protein anchors the chromosomal origin/ParB complex at a bacterial cell pole. *Cell* **134**(6):945–55.

[138] **Ebersbach, G.**, **Briegel, A.**, **Jensen, G.J.**, **Jacobs-Wagner, C.** (2008) A self-associating protein critical for chromosome attachment, division, and polar organization in *Caulobacter*. *Cell* **134**(6):956–68.

[139] **Ptacin, J.L.**, **Lee, S.F.**, **Garner, E.C.**, **Toro, E.**, **Eckart, M.**, **Comolli, L.R.**, **Moerner, W.E.**, **Shapiro, L.** (2010) A spindle-like apparatus guides bacterial chromosome segregation. *Nat Cell Biol* **12**(8):791–8.

[140] **Schofield, W.B.**, **Lim, H.C.**, **Jacobs-Wagner, C.** (2010) Cell cycle coordination and regulation of bacterial chromosome segregation dynamics by polarly localized proteins. *EMBO J* **29**(18):3068–81.

[141] **Shebelut, C.W.**, **Guberman, J.M.**, **van Teeffelen, S.**, **Yakhnina, A.A.**, **Gitai, Z.** (2010) *Caulobacter* chromosome segregation is an ordered multistep process. *Proc Natl Acad Sci U S A* **107**(32):14194–8.

[142] **Ptacin, J.L.**, **Gahlmann, A.**, **Bowman, G.R.**, **Perez, A.M.**, **von Diezmann, A.R.**, **Eckart, M.R.**, **Moerner, W.E.**, **Shapiro, L.** (2014) Bacterial scaffold directs pole-specific centromere segregation. *Proc Natl Acad Sci U S A* **111**(19):E2046–55.

[143] **Lam, H.**, **Schofield, W.B.**, **Jacobs-Wagner, C.** (2006) A landmark protein essential for establishing and perpetuating the polarity of a bacterial cell. *Cell* **124**(5):1011–23.

[144] **Laloux, G.**, **Jacobs-Wagner, C.** (2013) Spatiotemporal control of PopZ localization through cell cycle-coupled multimerization. *J Cell Biol* **201**(6):827–41.

[145] **Liu, G.**, **Draper, G.C.**, **Donachie, W.D.** (1998) FtsK is a bifunctional protein involved in cell division and chromosome localization in *Escherichia coli*. *Mol Microbiol* **29**(3):893–903.

[146] **Wang, L.**, **Lutkenhaus, J.** (1998) FtsK is an essential cell division protein that is localized to the septum and induced as part of the SOS response. *Mol Microbiol* **29**(3):731–40.

[147] **Yu, X.C.**, **Tran, A.H.**, **Sun, Q.**, **Margolin, W.** (1998) Localization of cell division protein FtsK to the *Escherichia coli* septum and identification of a potential N-terminal targeting domain. *J Bacteriol* **180**(5):1296–304.

[148] **Dubarry, N.**, **Possoz, C.**, **Barre, F.X.** (2010) Multiple regions along the *Escherichia coli* FtsK protein are implicated in cell division. *Mol Microbiol* **78**(5):1088–100.

[149] **Aussel, L.**, **Barre, F.X.**, **Aroyo, M.**, **Stasiak, A.**, **Stasiak, A.Z.**, **Sherratt, D.** (2002) FtsK is a DNA motor protein that activates chromosome dimer resolution by switching the catalytic state of the XerC and XerD recombinases. *Cell* **108**(2):195–205.

[150] **Yu, X.C.**, **Weihe, E.K.**, **Margolin, W.** (1998) Role of the C-terminus of FtsK in *Escherichia coli* chromosome segregation. *J Bacteriol* **180**(23):6424–8.

[151] **Massey, T.H.**, **Mercogliano, C.P.**, **Yates, J.**, **Sherratt, D.J.**, **Lowe, J.** (2006) Double-stranded DNA translocation: structure and mechanism of hexameric FtsK. *Mol Cell* **23**(4):457–69.

[152] **Bigot, S.**, **Saleh, O.A.**, **Cornet, F.**, **Allemand, J.F.**, **Barre, F.X.** (2006) Oriented loading of FtsK on KOPS. *Nat Struct Mol Biol* **13**(11):1026–8.

[153] **Bigot, S.**, **Saleh, O.A.**, **Lesterlin, C.**, **Pages, C.**, **El Karoui, M.**, **Dennis, C.**, **Grigoriev, M.**, **Allemand, J.F.**, **Barre, F.X.**, **Cornet, F.** (2005) KOPS: DNA motifs that control *E. coli* chromosome segregation by orienting the FtsK translocase. *EMBO J* **24**(21):3770–80.

[154] **Levy, O.**, **Ptacin, J.L.**, **Pease, P.J.**, **Gore, J.**, **Eisen, M.B.**, **Bustamante, C.**, **Cozzarelli, N.R.** (2005) Identification of oligonucleotide sequences that direct the movement of the *Escherichia coli* FtsK translocase. *Proc Natl Acad Sci U S A* **102**(49):17618–23.

[155] **Sivanathan, V.**, **Allen, M.D.**, **de Bekker, C.**, **Baker, R.**, **Arciszewska, L.K.**, **Freund, S.M.**, **Bycroft, M.**, **Lowe, J.**, **Sherratt, D.J.** (2006) The FtsK gamma domain directs oriented DNA translocation by interacting with KOPS. *Nat Struct Mol Biol* **13**(11):965–72.

[156] **Graham, J.E.**, **Sherratt, D.J.**, **Szczelkun, M.D.** (2010) Sequence-specific assembly of FtsK hexamers establishes directional translocation on DNA. *Proc Natl Acad Sci U S A* **107**(47):20263–8.

[157] **Löwe, J.**, **Ellonen, A.**, **Allen, M.D.**, **Atkinson, C.**, **Sherratt, D.J.**, **Grainge, I.** (2008) Molecular mechanism of sequence-directed DNA loading and translocation by FtsK. *Mol Cell* **31**(4):498–509.

[158] **Steiner, W.**, **Liu, G.**, **Donachie, W.D.**, **Kuempel, P.** (1999) The cytoplasmic domain of FtsK protein is required for resolution of chromosome dimers. *Mol Microbiol* **31**(2):579–83.

[159] **Lee, J.Y.**, **Finkelstein, I.J.**, **Arciszewska, L.K.**, **Sherratt, D.J.**, **Greene, E.C.** (2014) Single-molecule imaging of FtsK translocation reveals mechanistic features of protein-protein collisions on DNA. *Mol Cell* **54**(5):832–43.

[160] **Bigot, S.**, **Marians, K.J.** (2010) DNA chirality-dependent stimulation of topoisomerase IV activity by the C-terminal AAA+ domain of FtsK. *Nucleic Acids Res* **38**(9):3031–40.

[161] **Espeli, O.**, **Lee, C.**, **Marians, K.J.** (2003) A physical and functional interaction between *Escherichia coli* FtsK and topoisomerase IV. *J Biol Chem* **278**(45):44639–44.

[162] **Besprozvannaya, M.**, **Burton, B.M.** (2014) Do the same traffic rules apply? Directional chromosome segregation by SpoIIIE and FtsK. *Mol Microbiol* **93**(4):599–608.

[163] **Bath, J.**, **Wu, L.J.**, **Errington, J.**, **Wang, J.C.** (2000) Role of *Bacillus subtilis* SpoIIIE in DNA transport across the mother cell-prespore division septum. *Science* **290**(5493):995–7.

[164] **Wu, L.J.**, **Errington, J.** (1994) *Bacillus subtilis* SpoIIIE protein required for DNA segregation during asymmetric cell division. *Science* **264**(5158):572–5.

[165] **Wu, L.J.**, **Errington, J.** (1998) Use of asymmetric cell division and *spoIIIE* mutants to probe chromosome orientation and organization in *Bacillus subtilis*. *Mol Microbiol* **27**(4):777–86.

[166] **Leifson, E.** (1964) *Hyphomicrobium neptunium* Sp. N. *Antonie Van Leeuwenhoek* **30**:249–56.

[167] **Poindexter, J.L.S.**, **Cohen-Bazire, G.** (1964) The fine structure of stalked bacteria belonging to the family *Caulobacteraceae*. *J Cell Biol* **23**:587–607.

[168] **Wagner, J.K.**, **Brun, Y.V.** (2007) Out on a limb: how the *Caulobacter* stalk can boost the study of bacterial cell shape. *Mol Microbiol* **64**(1):28–33.

[169] **Wali, T.M.**, **Hudson, G.R.**, **Danald, D.A.**, **Weiner, R.M.** (1980) Timing of swarmer cell cycle morphogenesis and macromolecular synthesis by *Hyphomicrobium neptunium* in synchronous culture. *J Bacteriol* **144**(1):406–12.

[170] **Weiner, R.M.**, **Blackman, M.A.** (1973) Inhibition of deoxyribonucleic acid synthesis and bud formation by nalidixic acid in *Hyphomicrobium neptunium*. *J Bacteriol* **116**(3):1398–404.

[171] **Zerfas, P.M.**, **Kessel, M.**, **Quintero, E.J.**, **Weiner, R.M.** (1997) Fine-structure evidence for cell membrane partitioning of the nucleoid and cytoplasm during bud formation in *Hyphomonas* species. *J Bacteriol* **179**(1):148–56.

[172] **Hirsch, P.** (1974) Budding bacteria. *Annu Rev Microbiol* **28**(0):391–444.

[173] **Lee, K.C.**, **Webb, R.I.**, **Fuerst, J.A.** (2009) The cell cycle of the planctomycete *Gemmata obscuriglobus* with respect to cell compartmentalization. *BMC Cell Biol* **10**:4.

[174] **Schlesner, H.**, **Bartels, C.**, **Sittig, M.**, **Dorsch, M.**, **Stackebrandt, E.** (1990) Taxonomic and phylogenetic studies on a new taxon of budding, hyphal proteobacteria, *Hirschia baltica* gen. nov., sp. nov. *Int J Syst Bacteriol* **40**(4):443–51.

[175] **Waterbury, J.**, **Stanier, R.** (1977) Two unicellular cyanobacteria which reproduce by budding. *Arch Microbiol* **115**:249–257.

[176] **Whittenbury, R.**, **Dow, C.S.** (1977) Morphogenesis and differentiation in *Rhodomicrobium vannielii* and other budding and prosthecate bacteria. *Bacteriol Rev* **41**(3):754–808.

[177] **Brown, P.J.B.**, **Kysela, D.T.**, **Brun, Y.V.** (2011) Polarity and the diversity of growth mechanisms in bacteria. *Semin Cell Dev Biol* **22**(8):790–8.

[178] **Havenner, J.A.**, **McCardell, B.A.**, **Weiner, R.M.** (1979) Development of defined, minimal and complete media for the growth of *Hyphomicrobium neptunium*. *Appl Environ Microbiol* **38**(1):18–23.

[179] **Moore, R.L.**, **Weiner, R.M.**, **Gebers, R.** (1984) Genus *Hyphomonas* Pongratz 1957 nom. rev. emend., *Hyphomonas polymorpha* Pongratz 1957 nom. rev. emend., and *Hyphomonas neptunium* (Leifson 1964) comb. nov. emend. (*Hyphomicrobium neptunium*). *Int J Syst Bacteriol* **34**:71–73.

[180] **Nikitin, D.I.**, **Vishnewetskaya, O.**, **Chumakov, K.M.**, **Zlatkin, I.V.** (1990) Evolutionary relationship of some stalked and budding bacteria (genera *Caulobacter*, "*Hyphobacter*", *Hyphomonas* and *Hyphomicrobium*) as studied by the new integral taxonomical method. *Arch Microbiol* **153**(2):123–8.

[181] **Garrity, G.M.**, **Brenner, D.J.**, **Krieg, N.R.**, **Staley, J.R.** (2005) The Proteobacteria. Bergey's manual of systematic bacteriology, vol. 2, Part A-C. Springer, New York, 1040–1053.

[182] **Badger, J.H.**, **Eisen, J.A.**, **Ward, N.L.** (2005) Genomic analysis of *Hyphomonas neptunium* contradicts 16S rRNA gene-based phylogenetic analysis: implications for the taxonomy of the orders 'Rhodobacterales' and Caulobacterales. *Int J Syst Evol Microbiol* **55**(Pt 3):1021–6.

[183] **Badger, J.H.**, **Hoover, T.R.**, **Brun, Y.V.**, **Weiner, R.M.**, **Laub, M.T.**, **Alexandre, G.**, **Mrazek, J.**, **Ren, Q.**, **Paulsen, I.T.**, **Nelson, K.E.**, **Khouri, H.M.**, **Radune, D.**, **Sosa, J.**, **Dodson, R.J.**, **Sullivan, S.A.**, **Rosovitz, M.J.**, **Madupu, R.**, **Brinkac, L.M.**, **Durkin, A.S.**, **Daugherty, S.C.**, **Kothari, S.P.**, **Giglio, M.G.**, **Zhou, L.**, **Haft, D.H.**, **Selengut, J.D.**, **Davidsen, T.M.**, **Yang, Q.**, **Zafar, N.**, **Ward, N.L.** (2006) Comparative genomic evidence for a close relationship between the dimorphic prosthecate bacteria *Hyphomonas neptunium* and *Caulobacter crescentus*. *J Bacteriol* **188**(19):6841–50.

[184] **Poindexter, J.S.** (2006) Dimorphic prosthecate bacteria: the genera *Caulobacter, Asticcacaulis, Hyphomicrobium, Pedomicrobium, Hyphomonas and Thiodendron*. The Prokaryotes, vol. 5. Springer, New York, 72–90.

[185] **Brilli, M.**, **Fondi, M.**, **Fani, R.**, **Mengoni, A.**, **Ferri, L.**, **Bazzicalupo, M.**, **Biondi, E.G.** (2010) The diversity and evolution of cell cycle regulation in alpha-proteobacteria: a comparative genomic analysis. *BMC Syst Biol* **4**:52.

[186] **Ireland, M.M.**, **Karty, J.A.**, **Quardokus, E.M.**, **Reilly, J.P.**, **Brun, Y.V.** (2002) Proteomic analysis of the *Caulobacter crescentus* stalk indicates competence for nutrient uptake. *Mol Microbiol* **45**(4):1029–41.

[187] **Ong, C.J.**, **Wong, M.L.**, **Smit, J.** (1990) Attachment of the adhesive holdfast organelle to the cellular stalk of *Caulobacter crescentus*. *J Bacteriol* **172**(3):1448–56.

[188] **Schlimpert, S.**, **Klein, E.A.**, **Briegel, A.**, **Hughes, V.**, **Kahnt, J.**, **Bolte, K.**, **Maier, U.G.**, **Brun, Y.V.**, **Jensen, G.J.**, **Gitai, Z.**, **Thanbichler, M.** (2012) General protein diffusion barriers create compartments within bacterial cells. *Cell* **151**(6):1270–82.

[189] **Wagner, J.K.**, **Setayeshgar, S.**, **Sharon, L.A.**, **Reilly, J.P.**, **Brun, Y.V.** (2006) A nutrient uptake role for bacterial cell envelope extensions. *Proc Natl Acad Sci U S A* **103**(31):11772–7.

[190] **Weiner, R.M.** (2005) Genus *Hyphomonas*. Bergey's manual of systematic bacteriology. Springer, New York, 179–187.

[191] **Devine, R.A.**, **Weiner, R.M.** (1990) *Hyphomonas species* metabolise amino acids using Krebs cycle enzymes. *Microbios* **62**:137–153.

[192] **Jung, A.**, **Eisheuer, S.**, **Cserti, E.**, **Leicht, O.**, **Strobel, W.**, **Möll, A.**, **Schlimpert, S.**, **Kühn, J.**, **Thanbichler, M.** (2015) Molecular Toolbox for Genetic Manipulation of the Stalked Budding Bacterium *Hyphomonas neptunium*. *Appl Environ Microbiol* **81**(2):736–44.

[193] **Strobel, W.** (2010) Etablierung von genetischen Methoden zur Analyse der Zellteilung in *Hyphomonas neptunium*. Bachelor's thesis, Philipps University Marburg.

[194] **Ma, X.**, **Ehrhardt, D.W.**, **Margolin, W.** (1996) Colocalization of cell division proteins FtsZ and FtsA to cytoskeletal structures in living *Escherichia coli* cells by using green fluorescent protein. *Proc Natl Acad Sci U S A* **93**(23):12998–3003.

[195] **Cameron, T.A.**, **Anderson-Furgeson, J.**, **Zupan, J.R.**, **Zik, J.J.**, **Zambryski, P.C.** (2014) Peptidoglycan synthesis machinery in *Agrobacterium tumefaciens* during unipolar growth and cell division. *MBio* **5**(3):e01219–14.

[196] **Nguyen-Disteche, M.**, **Fraipont, C.**, **Buddelmeijer, N.**, **Nanninga, N.** (1998) The structure and function of *Escherichia coli* penicillin-binding protein 3. *Cell Mol Life Sci* **54**(4):309–16.

[197] **Kuru, E.**, **Hughes, H.V.**, **Brown, P.J.**, **Hall, E.**, **Tekkam, S.**, **Cava, F.**, **de Pedro, M.A.**, **Brun, Y.V.**, **VanNieuwenhze, M.S.** (2012) In Situ probing of newly synthesized peptidoglycan in live bacteria with fluorescent D-amino acids. *Angew Chem Int Ed Engl* **51**(50):12519–23.

[198] **Joyce, G.**, **Williams, K.J.**, **Robb, M.**, **Noens, E.**, **Tizzano, B.**, **Shahrezaei, V.**, **Robertson, B.D.** (2012) Cell division site placement and asymmetric growth in mycobacteria. *PLoS One* **7**(9):e44582.

[199] **Specht, M.**, **Dempwolff, F.**, **Schatzle, S.**, **Thomann, R.**, **Waidner, B.** (2013) Localization of FtsZ in *Helicobacter pylori* and consequences for cell division. *J Bacteriol* **195**(7):1411–20.

[200] **Raßbach, A.** (2013) Chromosomensegregation in *Hyphomonas neptunium*. Ph.D. thesis, Philipps University Marburg.

[201] **Koch, M.K.**, **McHugh, C.A.**, **Hoiczyk, E.** (2011) BacM, an N-terminally processed bactofilin of *Myxococcus xanthus*, is crucial for proper cell shape. *Molecular Microbiology* **80**(4):1031–1051.

[202] **Kühn, J.**, **Briegel, A.**, **Moerschel, E.**, **Kahnt, J.**, **Leser, K.**, **Wick, S.**, **Jensen, G.J.**, **Thanbichler, M.** (2010) Bactofilins, a ubiquitous class of cytoskeletal proteins

mediating polar localization of a cell wall synthase in *Caulobacter crescentus*. *EMBO J* **29**(2):327–39.

[203] **Lin, L.** (2013) Cytoskeletons as polar landmarks. Ph.D. thesis, PhD thesis, Philipps University Marburg.

[204] **Kelly, A.J.**, **Sackett, M.J.**, **Din, N.**, **Quardokus, E.**, **Brun, Y.V.** (1998) Cell cycle-dependent transcriptional and proteolytic regulation of FtsZ in *Caulobacter*. *Genes Dev* **12**(6):880–93.

[205] **Zhang, Y.** (2008) I-TASSER server for protein 3D structure prediction. *BMC Bioinformatics* **9**:40.

[206] **Bi, E.**, **Dai, K.**, **Subbarao, S.**, **Beall, B.**, **Lutkenhaus, J.** (1991) FtsZ and cell division. *Res Microbiol* **142**(2-3):249–52.

[207] **Crozat, E.**, **Meglio, A.**, **Allemand, J.F.**, **Chivers, C.E.**, **Howarth, M.**, **Venien-Bryan, C.**, **Grainge, I.**, **Sherratt, D.J.** (2010) Separating speed and ability to displace roadblocks during DNA translocation by FtsK. *EMBO J* **29**(8):1423–33.

[208] **Boch, J.**, **Bonas, U.** (2010) *Xanthomonas* AvrBs3 family-type III effectors: discovery and function. *Annu Rev Phytopathol* **48**:419–36.

[209] **Politz, M.C.**, **Copeland, M.F.**, **Pfleger, B.F.** (2013) Artificial repressors for controlling gene expression in bacteria. *Chem Commun (Camb)* **49**(39):4325–7.

[210] **Addinall, S.G.**, **Cao, C.**, **Lutkenhaus, J.** (1997) FtsN, a late recruit to the septum in *Escherichia coli*. *Mol Microbiol* **25**(2):303–9.

[211] **Zupan, J.R.**, **Cameron, T.A.**, **Anderson-Furgeson, J.**, **Zambryski, P.C.** (2013) Dynamic FtsA and FtsZ localization and outer membrane alterations during polar growth and cell division in *Agrobacterium tumefaciens*. *Proc Natl Acad Sci U S A* **110**(22):9060–5.

[212] **Wang, Y.**, **Jones, B.D.**, **Brun, Y.V.** (2001) A set of *ftsZ* mutants blocked at different stages of cell division in *Caulobacter*. *Mol Microbiol* **40**(2):347–60.

[213] **Wang, S.C.**, **West, L.**, **Shapiro, L.** (2006) The bifunctional FtsK protein mediates chromosome partitioning and cell division in *Caulobacter*. *J Bacteriol* **188**(4):1497–508.

[214] **He, B.** (2014) Study of a sociable molecule - Mapping the binding interfaces of the cell division regulator MipZ in *Caulobacter crescentus*. Ph.D. thesis, PhD thesis, Philipps University Marburg.

[215] **Kiekebusch, D.** (2011) Die P-loop ATPase MipZ - Mechanismus der Bildung eines Proteingradienten in einer prokaryotischen Zelle. Ph.D. thesis, Philipps University Marburg.

[216] **Ramamurthi, K.S.**, **Lecuyer, S.**, **Stone, H.A.**, **Losick, R.** (2009) Geometric cue for protein localization in a bacterium. *Science* **323**(5919):1354–7.

[217] **Ramamurthi, K.S.**, **Losick, R.** (2009) Negative membrane curvature as a cue for subcellular localization of a bacterial protein. *Proc Natl Acad Sci U S A* **106**(32):13541–5.

[218] **Oliva, M.A.**, **Halbedel, S.**, **Freund, S.M.**, **Dutow, P.**, **Leonard, T.A.**, **Veprintsev, D.B.**, **Hamoen, L.W.**, **Lowe, J.** (2010) Features critical for membrane binding revealed by DivIVA crystal structure. *EMBO J* **29**(12):1988–2001.

[219] **Stahlberg, H.**, **Kutejova, E.**, **Muchova, K.**, **Gregorini, M.**, **Lustig, A.**, **Muller, S.A.**, **Olivieri, V.**, **Engel, A.**, **Wilkinson, A.J.**, **Barak, I.** (2004) Oligomeric structure of the *Bacillus subtilis* cell division protein DivIVA determined by transmission electron microscopy. *Mol Microbiol* **52**(5):1281–90.

[220] **Kruse, T.**, **Bork-Jensen, J.**, **Gerdes, K.** (2005) The morphogenetic MreBCD proteins of *Escherichia coli* form an essential membrane-bound complex. *Mol Microbiol* **55**(1):78–89.

[221] **Ben-Yehuda, S.**, **Losick, R.** (2002) Asymmetric cell division in *B. subtilis* involves a spiral-like intermediate of the cytokinetic protein FtsZ. *Cell* **109**(2):257–66.

[222] **Eichenberger, P.**, **Fawcett, P.**, **Losick, R.** (2001) A three-protein inhibitor of polar septation during sporulation in *Bacillus subtilis*. *Mol Microbiol* **42**(5):1147–62.

[223] **Pogliano, J.**, **Osborne, N.**, **Sharp, M.D.**, **Abanes-De Mello, A.**, **Perez, A.**, **Sun, Y.L.**, **Pogliano, K.** (1999) A vital stain for studying membrane dynamics in bacteria: a novel mechanism controlling septation during *Bacillus subtilis* sporulation. *Mol Microbiol* **31**(4):1149–59.

[224] **Ben-Yehuda, S.**, **Rudner, D.Z.**, **Losick, R.** (2003) Assembly of the SpoIIIE DNA translocase depends on chromosome trapping in *Bacillus subtilis*. *Curr Biol* **13**(24):2196–200.

[225] **Wu, L.J.**, **Errington, J.** (1997) Septal localization of the SpoIIIE chromosome partitioning protein in *Bacillus subtilis*. *EMBO J* **16**(8):2161–9.

[226] **Jensen, R.B.** (2006) Analysis of the terminus region of the *Caulobacter crescentus* chromosome and identification of the dif site. *J Bacteriol* **188**(16):6016–9.

[227] **Touzain, F.**, **Petit, M.A.**, **Schbath, S.**, **El Karoui, M.** (2011) DNA motifs that sculpt the bacterial chromosome. *Nat Rev Microbiol* **9**(1):15–26.

[228] **Youngren, B.**, **Radnedge, L.**, **Hu, P.**, **Garcia, E.**, **Austin, S.** (2000) A Plasmid Partition System of the P1-P7par Family from the pMT1 Virulence Plasmid of *Yersinia pestis*. *Journal of bacteriology* **182**(14):3924–3928.

[229] **Tsokos, C.G.**, **Laub, M.T.** (2012) Polarity and cell fate asymmetry in *Caulobacter crescentus*. *Curr Opin Microbiol* **15**(6):744–50.

[230] **Ausubel, F.M.** (1988) Current protocols in molecular biology. *Greene Pub Associates, Wiley-Interscience* :New York.

[231] **Sambrook, J.**, **Fritsch, E.F.**, **Maniatis, T.** (1989) Molecular cloning: a laboratory manual. *Cold Spring Harbor Laboratory Press* :Cold Spring Harbor, N.Y.

[232] **Ely, B.** (1991) Genetics of *Caulobacter crescentus*. *Methods Enzymol* **204**:372–84.

[233] **Laemmli, U.K.** (1970) Cleavage of structural proteins during the assembly of the head of bacteriophage T4. *Nature* **227**(5259):680–5.

[234] **Gawronski, J.D.**, **Benson, D.R.** (2004) Microtiter assay for glutamine synthetase biosynthetic activity using inorganic phosphate detection. *Anal Biochem* **327**(1):114–8.

[235] **Waterhouse, A.M.**, **Procter, J.B.**, **Martin, D.M.**, **Clamp, M.**, **Barton, G.J.** (2009) Jalview Version 2–a multiple sequence alignment editor and analysis workbench. *Bioinformatics* **25**(9):1189–91.

[236] **Evinger, M.**, **Agabian, N.** (1977) Envelope-associated nucleoid from *Caulobacter crescentus* stalked and swarmer cells. *J Bacteriol* **132**(1):294–301.

[237] **Zimmer, J.** (2013) Analyse der Zellteilung in *Hyphomonas neptunium*. Bachelor's thesis, Philipps University Marburg.

[238] **Eisheuer, S.** (2011) Analyse der Zellteilung in *Hyphomonas neptunium*. Master's thesis, Philipps University Marburg.

[239] **Thanbichler, M.**, **Iniesta, A.A.**, **Shapiro, L.** (2007) A comprehensive set of plasmids for vanillate- and xylose-inducible gene expression in *Caulobacter crescentus*. *Nucleic Acids Res* **35**(20):e137.

[240] **Bendezu, F.O.**, **Hale, C.A.**, **Bernhardt, T.G.**, **de Boer, P.A.** (2009) RodZ (YfgA) is required for proper assembly of the MreB actin cytoskeleton and cell shape in *E. coli*. *EMBO J* **28**(3):193–204.

[241] **Heinrich, K.** (2011) Analyse der Chromosomensegregation in *Hyphomonas neptunium*. Bachelor's thesis, Philipps-Universität Marburg.

Acknowledgements

I want to express my gratitude to a number of people, who contributed in different ways to the completion of my thesis.

First and foremost, I want to thank my advisor Prof. Dr. Martin Thanbichler for giving me the opportunity to work on this fascinating project, for his great scientific ideas and good advices and his willingness to help.

I want to express my gratitude to the members of my thesis committee Prof. Dr. MD Lotte Søgaard-Andersen, Prof. Dr. Peter Graumann and Prof. Dr. Renate Renkawitz-Pohl. In particular, I want to thank Prof. Dr. MD Lotte Søgaard-Andersen for being my second reviewer. In addition I also want to thank my IMPRS committee member Dr. Lennart Randau.

I am indepted to our collaborators Yi-Wei Chang and Grant Jensen (CalTech, USA) for the electron cryo-tomograms, Jörg Kahnt (MPI Marburg, Dept. of Ecophysiology) for the MALDI/MS analyses and Thomas Heimerl (Phillips University Marburg, Dept. of Biology) for the electron micrographs.

My special thanks go to Maria Billini, Alexandra Jung and Wolfgang Strobel for proof-reading my thesis.

Spending hour after hour in the lab was made enjoyable by my group, who provided a pleasant working atmosphere with time for fun, legendary but almost forgotten cake sessions and helpful advices. For this, I want to thank all past and current lab members for the last years. My thank goes especially to my lab “neighbors” Julia and Wolle for nice lunch breaks, spreading good mood and all the fun. I want to thank Wolle in a special way for all the good times and fun activities, especially outside the lab. During the past four years we collected many memories, I will always treasure.

Additionally, I want to thank my bachelor student Jutta Zimmer, who made me laugh and filled the lab with a lot of fun, who contributed to this work and who became a good friend of mine.

In a special way, I want to thank my friends, who provided a lot of distraction and joy. Particularly, my beloved Lena, who is always there for me. I cannot imagine a life without our weekly phone calls and your support in any situation of life. Thank you for patiently enduring all of my problems and complaints during my PhD time.

At the end, I want to express my deepest gratitude to my parents and the rest of my family. Mom and Dad, you filled my life with love and fun and you are the pillar in my today's life. Words cannot express how grateful I am to be your daughter. I also want to thank my grandparents and the rest of my family for their support. I know that I can always count on you.

Erklärung

Ich versichere, dass ich meine Dissertation:

“Characterization of the division apparatus
in the budding bacterium *Hyphomonas neptunium*”

selbständig, ohne unerlaubte Hilfe angefertigt und mich dabei keiner anderen als der von mir ausdrücklich bezeichneten Quellen und Hilfen bedient habe. Die Dissertation wurde in der jetzigen oder einer ähnlichen Form noch bei keiner anderen Hochschule eingereicht und hat noch keinen sonstigen Prüfungszwecken gedient.

Marburg, den ....

Sabrina Eisheuer